UNIVERSITY OF CALIFORNIA SAN DIEGO

SAN DIEGO STATE UNIVERSITY

Probing NEMO-dependent mechanism and regulation of gene expression in the canonical NF-κB signaling pathway

A Dissertation submitted in partial satisfaction of the requirements
for the degree Doctor of Philosophy

in

Chemistry and Biochemistry

by

Sally Luong

Committee in charge:

University of California San Diego
- Professor Stacey Brydges
- Professor Simpson Joseph
- Professor Jin Zhang

San Diego State University
- Professor Tom Huxford, Chair
- Professor John Love

2026

The Dissertation of Sally Luong is approved, and it is acceptable in quality and form for publication on microfilm and electronically.

Chair

DEDICATION

I dedicate my work to my younger sister, Selena. Thank you for bringing out the best in me.

TABLE OF CONTENTS

LIST OF FIGURES

LIST OF TABLES

LIST OF ABBREVIATIONS

DD	Dimerization domain
EDA-ID	Hypohidrotic ectodermal dysplasia with immune deficiency
EMSA	Electrophoretic mobility shift assay
IBD	Inflammatory bowel disease
IκB	Inhibitor of NF-κB
IKK	Inhibitor of NF-κB kinase
IKK1/α	Inhibitor of NF-κB kinase 1/α
IKK2/β	Inhibitor of NF-κB kinase 2/β
IP	Incontinentia pigmenti
KBD	Kinase binding domain
LUBAC	Linear ubiquitin binding assembly complex
NBD	NEMO binding domain
NEMO	NF-κB essential modulator
NF-κB	Nuclear factor kappa B
NLS	Nuclear localization signal
NTD	N-terminal domain
RA	Rheumatoid arthritis
TAD	Transactivation domain
TNF-α	Tumor necrosis factor- α

ACKNOWLEDGEMENTS

I want to thank Dr. Tom Huxford for his mentorship and support throughout my years at SDSU. I want to also thank all my lab peers, past and present, you all have shaped the person and scientist I am now. Especially Matthew Mealka. You have been with me since the very beginning, and I cannot think of anyone better to share this experience with.

I am incredibly grateful to have friends inside and outside of the program that supported me and helped me scientifically, mentally, and physically. You have made research and life much more enjoyable. Thank you for being there for me and being in my life.

I am grateful for my family. My mom and dad for their support and understanding. My older brother, Kenny, just for being there. My grandma for being my inspiration. Selena, my younger sister, who I strive to be the best sister and role model for. And to Clark, I am very lucky and happy to have you by my side, thank you for closing out this chapter of life with me.

Thank you, Mikella Robinson and the SDSU Flow Core Facility, for helping me in sorting cells, troubleshooting, and technical support.

I would like to acknowledge CSUPERB for the 2022 CSUPERB Faculty-Graduate Student Research Collaboration Award and those who helped in receiving the 2023 Harry E. Hamber Memorial Scholarship. Thank you to the ACCEL program for their financial support and mentorship.

Chapter 2, 3 and 4, in part is currently being prepared for submission for publication of the material. Luong, Sally; Huxford, Tom. The dissertation author was the primary researcher and author of this material.

VITA

2019 Bachelor of Science in Chemistry emphasis in Biochemistry, San Diego State University

2026 Doctor of Philosophy in Chemistry, University of California San Diego/San Diego State University

ABSTRACT OF THE DISSERTATION

Probing NEMO-dependent mechanism and regulation of gene expression in the canonical NF-κB signaling pathway

by

Sally Luong

Doctor of Philosophy in Chemistry and Biochemistry

University of California San Diego, 2026

San Diego State University, 2026

Professor Tom Huxford, Chair

Nuclear factor-κB (NF-κB) is an inducible transcription factor involved in many cellular processes, such as inflammation, innate immune responses, and cell survival. The inhibitor of NF-κB Kinase (IKK) complex is central to the induction and nuclear translocation of NF-κB. Activation of IKK catalytic activity in response to TNF-α and other canonical inducers of NF-κB requires formation of non-degradative linear polyubiquitin chains and their association with its

NEMO subunit. NEMO, or NF-κB essential modulator, is a component of the IKK complex that is required for canonical activation of NF-κB. Without NEMO, the canonical pathway is disrupted and NF-κB cannot be induced to translocate into the nucleus. Past observations suggested that the IKK NEMO subunit, upon noncovalent association with linear polyubiquitin chains, mediates a second protein-protein interaction with the catalytic IKK2 subunit and "primes" the complex for kinase catalytic activity via activation loop phosphorylation. The purpose of this dissertation is to investigate the direct involvement of NEMO in promoting catalytically active IKK and NF-κB-mediated gene expression in response to TNF-α and to establish cell-based systems through which novel NEMO-dependent mechanisms of IKK regulation can be identified. To test the involvement of NEMO in canonical NF-κB signaling, mutations that disrupt the protein-protein interactions of NEMO can be introduced in HEK293T using CRISPR-Cas9 prime editing and the resulting mutant cell lines can then be used against various canonical inducers. We successfully generated two mutant NEMO cell lines: one engineered to disrupt the secondary binding site and the other to disrupt the linear ubiquitin binding site. Both mutations displayed varying degrees of decrease in TNF-α-induced NF-κB activation as evidenced by IKK2 phosphorylation, IκBα degradation, RelA accumulation in the nucleus, and target gene expression levels. Luciferase reporter assays further confirmed that disruption of the secondary binding site in NEMO resulted in significantly decreased levels of TNF-α-dependent NF-κB activation, though not to the same extent as cells mutated to disrupt the noncovalent interaction of NEMO with linear ubiquitin. Future studies will incorporate the validated NEMO mutations into another cell line capable of responding to canonical NF-κB inducers and further examine NEMO's involvement in canonical pathway activation.

Chapter 1 Introduction

1.1 NF-κB Pathway

Nuclear factor-kappa B (NF-κB)

Nuclear factor-κB (NF-κB) was first discovered in 1986 in David Baltimore's laboratory. Using a DNA binding electrophoretic mobility shift assay (EMSA) on transformed B-cell nuclear extracts, they discovered a nuclear factor bound that associates with a decameric DNA sequence within the intronic enhancer element of the kappa light-chain antibody gene[1–3]. The newly discovered nuclear factor was named after the cell type and location in which it was found and the gene containing the DNA sequence it bound to. Forty years of subsequent studies on NF-κB have significantly expanded upon its originally understood role, resulting the becoming to be a bit of a misnomer.

Baltimore and Sen demonstrated latent NF-κB DNA binding activity in non-B-cells by inducing Jurkat (a T lymphocyte cell line) and HeLa (a nonlymphoid cancer cell line) cells with an activating phorbol ester called phorbol 12-myristate 13-acetate (PMA)[2]. Böhnlein and others then showed that NF-κB not only binds to κ light-chain genes but also to the promoter of the interleukin-2 α receptor gene by combining the radiolabeled promoter sequence with nuclear extracts of stimulated Jurkat cells[4]. Baltimore and Baeuerle found that NF-κB is sequestered in the cytoplasm of resting cells by using dissociating agents, such as sodium deoxycholate and formamide, on the cytoplasmic fraction of unstimulated cells, detecting NF-κB activity[5]. From these discoveries, it is now understood that NF-κB is, in fact, a ubiquitous, inducible transcription factor. In unstimulated cells, NF-κB is retained in an inactive state within the cytoplasm through association with an inhibitor protein and responds to diverse stimuli by being released and translocating into the nucleus where it is able to bind to target gene DNA[6–8].

In mammals, NF-κB is a family of five polypeptides: p50, p52, RelA/p65, c-Rel, and RelB. It functions as either a homodimer or heterodimer, with the potential to form all 15 possible

combinations of these polypeptide subunits. The most prevalent and best understood NF-κB family transcription factor is the heterodimer of p50 and p65[9]. Two members of this mammalian NF-κB family, p50 and p52, are themselves generated in their mature forms via proteolytic digestion of the C-terminus of their respective precursor polypeptide, p105 and p100[10]. These precursor polypeptides contain a longer C-terminus with multiple ankyrin repeats and a death domain and, until the C-terminus is removed, acts to inhibit NF-κB.

All NF-κB family members share a conserved ~300 amino acids long N-terminal segment, known as the Rel homology region (RHR), which is responsible for dimer formation, nuclear localization, DNA binding, and interaction with its inhibitor[8]. Within the RHR, two well-folded protein domains play distinct roles: the N-terminal domain (NTD) is essential for DNA base sequence-specific binding, while the C-terminal dimerization domain (DD) supports both binding to DNA through ribose-phosphate backbone contacts and subunit dimerization. The nuclear localization signal (NLS), which is immediately C-terminal to the DD, is critical for nuclear translocation[11,12]. Each NF-κB protein also contains distinct elements that contribute to functional diversity. In p65, c-Rel, and RelB, transactivation domains (TAD) contribute to elevated target gene expression[13]. In contrast, p50 and p52 lack any C-terminal TAD region and instead possess a glycine-rich region (GRR)[11]. Consequently, homodimers of p50 or p52 bind DNA but fail to activate target gene expression without the involvement of additional transactivating factors. Additionally, RelB uniquely features an N-terminal leucine zipper, which is absent in the other NF-κB proteins (Figure 1.1).

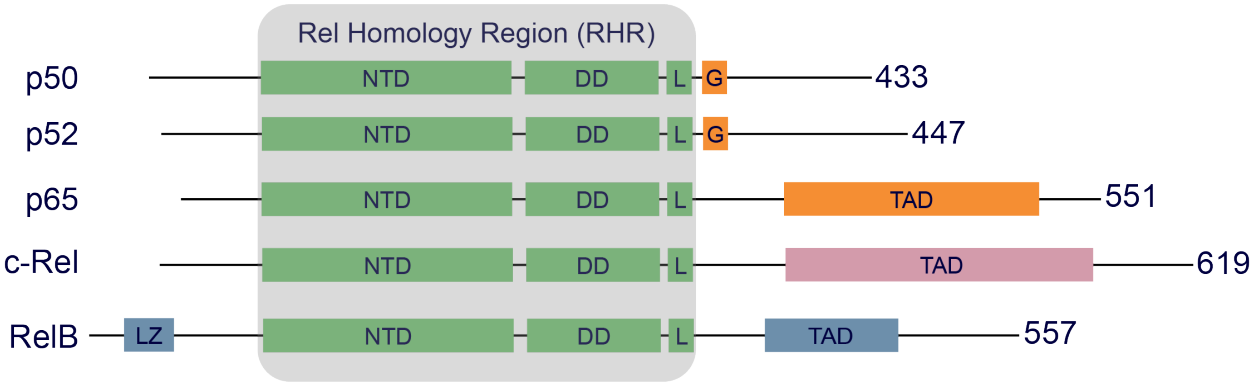

Figure 1.1: Schematic view of the mammalian NF-κB family polypeptide subunits and structured and functional domains.

Each of the five polypeptides contain the Rel homology region (RHR), which consists of an N-terminal domain (NTD), dimerization domain (DD), and nuclear localization signal (L). There is also a glycine-rich region (G) in p50 and p52, while p65, c-Rel, and RelB each possess transactivation domain (TAD). RelB has an N-terminal leucine zipper (LZ).

Inhibitor of nuclear factor-kappa B (IκB)

Inhibitor of NF-κB (IκB) was identified in 1988 in David Baltimore's laboratory after researchers observed that NF-κB activity was barely detectable in the cytosol of unstimulated cells, even though NF-κB was present[5]. Treatment of the cytosolic lysates with mild denaturing agents, such as deoxycholate, resulted in massive NF-κB DNA binding activity, suggesting that a noncovalently associated factor was responsible for inhibiting the nuclear localization and DNA binding of NF-κB. Following the discovery of this inhibitor of NF-κB, termed "IκB", scientists have identified several IκB proteins that can be classified into three groups: cytoplasmic, nuclear, and NF-κB precursor[14]. The "classical" cytoplasmic IκB proteins, which include IκBα, IκBβ, and IκBε, are found in the cytosol and they inhibit NF-κB by sequestering it there by masking its NLS and contributing their own cytoplasmic localization potential[15]. The nuclear IκB proteins, which consist of IκBζ, Bcl-3, IκBNS and IκBη, are typically not present in cells but, upon expression, accumulate in the nucleus. These nuclear IκB proteins can interact with otherwise inactive nuclear NF-κB dimers, such as the p50 homodimer, and function to activate selective target gene transcription[16]. As mentioned previously, the precursor proteins p105 and p100 give rise to the mature NF-κB p50 and p52 subunits, respectively. Both p105 and p100 are found in the cytoplasm and function similarly to typical IκB proteins by sequestering NF-κB in the cytoplasm[17,18].

Cytoplasmic IκB proteins have a centrally located ankyrin repeat domain flanked by an N-terminal signal-response region and a C-terminal PEST domain, which is rich in proline, glutamate, aspartate, serine, and threonine[19]. The ankyrin repeat domains of IκB bind to and mask the NLS of NF-κB, preventing its entry into the nucleus. When two serine residues (S32 and S36) within the N-terminal signal-response region of IκBα are phosphorylated by the IκB kinase (IKK) complex, IκBα becomes marked for degradation[20]. Subsequently, IκB is rapidly ubiquitinated by an SCF-type E3 ubiquitin-protein ligase and shortly thereafter is degraded by the 26 *S* Proteosome[21,22]. With IκB removed, NF-κB is released and free to translocate into the nucleus, where it can perform its function.

Inhibitor of nuclear factor-kappa B kinase (IKK) complex

IκB kinase (IKK) activity was first detected in 1996, when Chen and colleagues were studying the phosphorylation of IκBα. They discovered that site-specific phosphorylation of IκBα by partially purified cell lysates required the addition of ubiquitin and ATP for catalytic function[21]. The addition of ATP was self-explanatory, but addition of ubiquitin upstream of kinase catalytic activation was a novel observation that heralded the involvement of ubiquitin in novel non-degradative cell signaling mechanisms[20]. Two independent research teams subsequently identified one of this complex's kinase subunits, IKK1/α, and both kinase subunits, IKK1/α and IKK2/β, respectively[23,24]. The final subunit of the complex, NEMO/IKKγ, was found in a cell line unresponsive to NF-κB activation and in a separate study involving the sequencing of IKK-associated polypeptides[25,26].

The IKK complex is a heterotetramer, consisting of two enzymatically active kinase subunits, IKK1/IKKα and IKK2/IKKβ, as well as a scaffold-type accessory protein called IKKγ or NF-κB essential modulator (NEMO). IKK1 and IKK2 share over 50% amino acid identity and are 742 and 756 amino acids, respectively. Both display highly conserved structural features, including an N-terminal kinase domain (KD), followed by a ubiquitin-like domain (ULD), and a large scaffold/dimerization domain (SDD)[27]. At the C-terminal end of IKK1 and IKK2 is the NEMO-binding domain (NBD), a conserved sequence of amino acids that facilitates high-affinity noncovalent interaction with NEMO.

NEMO is a 419 amino acid protein, and its structure is less characterized. X-ray crystallography of relatively small portions of NEMO has revealed that its N-terminal region, known as the kinase-binding domain (KBD), exhibits a coiled-coil (CC) structure when complexed with the NBD from either IKK1 or IKK2. Additional regions of NEMO, termed "CC1" and "CC2," have also been characterized by X-ray crystallography and both adopt coiled-coil structures; CC1 was crystallized in the presence of the viral activator protein vFLIP, while CC2 dimerizes in noncovalent association with linear diubiquitin[28–30]. The NBD of IKK1 or IKK2 binds to the KBD

of NEMO, forming a heterodimer, while a region within the SDD of each IKK dimerizes to form the heterotetrameric IKK complex (Figure 1.2).

The IKK complex phosphorylates cytoplasmic IκB proteins, marking them for ubiquitination and degradation, thereby initiating NF-κB induction[27]. This process begins with the NEMO subunit of the IKK complex binding noncovalently to linear polyubiquitin chains, synthesized by the linear ubiquitin chain assembly complex (LUBAC)[29,31]. Some evidence suggests that, upon binding of linear ubiquitin, the complex undergoes a conformational change that enables NEMO to prime IKK2 for phosphorylation[32]. Serine residues at positions 176 and 180 in IKK1, or 177 and 181 in IKK2, are then phosphorylated by either another kinase, such as TAK1, or in *trans* by the IKK complex itself[33]. Once these residues are phosphorylated, the IKK complex is catalytically activate and can phosphorylate IκB proteins.

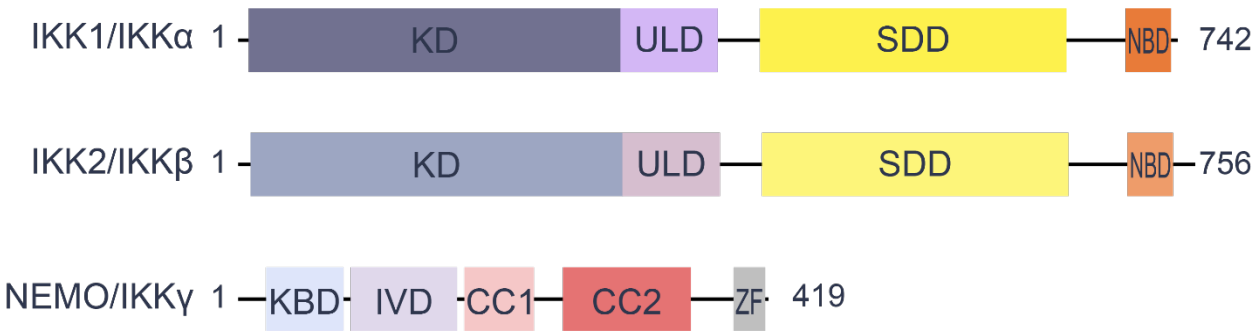

Figure 1.2: Schematic view of the IKK subunit proteins (IKK1, IKK2, and NEMO) and their structural domains.

IKK1 and IKK2, from N- to C-terminus, kinase domain (KD), ubiquitin-like domain (ULD), scaffold dimerization domain (SDD), and NEMO binding domain (NBD). NEMO, from N- to C-terminus, consists of kinase binding domain (KBD), intervening domain (IVD), coiled-coil domain 1 (CC1), coiled-coil domain 2 (CC2), and zinc finger (ZF).

NF-κB signaling pathway

NF-κB is activated through two main signaling pathways: canonical and noncanonical (or alternative), each triggered by external stimuli such as cytokines, cellular stress, and viral or bacterial components[33–35]. The canonical pathway requires both IKK2 and NEMO for activation and leads primarily to induction of NF-κB dimers containing p50, RelA, and c-Rel subunits[36]. In contrast, the noncanonical pathway is activated by a limited subset of cytokines of the greater tumor necrosis factor superfamily such as BAFF, CD40L, Lymphotoxin-β, and RANKL. This pathway depends on IKK1 independent of NEMO and the processing of p100 into p52, preferentially activating the NF-κB p52:RelB heterodimer[37]. Both pathways ultimately lead to free NF-κB dimers entering the nucleus, where they bind to κB DNA sequences and activate target gene expression.

Here, we focus on the canonical NF-κB activation pathway. In this pathway, the cell is stimulated by canonical inducers, such as inflammatory signals, growth factors, and bacterial or viral products, which activate their own specific receptors to initiate a signaling cascade[35]. Regardless of the particular stimulus, activation of the canonical pathway leads to LUBAC creating linear polyubiquitin chains that noncovalently binds with the CC2 domain of NEMO[31]. This interaction facilitates phosphorylation of serine residues 177 and 181 on IKK2, either by another kinase, such as TAK1, or through *trans* auto-phosphorylation. The activated IKK complex subsequently phosphorylates serine residues 32 and 36 on IκBα. This phosphorylation signals an E3 ubiquitin-protein ligase to attach lysine 48-linked ubiquitin to lysine 21 and 22 of IκBα, marking the protein for proteasomal degradation[38,39]. The 26 *S* proteasome then recognizes these ubiquitin chains on IκBα and degrades it, freeing the NF-κB dimer. The released NF-κB dimer can then translocate to the nucleus, bind to its target DNA sequence, and activate gene expression (Figure 1.3).

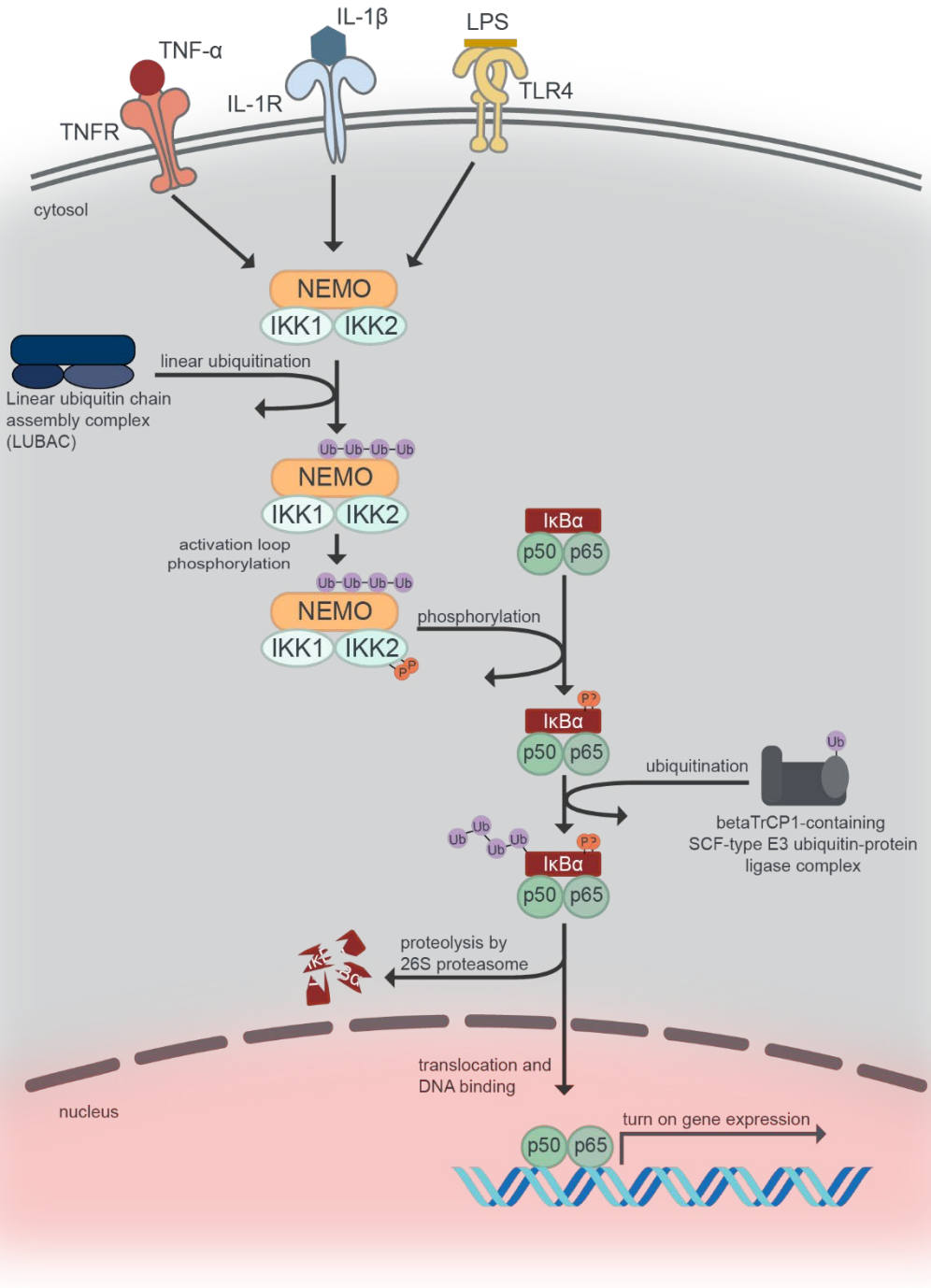

Figure 1.3: Schematic overview of canonical activation of NF-κB pathway.

1.2 Functions of NEMO

NEMO is a nonenzymatic and highly flexible scaffold protein that plays a critical role in the IKK complex. It is essential for the canonical activation of NF-κB. It can also associate noncovalently with linear polyubiquitin or K63-linked polyubiquitin and it is thought to undergo conformational changes to facilitate the activation of the IKK complex. Additionally, studies have shown that NEMO may also be modified through SUMOylation.

Ubiquitination of NEMO

NEMO has been found to bind various polyubiquitin chains, including linear (methionine 1, M1), lysine 11 (K11), lysine 48 (K48), and lysine 63 (K63) linkages, with the M1-linked chains exhibiting significantly higher affinity[40]. As previously mentioned, formative investigations into IKK demonstrated that NF-κB activation depends on non-degradative ubiquitin chains to promote catalytic activity by the IKK complex[20]. Early data indicated that K63-linked ubiquitin chains bound to NEMO, facilitating the activation of the NF-κB pathway by recruiting proteins necessary for the phosphorylation of IKK2, thereby activating the IKK complex[41–43]. Later studies demonstrated that M1-linked ubiquitin, rather than K63-linked ubiquitin as initially thought, is the critical component required for the IKK2-dependent canonical activation of NF-κB[29,44]. Further investigations into NEMO's binding to linear polyubiquitin, using circular dichroism (CD) spectroscopy and pull-down assays on mutant NEMO proteins, showed that NEMO undergoes a conformational change upon binding to M1-linked polyubiquitin[32,40]. This conformational change is believed to play a critical role in activating the IKK complex.

Conformational changes of NEMO

Evidence has shown there is conformational change in NEMO upon binding to M1-linked (linear) polyubiquitin. A 2015 study demonstrated that M1-linked polyubiquitin binding induces a conformational shift in NEMO, resulting in a functionally active complex and facilitating the recruitment of IκBα to IKK2[40]. A study in 2017 showed that NEMO transitions from a compact

resting conformation to an allosterically active state in response to binding M1-linked polyubiquitin chains, allowing it to overcome auto-inhibition[45]. In 2019, researchers highlighted the critical role of NEMO's intervening domain (IVD), which separates the KBD and CC1 regions, in activating downstream signaling[46]. They found that ligand-induced conformational changes in the IVD promoted IKK2 activation, while mutations within the IVD disrupted this process.

These past studies have established the concept of NEMO undergoing a conformational change upon binding to linear polyubiquitin. Building on this foundation, I am focusing on a 2022 study that further explores this phenomenon[32]. Scientists discovered that when NEMO non-covalently binds to linear polyubiquitin, it forms an additional contact with IKK2 at a site distinct from its KBD. They hypothesized that this interaction is facilitated by a conformational change in NEMO, allowing it to engage IKK2 through its C-terminus, thereby priming the complex for activation. After the conformational change in NEMO, IKK2 becomes catalytically active through phosphorylation.

Secondary binding site of NEMO

A 2022 study identified a secondary binding site on NEMO for IKK2 that is dependent on prior binding to linear polyubiquitin[32]. The secondary binding site was characterized by systematic mutagenesis of the NEMO amino acid sequence, precisely locating the region responsible for IKK2 interaction. Western blot analysis probing for phosphorylated IKK2 demonstrated that mutation of NEMO amino acids 385–389 to glycine completely abolished IKK2 activation, identifying this region as critical for the secondary binding interaction. This finding was further corroborated by a GST pull-down assay in which a peptide spanning NEMO amino acids 385–396 was incubated with IKK2 lysate, GST-NEMO lacking the kinase binding domain, and linear tetraubiquitin. The wild-type peptide competitively bound to IKK2 and interfered with GST-NEMO pull-down of IKK2, whereas a peptide carrying the 385–389 glycine substitutions failed to compete, allowing GST-NEMO to pull down IKK2 unimpeded. Together,

these results explain NEMO amino acids 385–389 is the secondary IKK2 binding site and demonstrate that this interaction is required for full IKK2 activation downstream of linear polyubiquitin binding.

1.3 NF-κB in human diseases

NF-κB is a ubiquitous transcription factor present in nearly all cell types and responsive to a broad range of stimuli. Its central role in regulating gene expression programs governing inflammation, cell survival, and immune responses. Dysregulation of NF-κB signaling has been implicated in a wide spectrum of human diseases, including chronic inflammatory conditions, autoimmune disorders, and cancer [47,48].

Inflammatory diseases

NF-κB drives the expression of numerous inflammatory genes, including proinflammatory cytokines, chemokines, and inflammatory mediators, establishing it as a central regulator of the inflammatory response[49,50]. While normally transient, sustained NF-κB activation due to genetic or dysregulation in the pathway contributes significantly to disease progression and tissue pathology. The pathological consequences of chronic NF-κB activation are evident in inflammatory diseases such as rheumatoid arthritis (RA) and inflammatory bowel disease (IBD). RA is an autoimmune disease characterized by synovial inflammation, autoantibody production, and bone and cartilage deformation[51]. The synovium of RA patients demonstrates significantly higher NF-κB activity compared to normal control individuals[52]. Similarly, increased NF-κB activity has been observed in the intestinal tissues of IBD patients with ulcerative colitis and Crohn's disease, respectively. Nuclear extracts of the lamina propria of those patients showed higher levels of NF-κB than in normal controls[53].

Cancer

NF-κB has been found to be associated with many types of cancer, including lung cancer, pancreatic cancer, lymphoma, and leukemia. NF-κB-related cancers can arise from viral infections, chromosomal mutations, and persistent inflammation[54,55]. In their original paper on the subject, Hanahan and Weinberg proposed six defining "Hallmarks of Cancer" that underlie the development and pathology of nearly all cancers: 1) self-sufficiency in growth signals; 2)

insensitivity to growth inhibition; 3) evasion of apoptosis; 4) immortalization; 5) sustained angiogenesis; and 6) tissue invasion and metastasis[54,56]. Consistent with these hallmarks, NF-κB is implicated in several of these processes.

In a study investigating a chemokine, CCL5, known to promote cancer cell migration and metastasis, researchers used A549, a human lung cancer cell line, to show that CCL5-induced cell migration occurred through the NF-κB signaling pathway. When the NF-κB pathway was inhibited with either an inhibitor of NF-κB induction or a proteasome inhibitor to block IκB degradation, cell migration reduced drastically[57]. In a study on anti-tumor compound pyrazole, they showed that it suppressed gene expression of TNF-α and the NF-κB p65 subunit in A549 cells, resulting in decreased cell proliferation and inflammation[58]. A different study on basal cell carcinoma cells showed that NF-κB induced stromal cell-derived factor 1 alpha (SDF-1α) to enhance tumor angiogenesis through upregulation of IL-6[59,60]. These findings illustrate the prominent role of NF-κB in cancer, and given its capacity to regulate hundreds of genes, its involvement in tumor progression is unsurprising.

1.4 NEMO-linked diseases

Incontinentia pigmenti (IP)

Incontinentia pigmenti (IP) is an X-linked genetic disorder caused by mutations in the IKBKG gene, which encodes NEMO[61]. The disease is embryonically lethal in males and leads to severe abnormalities in the skin, teeth, hair, and eyes of affected females[62]. A genetic study on IP patient cells identified mutations within IKBKG gene as the cause. Upon TNF-α stimulation, these cells failed to degrade IκB or activate NF-κB, confirming pathway dysfunction[62]. In a separate study attempting to generate NEMO-deficient mice, researchers observed that homozygous deletion of NEMO was embryonically lethal, with embryos beginning to die around E12.5 due to massive liver apoptosis[63]. NEMO-deficient mouse embryonic fibroblasts (MEFs) isolated at this stage were unresponsive to stimulation by TNF-α, LPS, or IL-1β, indicating inactivation of the NF-κB pathway. Female heterozygous NEMO-deficient mice survived beyond embryogenesis and exhibited skin abnormalities resembling those seen in IP patients. IP is caused by different mutations in IKBKG, a mutational analysis of 122 IP patients revealed that the most recurrent mutation in IP is a deletion spanning exons 4 – 10 in the IKBKG gene[64].

Ectodermal dysplasia with anhidrosis and immunodeficiency (EDA-ID)

EDA-ID is a rare X-linked disorder that affects innate and adaptive immunity and the development of ectodermal derived structures, such as eccrine gland, hair follicles, and teeth[65–67]. EDA itself occurs due to mutation in the gene ED1 or DL[68,69]. ED1 is the gene that encodes for ectodysplasin, a membrane-associated protein produced in cell types and tissues of ectodermal origin. DL is the gene that encodes for a putative ectodysplasin receptor. Most patients that suffer from EDA were found to have recurrent infections that led to the diagnosis of also having immunodeficiency, hence EDA-ID[65]. The mutations found in IKBKG, the gene encoding for NEMO, impaired LPS and TNF-α induced NF-κB activation and did not abolish it like IP[65,70].

NEMO and cancer

NEMO has been implicated in several malignancies, including hepatocellular, pancreatic, renal, and small cell lung cancers. Its role in tumor development is complex and context-dependent, having been shown to both promote and suppress tumorigenesis depending on the cell type and whether its function is mediated through NF-κB-dependent or -independent mechanisms[67]. In hepatocellular carcinoma (HCC), NEMO-mediated NF-κB activation in hepatocytes has an essential physiological function to prevent the spontaneous development of steatohepatitis and hepatocellular carcinoma, identifying NEMO as a tumor suppressor in the liver[71]. In contrast, ablation of NEMO in a relevant mouse model of small cell lung cancer (SCLC) strongly delayed tumor onset and growth, resulting in considerably prolonged survival, indicating a tumor-promoting role in this context[72]. In pancreatic cancer, NEMO deletion robustly suppresses the NF-κB pathway, eliminating the oncogene-induced senescence barrier and accelerating pancreatic ductal adenocarcinoma progression[73]. Together, these findings underscore that NEMO's contribution to cancer is highly tissue-specific and cannot be generalized across cancer types, highlighting the importance of understanding its precise molecular mechanisms in each context.

1.5 Clustered regularly interspaced short palindromic repeats (CRISPR) — CRISPR-associated protein 9 (CRISPR-Cas9)

CRISPR-Cas9 system

The CRISPR-Cas system was developed in 2013 to edit genomes by manipulating a bacterial enzyme that was originally found as a defense mechanism against viral infections[74,75]. CRISPR-associated proteins (Cas) are a family of proteins that hold DNA manipulating capabilities, like other proteins such as helicases, nucleases, and DNA-binding proteins[74]. There are two classes of Cas proteins and are further categorized into multiple types and subtypes[74,76,77]. The most commonly used Cas protein is *Streptococcus pyogenes* Cas9 (SpCas9). The utilization of a single guide RNA (sgRNA) and the protospacer adjacent motif (PAM) site is how the CRISPR-Cas system recognizes the desired sequence. Cas9 has a specific PAM sequence, 5'-NGG-3', where "N" can be any of the four nucleotide bases[75]. The Cas9 endonuclease recruits sgRNA and forms a ribonucleoprotein, that can locate, bind, and cleave the specific DNA target[78]. Once the sgRNA is attached to its target sequence, Cas9 creates a double-stranded break in the sequence and then the DNA is repaired through either two endogenous self-repair systems, the non-homologous end joining (NHEJ) pathway or the homology-directed repair (HDR) pathway[77]. CRISPR-Cas9 technology has been modified in various ways to improve the precision and efficiency of genome editing[79]. One such advancement is prime editing, developed by Anzalone, *et al.* in 2019, which fuses a reverse transcriptase to a Cas9 nickase paired with an engineered prime editing guide RNA (pegRNA)[80]. Unlike conventional CRISPR-Cas9, prime editing does not require double-strand breaks or donor DNA templates, making it a versatile tool capable of introducing precise substitutions, insertions, and deletions with reduced risk of unintended indel formation.

Prime editing

In 2019, David Liu's laboratory generated a novel technique of editing genes using a catalytically impaired Cas9 linked to a reverse transcriptase called prime editing (PE)[80]. Cas9(H840A) nickase fused to a Moloney murine leukemia virus (M-MLV) reverse transcriptase (RT) with five single-point mutations is used in place of Cas9 in the PE system[77,79,81]. A larger guide RNA used for PE is dubbed prime editing guide (peg) RNA alongside another smaller guide RNA used to favor the mutation called nicking guide (ng) RNA. The pegRNA is comprised of four regions that work together to bind and incorporate the desired edit. The four regions are: 1) the primer binding site (PBS), which binds to the DNA strand that will contain the edit, 2) the reverse transcriptase template (RTT), which holds the edit, 3) the spacer, which binds to the non-edited strand, and lastly 4) the scaffold, which is needed for Cas9 recruitment[82].

The three components, the Cas9-RT complex, pegRNA, and ngRNA, are transfected together into a cell and edits the DNA without any double-stranded breaks. The Cas9-RT complex recruits the pegRNA, creating a ribonucleoprotein complex, and searches for its intended target sequence. Mutated Cas9 nicks one strand of the DNA, the pegRNA binds to both strands of DNA, and then the reverse transcriptase comes and extends the RTT region of the pegRNA. Cas9-RT: pegRNA complex releases from the DNA and leaves a flap on one strand of the DNA. At the same time, the Cas9-RT: pegRNA complex is mutating the sequence, another Cas9-RT binds to the ngRNA, creating Cas9-RT: ngRNA complex and nicking the opposite strand of the mutation, promoting using the edited DNA strand as a template. Through endogenous DNA repair systems, the mutation is integrated into the DNA or reverted back to its original sequence (Figure 1.4).

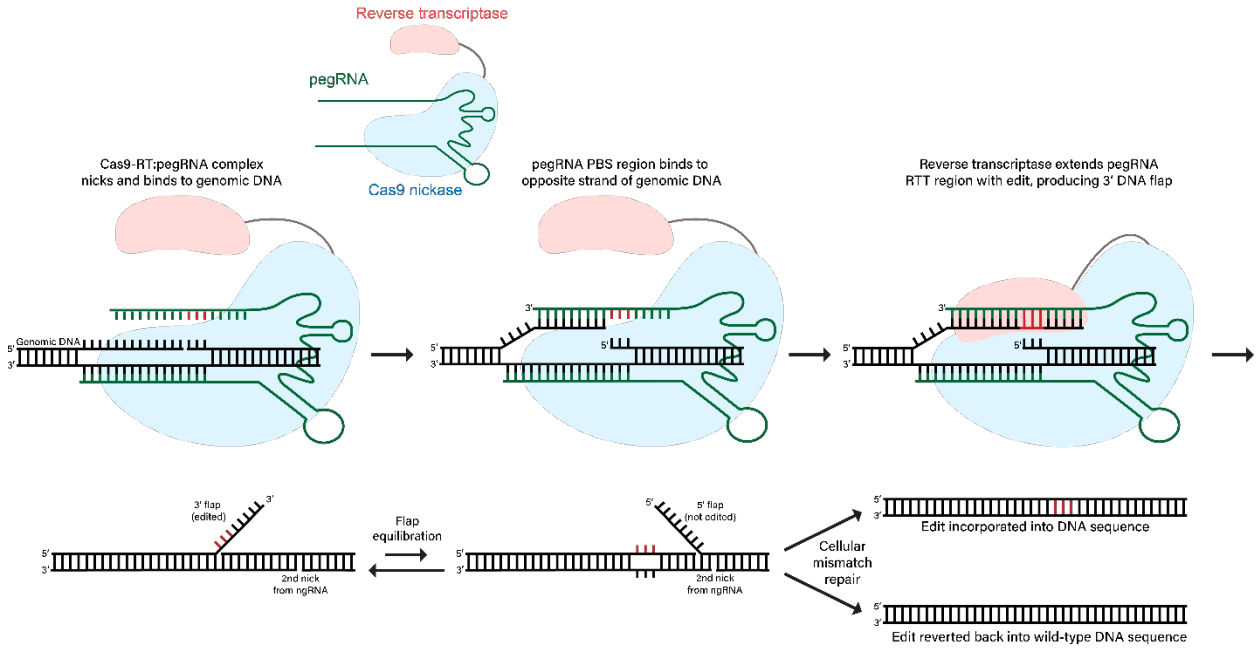

Figure 1.4: Steps of proposed prime editing mechanism for editing genomic DNA.

1.6 Cell lines

Human embryonic kidney (HEK) 293T

HEK293 cell lines is a commonly used immortalized cell line that was created by transfecting a primary human embryonic kidney of female origin with sheared Adenovirus 5 DNA[83,84]. These cells are noted as a hypotriploid karyotype but considered more of an adrenal gland phenotype based on its basal gene expression[85,86]. These cells are widely used in research to study cell signaling, protein interactions, and protein expression. Further mutations on HEK293 cells generated new derivatives, making them more suitable for viral and protein expression, suspension culture, and more. HEK293T cell lines is a popular derivative of the original HEK293 cell lines, where it has been stably transfected with SV40 T protein expression plasmid[87,88]. HEK293T cells are used more commonly than other derivatives because of their easy maintenance, higher transfection rate, and favorable protein and viral expression[89]. In the context of this study, HEK293T cells were selected for their high transfection efficiency, ease of culture, and well-established use as a model cell line in literature.

U-2 OS human osteosarcoma

U-2 OS cell lines are human osteosarcoma derived from moderately differentiated sarcoma of the tibia of a 15 year-old female[90]. The cell lines were characterized to be hypertriploid and exhibit karyotypes with a high incidence of aneuploidy and structural rearrangements and alterations[91,92]. They are usually used in research studies pertaining to bone formation, bone tumor progression and metastasis, and arthritis. U-2 OS cells were selected for their well-characterized and intact NF-κB activation pathway, responsiveness to a broader range of canonical NF-κB inducers compared to HEK293T cells, high transfection efficiency, and established use in both gene editing and NF-κB signaling studies.

1.7 Focus of Study

The canonical signaling pathway of NF-κB has been extensively studied. Practically every signature aspect in the pathway has been identified, from the requirement for phosphorylation at the activation loop of the IKK2 subunit to binding interactions between NF-κB and DNA. Within the pathway, IKK2 activation loop phosphorylation is dependent upon the presence of NEMO, a protein that has shown to exhibit a loose, elongated structure that undergoes numerous post-translational modifications, associates with diverse cellular proteins, and is capable of homotypic self-association at several regions dependent upon interaction with diverse cellular and viral factors. Among the cellular signaling factors that can induce coiled-coil dimer formation between two complex-associated NEMO subunits is its noncovalent association with linear polyubiquitin. However, we do not know how NEMO integrates this or other upstream signaling events in order to exert control over the canonical NF-κB signaling pathway. In previous studies of NEMO, scientists used KO NEMO mouse cell lines and retroviral transfections to overexpress mutated NEMO in mouse and human cell lines. For my study, I will be employing a less physiologically disruptive genetic approach of introducing targeted mutations. CRISPR-Cas9 will be used to introduce mutations into the IKBKG gene of HEK293T cells. I will be generating a set of mutated cell lines that I can use to test the hypothesis that NEMO integrates the various canonical signals in ways that lead to NF-κB-dependent gene expression. If true, then this work should point to novel potential therapeutic strategies for interfering with NF-κB activation in response to specific inducing stimuli without entirely blocking the beneficial effects of this fundamental transcription factor system.

NEMO mutations

The four respective mutations that will be introduced into the X chromosome IKBKG gene are: 1) an 8 base pair (bp) deletion in Exon 1 to completely eliminate NEMO expression, 2) a single bp mutation to change aspartic acid 311 to asparagine and disrupt association with linear

polyubiquitin[29,93], 3) a 18 bp mutation of amino acids 384-389 to all glycine to impair the proposed secondary interaction with IKK2[32], and 4) a single point mutation of glutamic acid 391 into a stop codon to prematurely truncate NEMO prior to its C-terminal zinc finger domain[66].

Chapter 2 Materials and Methods

2.1 Cell lines

HEK293T cell line maintenance

HEK293T cells were purchased from American Type Culture Collection (ATCC) and KO NEMO HEK293T cells were purchased from AbCam. Cells were grown in its complete media which is comprised of DMEM/F-12 (ThermoFisher) supplemented with 10% FBS (Gibco). HEK293T cells were quickly thawed in a 37℃-water bath and placed in a T75 flask (Corning) containing 12 mL of pre-warmed complete media. Cells were passaged every 2 – 3 days when the confluency of cells reached 70% or more. To passage cells, existing media was aspirated, and the cells were washed with 1X Dulbecco's phosphate buffered saline (DPBS) (Gibco). The 1X DPBS was aspirated and 2 mL of 0.25% Trypsin-EDTA (Gibco) or TrypLE™ Express Enzyme (Gibco) was added and let sit for 1-5 minutes until the cells detached from the bottom of the flask. 8 mL of complete media was then added to the cells to neutralize the trypsin and moved to a 15 mL conical tube. 5 mL of 1X DPBS was used to wash the existing used flask and aspirated out. T75 flasks were reused up to three times before passaging into new flasks. 10-14 mL of complete media was added to the flask and then 0.5-1 mL of the cells were added to the flask after to achieve a total of 1 million cells. The cell suspension was gently mixed by pipetting up and down several times with a serological pipette. The cells were then checked under a confocal microscope (Ziess) and placed in a 5% CO_2 incubator.

Transfecting HEK293T

Transfection protocol provided by ThermoFisher for Lipofectamine 2000 was altered for the experiment. 0.25×10^6 cells were seeded into 6-well culture plates (Corning) overnight. pCMV-PE2-P2A-GFP and ngRNA was combined with 450 µL Opti-MEM™ (Gibco) and split into three tubes before adding respective pegRNA. In a separate tube, Lipofectamine 2000 (ThermoFisher) was mixed with Opti-MEM™. Equal volumes of Lipofectamine/Opti-MEM™

were combined with plasmid/Opti-MEM™, mixed well by pipetting up and down, and let incubate at room temperature for a minimum of 10 minutes. The incubated mixture was then added to its respective well in a dropwise manner. Each well should contain 400 ng pCMV-PE2-P2A-GFP, 600 ng pegRNA, 400 ng ngRNA, and 12 µL Lipofectamine 2000. The first transfected cells were imaged three days later on the ImageXpress® Pico Automated Cell Imaging System (Molecular Devices) to confirm GFP expression. For all the following transfected cells, they were immediately used for fluorescence activated cell sorting (FACS) or resuspended in cryopreservation media to be stored in liquid nitrogen for future use.

U-2 OS cell line maintenance

U-2 OS cells (ATCC) were maintained in McCoy's 5A Modified Medium (Gibco) supplemented with 10% FBS (complete media). For thawing, cells were rapidly warmed in a 37°C water bath, transferred to 9 mL of pre-warmed complete media, and centrifuged at 120 × g for 10 minutes. The supernatant was aspirated, and the cell pellet was resuspended and seeded into a T75 flask containing 12 mL of complete media, then incubated at 37°C in a 5% CO_2 atmosphere for 15 minutes before routine culture. Cells were passaged at a 1:3–1:6 split ratio upon reaching 70–80% confluency, approximately every 2–3 days, following the same procedure used for HEK293T cells.

Transfecting U-2 OS

U-2 OS cells were seeded at a density of 0.1×10^5 cells/mL and 2 mL volume in a 6-well plate. When the cells were 70-80% confluent, they were transfected with the same DNA concentration as HEK293T cells, except for the transfection agent. Lipofectamine 3000 (ThermoFisher) and its protocol was used. 2.5 µL of Lipofectamine 3000 was added to 125 µL Opti-MEM and P3000 reagent was added with the DNA and 125 µL Opti-MEM. The transfection reagent, DNA, and P3000 reagent were combined and incubated for 10-15 minutes before adding to the cells. For 6G NEMO, 20-39-13 pegRNA plasmid was used along with -37 ngRNA plasmid.

For D311N, 6-16-14 pegRNA plasmid and -70 ngRNA was used. Cells were incubated for 3-4 days with transfection material and then sorted using flow cytometry or cryopreserved for future sort.

Cell cryopreservation

Unused cells from each passage were centrifuged at 100 × g for 10 minutes. The supernatant was aspirated, and the cell pellet was resuspended in cryopreservation media at a density of at least 1×10^6 cells/mL. HEK293T cells were resuspended in DMEM/F-12 supplemented with 10% FBS and 10% dimethyl sulfoxide (DMSO; Sigma-Aldrich), while U-2 OS cells were resuspended in McCoy's 5A Modified Medium supplemented with 10% FBS and 5% DMSO. Cells were aliquoted into 1 mL volumes in 1.5 mL cryopreservation tubes (Corning) and placed within a Styrofoam insulated container to achieve a controlled cooling rate of approximately 1°C/minute. The insulated container was transferred to a −80°C freezer overnight, after which cryotubes were stored at −80°C for up to one week before being transferred to liquid nitrogen for long-term storage.

2.2 Generating mutant NEMO cell lines

CRISPR prime editing 3 oligos

The sequences to construct the ngRNA and pegRNA plasmids were generated by https://primedesign.pinellolab.partners.org/ and http://pegfinder.sidichenlab.org/[94,95]. The sequence of NEMO with the appropriate mutations to knockout, disrupt linear ubiquitin binding, disrupt secondary IKK2 binding, and remove zinc finger activity were inputted into PrimeDesign (Table 2.1). The website generated different lengths of RTT, PBS and ngRNA. The selected constructs were listed in the table below based on the recommended length of RTT and PBS according to the paper that first reported Prime Editing[80]. The individual oligos were ordered from Integrated DNA Technologies (IDT) and annealed together by combining the top and bottom oligonucleotides (100 μM) with annealing buffer (10 mM Tris-HCl pH 8.5, 50 mM NaCl). The mixture was heated to 95℃ for 3 minutes and then cooled at 0.1℃ per second to 22℃ using a thermocycler (Bio-Rad iCycler). The annealed oligo was then diluted with MilliQ (MQ) water to a concentration of 1 μM.

Plasmids

pCMV-PE2-P2A-GFP (Addgene #132776) and pU6-pegRNA-GG-acceptor (Addgene #132777) was a gift from David Liu. BPK1520 (Addgene #65777) a gift from Keith Joung. All plasmids were streaked onto LB Ampicillin (Amp) plates[80,96]. pCMV-PE2-P2A-GFP and BPK1520 plates were incubated at 37℃ while pU6-pegRNA-GG-acceptor plates was incubated at 30℃. Plasmids were isolated and purified through in-house miniprep protocol (Appendix).

Constructing ngRNA

BPK1520 plasmid was digested with BsmBI (New England BioLabs) at 37℃ and was run on a 0.8% agarose gel in 1X TAE buffer. A band around 2,300 bp was excised out and gel extracted with QIAquick Gel Extraction Kit (Qiagen). The extracted plasmid was incubated with the

annealed ngRNA oligo and T4 Ligase (New England BioLabs) at 24℃ for 10 minutes. The ligation mixture was left on ice for 5 minutes before transformation into DH5α cells and subsequently cultured to purify the ligated plasmid using Plasmid *Plus* Maxi Kit (Qiagen). Sanger sequencing with primers pegRNA 5' sequence primer (5'-CAGGGTTATTGTCTCATGAGCGG-3') and the oS280 primer (5'-GACTATCATATGCTTACCGT-3') was used to verify correct insertion.

Constructing pegRNA

pU6-pegRNA-GG-acceptor plasmid was digested with BsaI (New England BioLabs) at 37℃ and was run on a 1% agarose gel in 1X TAE buffer. A band around 2,100 bp was excised out and gel extracted with GeneJET Gel Extraction Kit (ThermoFisher) to isolate digested pegRNA plasmid. A modified golden gate assembly procedure from Anzalone et. Al (2019) was used. The digested pU6-pegRNA-GG-acceptor plasmid, annealed spacer oligonucleotide, annealed scaffold oligonucleotide, annealed extension oligonucleotide, BsaI (New England BioLabs), and T4 Ligase (New England BioLabs) were combined and run on a pegRNA PCR cycle on an iCycler (Bio-Rad) (Appendix). The same annealed scaffold oligonucleotide was used for all pegRNA plasmid construction. All plasmids were purified with Plasmid *Plus* Maxi Kit (Qiagen) and verified through Sanger sequencing using pegRNA 5' sequence primer (5'-CAGGGTTATTGTCTCATGAGCGG-3') and the oS280 primer (5'-GACTATCATATGCTTACCGT-3').

Table 2.1: Scaffold oligonucleotide sequences

Scaffold Oligonucleotide	Sequence (5' – 3')
Top	AGAGCTAGAAATAGCAAGTTAAAATAAGGCTAGTCCGTTATCAACT TGAAAAAGTGGCACCGAGTCG
Bottom	GCACCGACTCGGTGCCACTTTTTCAAGTTGATAACGGACTAGCCTT ATTTTAACTTGCTATTTCTAG

Table 2.2: Sequences of pegRNAs and sgRNAs used to incorporate mutation into HEK293T cells.

pegRNA	spacer sequence	3' extension	PBS length (nt)	RT template length (nt)
8-bp KO 17-25-10	AGCCGGAAGC GTGGTAGGGA	GTCCCAGTTTCGCGGTCGCCCTTCCCTA CCACGCT	10	25
8-bp KO 17-25-13	AGCCGGAAGC GTGGTAGGGA	GTCCCAGTTTCGCGGTCGCCCTTCCCTA CCACGCTTCC	13	25
8-bp KO 17-25-16	AGCCGGAAGC GTGGTAGGGA	GTCCCAGTTTCGCGGTCGCCCTTCCCTA CCACGCTTCCGGC	16	25
QRRSPP2 0-39-10	AGAAGTCAGG TGGCTCCTCG	TCCCCTGGCCCTGCCCAGCggcggcggc ggcggcggcGAGGAGCCACCT	10	39
QRRSPP2 0-39-13	AGAAGTCAGG TGGCTCCTCG	TCCCCTGGCCCTGCCCAGCggcggcggc ggcggcggcGAGGAGCCACCTGAC	13	39
QRRSPP2 0-39-16	AGAAGTCAGG TGGCTCCTCG	TCCCCTGGCCCTGCCCAGCggcggcggc ggcggcggcGAGGAGCCACCTGACTTC	16	39
D311N6-16-14	CCAGGCGGAT ATCTACAAGG	GCCTGGAAGTtCGCCTTGTAGATATCCG CC	14	16
D311N6-21-16	CCAGGCGGAT ATCTACAAGG	TCTCAGCCTGGAAGTtCGCCTTGTAGAT ATCCGCCTG	16	21
D311N6-28-16	CCAGGCGGAT ATCTACAAGG	GCCTGCCTCTCAGCCTGGAAGTtCGCCT TGTAGATATCCGCCTG	16	28
E391X11	GCAGAAGTCA GGTGGCTCCT	CCCCCCCGAGtAGCCACCTGACTTCT	15	11
E391X13	GCAGAAGTCA GGTGGCTCCT	AGCCCCCCCGAGtAGCCACCTGACTTCT	15	13
E391X15	GCAGAAGTCA GGTGGCTCCT	GGAGCCCCCCCGAGtAGCCACCTGACTT CT	15	15

All sequences are shown in 5' to 3' orientation. pegRNAs are a concatenation of the spacer sequence, the sgRNA scaffold, and the 3' extension (contains PBS and RT template).

Table 2.3: Sequences of ngRNA used for each respective mutation, shown in 5' to 3' orientation.

ngRNA	Sequence	Nick-to-peg distance (nt)
KO NEMO	GGTGTCATAGCTGTGGGATC	-37
QRRSPP NEMO	GAGCCTACCTCTCCTCTCCCC	-37
D311N NEMO	GCACCCACCAGGCACTGCGCC	-70
E391X NEMO	GCATGAGTGGCCTGTGAGACC	133

Flow cytometry

The transfected cells were sorted after transfection or after one passage if the transfected cells were cryopreserved to be sorted at a later date. Cells were aspirated and washed with 1X DPBS. The cells were detached using TrypLE™ Express Enzyme (Gibco) followed by enzyme deactivation with respective cell line complete media. The cells were transferred into 15 mL conical tubes (Falcon). 10 µL of the resuspended cells were diluted with 10 µL Trypan Blue (ThermoFisher) and counted using the Countess™ cell counting chamber slides (ThermoFisher) and Countess™ Automated Cell Counter (ThermoFisher). The remaining cells in the 15 mL conical tube were spun down at 100 x g for 5 minutes at room temperature. The cells were washed twice with ice-cold FACS buffer (3% FBS 1X DPBS) and centrifuged at 100 × g for 5 minutes at 4°C. The pellet cells were resuspended in 200 – 500 µL of FACS buffer to achieve a cell density of 10×10^6 cells per mL. The resuspended cells were kept on ice until used for flow cytometry. The cells were isolated into 1 cell/well into a 96-well plate (Corning) containing 100 µL of boosted media (20% FBS, 1% Pen/Strep, DMEM/F-12 media or McCoy's 5A modified media) using a FACS Melody™ Cell Sorter (BD Biosciences). After sorting, the 96-well plates were kept on ice before moving into a 37°C incubator with 5% CO_2.

Processing sorted single cells

The single cell 96-well plates were left undisturbed aside from monitoring in a 37°C incubator with 5% CO_2 for at least a week. After three days and every other day afterwards, the cells were monitored under a confocal light microscope. When the media turned a more yellow color or after a week in the incubator, 100 µL boosted media was added to existing media and then every other day afterwards the media was replaced with the cell line's complete media. When the cells were 70-90% confluent or grew in a sizable upward manner, they were transferred into 24-well plates by sloughing off cells with complete media or detached with TrypLE™. Cells were transferred from 24-well plates into 6-well plates (Corning).

Once the cells were 70 – 90% confluent in the 6-well plates, the existing media was aspirated, and the cells were sloughed off with 1 mL of media. 0.5 mL of cells were moved to 1.5 mL microcentrifuge tubes and pelleted at 1000 × g for 5 minutes. The media was aspirated, and the cell pellet was stored in the -80°C freezer. The pellet can be used for direct PCR lysis immediately or kept at -20°C until future use. The other 0.5 mL cell suspension was cryopreserved. The cryotubes are then placed in a Styrofoam container overnight in a -80°C freezer and later moved to a liquid nitrogen dewar.

Extracting genomic DNA and PCR amplification

Genomic DNA (gDNA) extraction and PCR sample preparation were performed using the Platinum™ Direct PCR Universal Master Mix (Thermo Fisher) following the manufacturer's protocol. Briefly, cell pellets were resuspended in 20 µL of the provided lysis buffer supplemented with 0.6 µL proteinase K and incubated at room temperature for 1 minute to less than 4 hours. Samples were then heat-inactivated at 98°C for 1 minute, followed by centrifugation at maximum speed for 1–5 minutes at room temperature, and stored at –20°C prior to PCR. Freeze-thaw

cycling facilitated separation of cell debris from the supernatant, and 1 μL of the clarified supernatant was used as template for PCR amplification.

The exon 1 and exon 8–10 regions of the IKBKG gene on chromosome X (GRCh38.p14) were amplified using primers designed with NIH Primer-BLAST and synthesized by Integrated DNA Technologies (IDT). The exon 1 region was amplified using the forward primer 5'-GCCGGCGTGCTTATCATTAC-3' and reverse primer 5'-GTTGTCTTGCAAAACGAGCA-3'. The exon 8–10 region was amplified using the forward primer 5'-TCTCCTCTGTCGTTTTGGGC-3' and reverse primer 5'-GGAAGGCCCCAGTCTTGACT-3'.

Sequencing mutated cell line

Amplified PCR products were resolved on a 1% agarose gel alongside a 1 kb Plus DNA ladder (GeneRuler™) and a no-template negative control. For the NEMO knockout construct, a band at 680 bp was excised; for all remaining NEMO mutant cell lines, a band at 2,100 bp was excised. Gel extraction was performed using the GeneJET Gel Extraction Kit (Thermo Fisher), and purified PCR products were eluted in 30 μL of the supplied elution buffer. DNA concentration was quantified using the NanoPhotometer N50-Go (Implen).

Purified PCR products were mixed with the appropriate forward primer and submitted to either Retrogen, Inc. or GeneWiz for Sanger sequencing. The exon 1 forward primer (5'-TGGCGGACTCAGACTTCTCT-3') was used to verify the NEMO knockout; the exon 8 forward primer (5'-CGCCGACGTATCTGTTTCCT-3') was used to verify the linear polyubiquitin-binding mutation (D311N); and the exon 10 forward primer (5'-ACATGAGTGGCCTGTGAGAC-3') was used to verify both the QRRSPP and zinc finger (E391X) mutations. Resulting chromatograms were analyzed using Chromas and Serial Cloner to confirm successful introduction of each mutation. Cell lines confirmed to carry the correct mutation were subsequently thawed, expanded, and aliquoted into 2 mL cryotubes in cryopreservation media for long-term storage.

Verifying mutated cell line with western blot

The cells with homozygous mutations were stimulated with 10 ng/mL TNF-α and its cell extracts were used for western blot following nuclear extract kit (Active Motif®) instructions. For TNF-α induction, the cells were seeded the day before onto 100 mm cell culture dishes (Corning) to a total volume of 10 mL and 2 – 2.5 × 10^6 cells. The following day or when the cells are at 70 – 90% confluency, the media was replaced with complete media supplemented with 10 ng/mL TNF-α for time range of 0, 10, and 30 minutes. After each timepoint, the media is aspirated, and the cells are washed with ~3-4 mL of ice-cold 1X PBS supplemented with phosphatase inhibitor. The cells were sloughed off with ~1-1.5 mL ice-cold 1X PBS and phosphatase inhibitor and transferred into 1.5 mL Eppendorf tubes. The tubes were centrifuged for 1-3 minutes at 500 × g. The supernatant is aspirated, and cell pellets are either frozen at -80°C or used immediately. Nuclear and cytoplasmic extracts were separated using nuclear extract kit (Active Motif®) and their protein concentrations were measured using Bradford assay or BCA assay.

The extracts were normalized and loaded onto a 4 – 20% Stain Free SDS-PAGE gel (Bio-Rad). The gels were run at 120V for 50 – 60 minutes, imaged on Chemi-Doc (Bio-Rad) and then transferred onto nitrocellulose membrane on Turbo Transfer (Bio-Rad). The membrane was blocked for an hour at room temperature with blocking buffer (5% BSA in 1X TBST) then probed with primary antibody overnight at 4°C. The membrane is then washed three times at room temperature with 1X TBST for 5 minutes, subsequently incubated with blocking buffer for 30 minutes. 1 μL of secondary antibody is added to the membrane with the blocking buffer and incubated on an orbital shaker at room temperature for an hour. The washing step is repeated, and ECL substrate (Bio-Rad) is added onto the membrane and imaged on the Chemi-Doc (Bio-Rad).

2.3 Cell stimulation

Reconstitution of stimuli

Six NF-κB inducers were used in this study, with reconstitution and storage conditions optimized for each reagent. Tumor necrosis factor-α (TNF-α; Sigma-Aldrich) was reconstituted in nuclease-free water to a stock concentration of 100 µg/mL, aliquoted into 10 µL working volumes, and stored at −20°C; cells were treated at a final concentration of 10 ng/mL. Lipopolysaccharide (LPS; E. coli O111:B4; Sigma-Aldrich) was reconstituted in DPBS to 1 mg/mL, further diluted to a working stock of 0.1 mg/mL, aliquoted, and stored at −20°C; the final treatment concentration was 1 µg/mL. Interleukin-1β (IL-1β; Sigma-Aldrich) was reconstituted in filter-sterilized 0.5% BSA (Thermo Fisher) in DPBS to a stock concentration of 100 ng/µL, aliquoted, and stored at −20°C; cells were treated at 10 ng/mL. Flagellin (Salmonella typhimurium; Sigma-Aldrich) was reconstituted in nuclease-free water to 10 ng/µL, aliquoted into working volumes, and stored at −20°C; the final treatment concentration was 10 ng/mL. Phorbol myristate acetate (PMA; InvivoGen) was initially dissolved in DMSO by vortexing, further diluted in nuclease-free water to a stock concentration of 5 mg/mL, aliquoted, and stored at −20°C; cells were treated at 1 µg/mL. Sphingosine-1-phosphate (S1P; Enzo) was reconstituted in 2 mL methanol and divided into 100 µL aliquots stored at −20°C. Prior to use, methanol was evaporated from a single aliquot under dry nitrogen, and the residue was resuspended in 4 mg/mL BSA (Thermo Fisher) in nuclease-free water (Gibco) to achieve a working concentration of 125 µM; cells were treated at a final concentration of 1 µM, and resuspended S1P was stored at 4°C and used within one week.

Stimulating cells

Cells were seeded the day before onto 100 mm cell culture dishes (Corning) to a total volume of 10 mL and 1 – 2 × 10^6 cells or onto 6-well cell culture plates (Corning) to a total volume of 2 mL and 0.2 × 10^6 cells. The following day or when the cells are at 70 – 90% confluency, the

cell's media is replaced with complete media supplemented with varying concentrations based respective to the stimulus. Cells were stimulated at various time points. After each time point, the media is aspirated, and the cells are washed with ~0.5-4 mL of ice-cold 1X PBS supplemented with phosphatase inhibitor per Active Motif nuclear extraction kit instructions. The cells were sloughed off with ~1-1.5 mL ice-cold 1X PBS and phosphatase inhibitor and then transferred into 1.5 mL Eppendorf tubes and kept on ice. For U-2 OS cells, the cells were detached by TrypLE, neutralized and pelleted before proceeding to the washing step with ice-cold 1X PBS with phosphatase inhibitor. The tubes were centrifuged for 5 minutes at 500 × g at 4℃. The supernatant is aspirated, and cell pellets are either frozen at -80℃ for future use or used immediately.

2.4 Western Blot

Sample preparation

Nuclear and cytoplasmic fractions and whole-cell lysates were prepared using the nuclear extract kit (Active Motif®). Protein concentrations were measured using Bradford Reagent Dye (Bio-Rad). The sample dye extracts were normalized to 5-10 µg and mixed with 4X Laemmli dye (Bio-Rad) or in-house 4X Laemmli dye. Sample dyes were immediately used to load gels or kept at -20°C for future use.

Antibodies

The following primary antibodies were used: anti-GAPDH mouse (1:1,000; Santa Cruz Biotechnology, cat. #sc-47724), anti-GAPDH rabbit (1:1,000; Invitrogen/Thermo Fisher, cat. #MA5-33140), anti-Lamin A/C mouse (1:1,000; Santa Cruz Biotechnology, cat. #sc-7293), anti-β-actin rabbit (1:1,000; Cell Signaling Technology, cat. #4970), anti-IKKβ rabbit (1:2,000; Cell Signaling Technology, cat. #8943), anti-IKKγ mouse (1:1,000; Santa Cruz Biotechnology, cat. #sc-166398), anti-IKKγ rabbit (1:1,000; Cell Signaling Technology, cat. #79154), anti-IκBα mouse (1:10,000; Cell Signaling Technology, cat. #4814), anti-NF-κB p65 rabbit (1:2,500; Cell Signaling Technology, cat. #8242), anti-phospho-IκBα (Ser32) rabbit (1:1,000; Cell Signaling Technology, cat. #2859), anti-phospho-NF-κB p65 (Ser536) rabbit (1:1,000; Cell Signaling Technology, cat. #3033), and anti-phospho-IKKα/β (Ser176/180) rabbit (1:1,000; Cell Signaling Technology, cat. #2697). HRP-conjugated secondary antibodies for western blotting were used at 1:10,000 and included anti-mouse IgG (Cell Signaling Technology, cat. #7076) and anti-rabbit IgG (Cell Signaling Technology, cat. #7074). For immunofluorescence, goat anti-rabbit IgG (H+L) Alexa Fluor Plus 488 (1:10,000; Invitrogen/Thermo Fisher, cat. #A32731) and goat anti-mouse IgG (H+L) Alexa Fluor Plus 647 (1:10,000; Invitrogen/Thermo Fisher, cat. #A32728) secondary antibodies were used.

SDS-PAGE gel and transfer

5-10 µg protein dye samples were loaded onto a 4 – 20% Mini-PROTEAN™ TGX Stain-Free™ Protein Gels (Bio-Rad) with a protein ladder, Precision Plus Protein Standards All Blue or Precision Plus Protein Dual Color standards. The gels were run at 120V for 60 minutes on a Criterion Cell (Bio-Rad) in a mini-PROTEAN gel cassette (Bio-Rad). Two blotting pads and a nitrocellulose membrane were soaked in 1X Turbo Transfer buffer (Bio-Rad). The western blot "sandwich" was assembled by placing one blotting pad on the bottom followed by nitrocellulose membrane, gel, and lastly another blotting pad on top. The "sandwich" was gently rolled out with a roller to remove excess 1x transfer buffer and remove bubbles. The "sandwich" was then placed on the Turbo Transfer cassette tray, gel side up, and ran on Turbo Transfer machine (Bio-Rad). The setting of the transfer is dependent on the size and quantity of the "sandwich".

Immunoblot

The transferred membrane was briefly rinsed with 1X TBST to remove residual transfer buffer, then blocked for 1 hour at room temperature in blocking buffer (5% BSA in 1X TBST) on an orbital shaker. Primary antibodies were diluted at their respective concentrations in blocking buffer and incubated with the membrane overnight at 4°C or for 2 hours at room temperature on an orbital shaker. Following primary antibody incubation, the membrane was washed three times with 1X TBST for 5 minutes per wash, then blocked again with blocking buffer for 30 minutes. HRP-conjugated or fluorescent secondary antibodies were added to the membrane in blocking buffer at a minimum dilution of 1:10,000 and incubated for 1 hour at room temperature on an orbital shaker, followed by three additional 5-minute washes with 1X TBST. Primary antibodies were either discarded or stored with 0.02% sodium azide at 4°C for future use.

For HRP-based detection, excess liquid was removed by gently blotting the edge of the membrane against a KimWipe™ (Kimtech Science™). Clarity Max ECL Substrate (Bio-Rad) was prepared in a 1:1 ratio per the manufacturer's instructions and applied to cover the entire

membrane surface. A total volume of 1 mL was used for a standard mini SDS-PAGE gel-sized membrane. The membrane was briefly dried before being placed onto the ChemiDoc MP Imaging System (Bio-Rad) tray and imaged using the chemiluminescence setting. For fluorescent detection, the membrane was similarly dried with a KimWipe™ following the final wash and imaged using the fluorescence channel corresponding to the emission spectra of the secondary antibody dye on the ChemiDoc MP Imaging System (Bio-Rad). Western blot images were analyzed and processed using ImageJ.

2.5 Reverse Transcriptase-Qualitative Polymerase Chain Reaction (RT-qPCR)

RNA isolation

Cells grown in 6-well tissue culture plates (Corning) were harvested using 1 mL of TRIzol™ reagent (Thermo Fisher) per well. Harvested samples were either stored at −20°C or immediately processed for RNA extraction following the manufacturer's protocol. The RNA pellet was air-dried and resuspended in 50 µL of nuclease-free water (Invitrogen), and RNA concentration was quantified using the NanoPhotometer N50-Go (Implen). Purified RNA was either used immediately for cDNA synthesis or stored at −80°C until further use.

cDNA generation

High-Capacity RNA-to-cDNA™ Kit was used to convert total RNA to cDNA, following the manufacturers protocol. The Bio-Rad iCycler was the thermocycler used. cDNA concentration was measured on the NanoPhotometer® N50-Go (Implen), diluted into 5 ng/µL stocks before storing at -20°C.

Qualitative PCR

All qPCR experiments were performed on the CFX Connect Real-Time PCR Detection System (Bio-Rad) using PowerTrack SYBR Green Master Mix (Thermo Fisher) in a 10 µL reaction volume following the manufacturer's protocol. Each reaction contained 5 ng of cDNA and 0.4 µM of each forward and reverse primer. Reactions were assembled by first combining cDNA with yellow sample buffer in a 0.2 mL 8-tube PCR strip (Bio-Rad). A master mix consisting of PowerTrack SYBR Green Master Mix, primers, and nuclease-free water was prepared separately, then added to the cDNA and mixed by pipetting. Tubes were sealed with 0.2 mL flat PCR tube caps (Bio-Rad) and briefly centrifuged prior to loading onto the instrument. A no-template control (NTC) was included in every run to detect potential contamination. All experiments were performed in biological and technical triplicates.

Table 2.4: qPCR primer sequences.

Primer	Sequence (5' – 3')
GAPDH Forward	GGAAGGTGAAGGTCGGAGTC
GAPDH Reverse	GAGTTAAAAGCAGCCCTGGTG
IL6 Forward	GACAAACAAATTCGGTACATCC
IL6 Reverse	GCAAGTCTCCTCATTGAATCC
NKFBIA Forward	GCTGAAGAAGGAGCGGCTACT
NFKBIA Reverse	TCGTACTCCTCGTCTTTCATGGA
NFKBIZ Forward	ACACCCACAAACCAACTCTGG
NFKBIZ Reverse	TGCTGAACACTGGAGGAAGTC
TNFAIP3 Forward	TCCTCAGGCTTTGTATTTGAGC
TNFAIP3 Reverse	TGTGTATCGGTGCATGGTTTTA
SOD1 Forward	AAAGATGGTGTGGCCGATGT
SOD1 Reverse	CAAGCCAAACGACTTCCAGC
CFLAR Forward	ATGAAGATACGGGCCACACG
CFLAR Reverse	TTCGTGCCCTCATCCAACAA

Relative Gene Expression Calculation

Relative gene expression was calculated using the 2^−ΔΔCt method, where ΔΔCt represents the difference between the ΔCt of the experimental sample and the ΔCt of the baseline sample (0-minute time point). ΔCt represents the difference between the Ct value of the gene of interest and the Ct value of the reference housekeeping gene. Fold change in gene expression was calculated as 2^−ΔΔCt, where a value of 1 represents no change relative to the baseline.

Statistics

Statistical significance between time points and cell lines for each gene was determined by two-way ANOVA using GraphPad Prism software, with a minimum significance threshold of $P < 0.05$.

2.6 NF-κB Luciferase Reporter Assay

pNL3.2.NF-κB-RE vector preparation

pNL3.2.NF-κB-RE[NlucP/NF-κB-RE/Hygro] vector was purchased from Promega and transformed into DH5α *E. coli* cells and plated onto LB Amp plates. The transformed cells were grown overnight in a 37°C incubator then a single colony was picked to make a 60 mL bacterial culture for plasmid preparation using the Plasmid *Plus* Maxi Kit (Qiagen).

HEK293T hygromycin kill curve

To determine the optimal hygromycin selection concentration, all cell lines were seeded onto 6-well tissue culture plates (Corning) at a density of 4.0×10^4 cells/mL in a total volume of 2 mL per well and allowed to recover overnight in a 5% CO_2, 37°C incubator. Hygromycin was prepared in complete media at the following concentrations: 50, 100, 250, 500, and 1,000 μg/mL. Following overnight recovery, the existing media was replaced with hygromycin-supplemented complete media at the respective concentrations; a negative control received complete media without hygromycin. Cell viability was monitored daily for 12 days, and media was replaced every two days with fresh hygromycin-supplemented complete media at the corresponding concentration. The lowest concentration that resulted in complete cell death within 7–10 days was determined to be 250 μg/mL, which was subsequently used as the selection concentration for cells transfected with the hygromycin-resistance-encoding pNL3.2.NF-κB-RE vector.

pNL3.2.NF-κB-RE transfection

To optimize Lipofectamine 2000 transfection conditions, cells were seeded at 0.5×10^5 cells/mL in a total volume of 1 mL per well in a 12-well tissue culture plate (Corning), with six wells allocated per cell line. Cells were allowed to recover overnight in a 5% CO_2, 37°C incubator prior to transfection. The Lipofectamine 2000 (Thermo Fisher) protocol was modified as follows: the first well served as an untransfected negative control, while the remaining five wells were transfected with 2, 4, 6, 8, and 10 μL of Lipofectamine 2000, respectively. All transfected wells

received 300 ng of the pNL3.2.NF-κB-RE vector. Following transfection, cells were allowed to recover for 3 days in the 5% CO_2, 37°C incubator.

After the recovery period, the media was aspirated and replaced with complete media supplemented with 250 μg/mL hygromycin for selection of stably transfected cells. Hygromycin-supplemented media was refreshed every 2–3 days, and cells were monitored until stable transfectants were established. Successfully transfected cells were subsequently expanded and either cryopreserved in cryopreservation media or used immediately for NF-κB luciferase assays.

Promega Nano-Glo luciferase assay

NF-κB transcriptional activity was measured using a modified Nano-Glo® Luciferase Assay System (Promega) in cells stably transfected with the pNL3.2.NF-κB-RE[NlucP/NF-κB-RE/Hygro] vector. Cells were seeded at 20,000 cells per well in a total volume of 100 μL in a 96-well plate and allowed to recover overnight in a 37°C, 5% CO_2 incubator. All assays were performed in biological and technical triplicates.

Induction media was prepared by supplementing complete media with TNF-α to a final concentration of 20 ng/mL. Complete media without TNF-α served as the negative control. Following overnight recovery, the existing media was aspirated and replaced with either induction or control media. Cells were incubated with induction media for time points ranging from 10 minutes to 5 hours to assess NF-κB pathway activation kinetics. At 5–10 minutes before each designated time point, the plate was removed from the incubator to acclimate to room temperature. Subsequently, 100 μL of Nano-Glo® luciferase reagent was added to each well and mixed thoroughly by pipetting. The plate was incubated at room temperature for 3 minutes before luminescence was measured at 460 nm on the CLARIOstar plate reader (BMG Labtech). Fold induction was calculated by dividing the average relative light units (RLU) of induced cells by the average RLU of the lowest recorded time point.

Statistics

Statistical significance between control and induced cells was determined by two-way ANOVA using GraphPad Prism software, with a minimum significance threshold of $P < 0.05$.

2.7 NF-κB inhibitor assay

Inhibitors

MLN120B, BMS-345541, and Hoipin-8 were purchased from MedChemExpress and reconstituted in DMSO (Sigma-Aldrich) to a stock concentration of 10 mM. Stocks were aliquoted into working volumes and stored at −80°C until use.

Inhibitor assay

Cells were seeded at 2.0×10^5 cells per well in a 6-well tissue culture plate (Corning) and allowed to adhere overnight in a 5% CO_2, 37°C incubator. Prior to treatment, each inhibitor was diluted to a final concentration of 10 μM in serum-free media and applied to cells by replacing the existing media. Cells were incubated with the inhibitor-containing media for 24 hours or 1 hour at 5% CO_2, 37°C, after which the media was replaced with complete media containing 10 ng/mL TNF-α for 30 minutes to stimulate NF-κB activation for western blot or 5 hours for luciferase assay.

Statistics

Statistical significance between control and inhibitor-treated cells was determined by two-way ANOVA using GraphPad Prism software, with a minimum significance threshold of $P < 0.05$.

Acknowledgements

Chapter 2, in part is currently being prepared for submission for publication of the material. Luong, Sally; Huxford, Tom. The dissertation author was the primary researcher and author of this material.

Chapter 3 Preparation of mutant NEMO HEK293T cell lines by CRISPR-Cas9 prime editing

Introduction

Human NEMO (NF-κB Essential Modulator), encoded by the IKBKG gene, is largely disordered scaffolding protein, with several regions defined by their binding properties and only partial structural data available to date[97]. NEMO plays an indispensable role in canonical NF-κB signaling by serving as the regulatory subunit of the IκB kinase (IKK) complex, bridging upstream signaling events to the activation of IKK2 and subsequent NF-κB nuclear translocation[32]. Understanding the precise molecular mechanisms by which NEMO facilitates IKK complex activation remains a key challenge in the field, particularly given its structural flexibility and its multiple distinct protein-protein interaction interfaces.

Several binding mechanisms within NEMO are critical to its function in NF-κB activation, including its association with linear polyubiquitin chains via the coiled-coil 2 (CC2) domain, its secondary interaction with IKK2, and the regulatory role of its C-terminal zinc finger domain[29,32,98]. Disrupting these interactions individually within a cellular context would allow for the dissection of their relative contributions to canonical NF-κB signaling and provide insight into how NEMO coordinates IKK complex assembly and activation.

To investigate these mechanisms, CRISPR-Cas9 prime editing was employed to introduce precise endogenous mutations into the IKBKG gene in HEK293T cells. Unlike traditional CRISPR-Cas9, which relies on double-strand breaks and error-prone non-homologous end joining (NHEJ), prime editing enables the direct installation of specific point mutations and small insertions or deletions with minimal off-target effects and without requiring a donor DNA template[80]. HEK293T cells were selected as the model system for their robust response to TNF-α-induced canonical NF-κB activation, high transfection efficiency, and ease of maintenance in culture. Four mutations were introduced to disrupt distinct aspects of NEMO function: an 8 bp deletion in exon 1 to eliminate NEMO expression, a D311N substitution to disrupt linear

polyubiquitin binding, a 6G substitution at positions 384–389 to impair secondary IKK2 binding, and an E391X truncation to disrupt the zinc finger domain. The generation, validation, and functional characterization of these mutant cell lines using canonical TNF-α stimulation are described in this chapter.

Results

3.1 Sequences of prime editing CRISPR-Cas9 plasmids

Sequences of all pegRNA and ngRNA plasmids were verified by Sanger sequencing through Retrogen using the primers described previously, and the confirmed sequences were assembled into the pU6-pegRNA-GG-acceptor and BPK1520 plasmids, respectively, using Serial Cloner (Figures 3.1 – 3.6). Multiple independent plasmid constructs were generated for each of the four NEMO mutations and used to transfect HEK293T cells. Following transfection and selection, only three of the four intended NEMO mutant cell lines (6G, D311N, and E391X) were successfully verified. Despite repeated attempts with multiple independent constructs, the NEMO knockout cell line could not be generated in HEK293T cells and were excluded from further analysis. A list of all oligos used for attempted constructs are provided in the Appendix.

pU6-pegRNA-GG-QRSSPP-20-39-13:

gacgtcgctagctgtacaaaaaagcaggctttaaaggaaccaattcagtcgactggatccggtaccAAGG
TCGGGCAGGAAGAGGGCCTATTTCCCATGATTCCTTCATATTTGCATATACGATACAAGGCTGTTAGAGA
GATAATTAGAATTAATTTGACTGTAAACACAAAGATATTAGTACAAAATACGTGACGTAGAAAGTAATAA
TTTCTTGGGTAGTTTGCAGTTTTAAAATTATGTTTTAAAATGGACTATCATATGCTTACCGTAACTTGAA
AGTATTTCGATTTCTTGGCTTTATATATCTTGTGGAAAGGACGAAACACCG**agaagtcaggtggctcctc**
ggtttt**agagctagaaatagcaagttaaaataaggctagtccgttatcaacttgaaaaagtggcaccgag**
tcggtgc**TCCCCTGGCCCTGCCCAGCGGCGGCGGCGGCGGCGAGGAGCCACCTGAC**ttttttaagc
ttgggccgctcgaggtacctctctacatatgacatgtgagcaaaaggccagcaaaaggcCAGGAACCGTA
AAAAGGCcgcgttgctggcgtttttccataggctccgccccccctgacgagcatcacaaaaatcgacgctc
aagtcagaggtggcgaaacccgacaggactataaagataccaggcgtttccccctggaagctccctcgtg
cgctctcctgttccgaccctgccgcttaccggatacctgtccgcctttctcccttcgggaagcgtggcgc
tttctcatagctcacgctgtaggtatctcagttcggtgtaggtcgttcgctccaagctgggctgtgtgca
cgaaccccccgttcagcccgaccgctgcgccttatccggtaactatcgtcttgagtccaacccggtaaga
cacgacttatcgccactggcagcagccactggtaacaggattagcagagcgaggtatgtaggcggtgcta
cagagttcttgaagtggtggcctaactacggctacactagaagaacagtatttggtatctgcgctctgct
gaagccagttaccttcggaaaaagagttggtagctcttgatccggcaaacaaaccaccgctggtagcggt
ggtttttttgtttgcaagcagcagattacgcgcagaaaaaaaggatctcaagaagatcctttgatctttt
ctacggggtctgacgctcagtggaacgaaaactcacgttaagggattttggtcatgagattatcaaaaag
gatcttcacctagatccttttaaattaaaaatgaagttttaaatcaatctaaagtatatatgagtaaact
tggtctgacagttaccaatgcttaatcagtgaggcacctatctcagcgatctgtctatttcgttcatcca
tagttgcctgactccccgtcgtgtagataactacgatacgggagggcttaccatctggccccagtgctgc
aatgataccgcgagatccacgctcaccggctccagatttatcagcaataaaccagccagccggaagggcc
gagcgcagaagtggtcctgcaactttatccgcctccatccagtctattaattgttgccgggaagctagag
taagtagttcgccagttaatagtttgcgcaacgttgttgccattgctacaggcatcgtggtgtcacgctc
gtcgtttggtatggcttcattcagctccggttcccaacgatcaaggcgagttacatgatcccccatgttg
tgcaaaaaagcggttagctccttcggtcctccgatcgttgtcagaagtaagttggccgcagtgttatcac
tcatggttatggcagcactgcataattctcttactgtcatgccatccgtaagatgcttttctgtgactgg
tgagtactcaaccaagtcattctgagaatagtgtatgcggcgaccgagttgctcttgcccggcgtcaata
cgggataataccgcgccacatagcagaactttaaaagtgctcatcattggaaaacgttcttcggggcgaa
aactctcaaggatcttaccgctgttgagatccagttcgatgtaacccactcgtgcacccaactgatcttc
agcatcttttactttcaccagcgtttctgggtgagcaaaaacaggaaggcaaaatgccgcaaaaaagggа
ataagggcgacacggaaatgttgaatactcatactcttccttttcaatattattgaagcatttatcagg
gttattgtctcatgagcggatacatatttgaatgtatttagaaaaataaacaaatagggGttccgcgcac
atttccccgaaaagtgccacct

Figure 3.1: Annotated 6G pegRNA construct sequence that generated successfully mutated NEMO cell lines.

The pegRNA construct contains the following components: a U6 promoter site (uppercase and underlined), a spacer sequence (lowercase bold), a sgRNA scaffold (lowercase and underlined), a 3' extension containing the primer binding site (PBS) and reverse transcriptase (RT) template (uppercase bold), and the pU6-pegRNA-GG-acceptor backbone (lowercase).

pU6-pegRNA-GG-D311N-6-16-14:

gacgtcgctagctgtacaaaaaagcaggctttaaaggaaccaattcagtcgactggatccggtaccAAGG
TCGGGCAGGAAGAGGGCCTATTTCCCATGATTCCTTCATATTTGCATATACGATACAAGGCTGTTAGAGA
GATAATTAGAATTAATTTGACTGTAAACACAAAGATATTAGTACAAAATACGTGACGTAGAAAGTAATAA
TTTCTTGGGTAGTTTGCAGTTTTAAAATTATGTTTTAAAATGGACTATCATATGCTTACCGTAACTTGAA
AGTATTTCGATTTCTTGGCTTTATATATCTTGTGGAAAGGACGAAACACCG**ccaggcggatatctacaag**
ggttttagagctagaaatagcaagttaaaataaggctagtccgttatcaacttgaaaaagtggcaccgag
tcggtgc**GCCTGGAAGTTCGCCTTGTAGATATCCGCC**ttttttaagcttgggccgctcgaggtacctct
ctacatatgacatgtgagcaaaaggccagcaaaaggcCAGGAACCGTAAAAAGGCcgcgttgctggcgtt
tttccataggctccgccccctgacgagcatcacaaaaatcgacgctcaagtcagaggtggcgaaacccg
acaggactataaagataccaggcgtttccccctggaagctccctcgtgcgctctcctgttccgaccctgc
cgcttaccggatacctgtccgcctttctcccttcgggaagcgtggcgctttctcatagctcacgctgtag
gtatctcagttcggtgtaggtcgttcgctccaagctgggctgtgtgcacgaacccccgttcagcccgac
cgctgcgccttatccggtaactatcgtcttgagtccaacccggtaagacacgacttatcgccactggcag
cagccactggtaacaggattagcagagcgaggtatgtaggcggtgctacagagttcttgaagtggtggcc
taactacggctacactagaagaacagtatttggtatctgcgctctgctgaagccagttaccttcggaaaa
agagttggtagctcttgatccggcaaacaaaccaccgctggtagcggtggtttttttgtttgcaagcagc
agattacgcgcagaaaaaaaggatctcaagaagatcctttgatcttttctacggggtctgacgctcagtg
gaacgaaaactcacgttaagggattttggtcatgagattatcaaaaaggatcttcacctagatccttttta
aattaaaaatgaagttttaaatcaatctaaagtatatatgagtaaacttggtctgacagttaccaatgct
taatcagtgaggcacctatctcagcgatctgtctatttcgttcatccatagttgcctgactccccgtcgt
gtagataactacgatacgggagggcttaccatctggccccagtgctgcaatgataccgcgagatccacgc
tcaccggctccagatttatcagcaataaaccagccagccggaagggccgagcgcagaagtggtcctgcaa
ctttatccgcctccatccagtctattaattgttgccgggaagctagagtaagtagttcgccagttaatag
tttgcgcaacgttgttgccattgctacaggcatcgtggtgtcacgctcgtcgtttggtatggcttcattc
agctccggttcccaacgatcaaggcgagttacatgatcccccatgttgtgcaaaaaagcggttagctcct
tcggtcctccgatcgttgtcagaagtaagttggccgcagtgttatcactcatggttatggcagcactgca
taattctcttactgtcatgccatccgtaagatgcttttctgtgactggtgagtactcaaccaagtcattc
tgagaatagtgtatgcggcgaccgagttgctcttgcccggcgtcaatacgggataataccgcgccacata
gcagaactttaaaagtgctcatcattggaaaacgttcttcggggcgaaaactctcaaggatcttaccgct
gttgagatccagttcgatgtaacccactcgtgcacccaactgatcttcagcatcttttactttcaccagc
gtttctgggtgagcaaaaacaggaaggcaaaatgccgcaaaaaagggaataagggcgacacggaaatgtt
gaatactcatactcttcctttttcaatattattgaagcatttatcagggttattgtctcatgagcggata
catatttgaatgtatttagaaaaataaacaaatagggttccgcgcacatttccccgaaaagtgccacct

Figure 3.2: Annotated D311N pegRNA construct sequence that generated successfully mutated NEMO cell lines.

The pegRNA construct contains the following components: a U6 promoter site (uppercase and underlined), a spacer sequence (lowercase bold), a sgRNA scaffold (lowercase and underlined), a 3' extension containing the primer binding site (PBS) and reverse transcriptase (RT) template (uppercase bold), and the pU6-pegRNA-GG-acceptor backbone (lowercase).

pU6-pegRNA-GG-E391X-13:

gacgtcgctagctgtacaaaaaagcaggctttaaaggaaccaattcagtcgactggatccggtaccAAGG
TCGGGCAGGAAGAGGGCCTATTTCCCATGATTCCTTCATATTTGCATATACGATACAAGGCTGTTAGAGA
GATAATTAGAATTAATTTGACTGTAAACACAAAGATATTAGTACAAAATACGTGACGTAGAAAGTAATAA
TTTCTTGGGTAGTTTGCAGTTTTAAAATTATGTTTTAAAATGGACTATCATATGCTTACCGTAACTTGAA
AGTATTTCGATTTCTTGGCTTTATATATCTTGTGGAAAGGACGAAACACCG**cagaagtcaggtggctcct**
gttttagagctagaaatagcaagttaaaataaggctagtccgttatcaacttgaaaaagtggcaccgagt
cggtgc**AGCCCCCCCGAGTAGCCACCTGACTTCT**ttttttaagcttgggccgctcgaggtacctctcta
catatgacatgtgagcaaaaggccagcaaaaggcCAGGAACCGTAAAAAGGCcgcgttgctggcgttttt
ccataggctccgccccctgacgagcatcacaaaaatcgacgctcaagtcagaggtggcgaaacccgaca
ggactataaagataccaggcgtttcccccctggaagctccctcgtgcgctctcctgttccgaccctgccgc
ttaccggatacctgtccgcctttctcccttcgggaagcgtggcgctttctcatagctcacgctgtaggta
tctcagttcggtgtaggtcgttcgctccaagctgggctgtgtgcacgaacccccccgttcagcccgaccgc
tgcgccttatccggtaactatcgtcttgagtccaacccggtaagacacgacttatcgccactggcagcag
ccactggtaacaggattagcagagcgaggtatgtaggcggtgctacagagttcttgaagtggtggcctaa
ctacggctacactagaagaacagtatttggtatctgcgctctgctgaagccagttaccttcggaaaaaga
gttggtagctcttgatccggcaaacaaaccaccgctggtagcggtggtttttttgtttgcaagcagcaga
ttacgcgcagaaaaaaaggatctcaagaagatcctttgatcttttctacggggtctgacgctcagtggaa
cgaaaactcacgttaagggattttggtcatgagattatcaaaaaggatcttcacctagatccttttaaat
taaaaatgaagttttaaatcaatctaaagtatatatgagtaaacttggtctgacagttaccaatgcttaa
tcagtgaggcacctatctcagcgatctgtctatttcgttcatccatagttgcctgactccccgtcgtgta
gataactacgatacgggagggcttaccatctggccccagtgctgcaatgataccgcgagatccacgctca
ccggctccagatttatcagcaataaaccagccagccggaagggccgagcgcagaagtggtcctgcaactt
tatccgcctccatccagtctattaattgttgccgggaagctagagtaagtagttcgccagttaatagttt
gcgcaacgttgttgccattgctacaggcatcgtggtgtcacgctcgtcgtttggtatggcttcattcagc
tccggttcccaacgatcaaggcgagttacatgatcccccatgttgtgcaaaaaagcggttagctccttcg
gtcctccgatcgttgtcagaagtaagttggccgcagtgttatcactcatggttatggcagcactgcataa
ttctcttactgtcatgccatccgtaagatgcttttctgtgactggtgagtactcaaccaagtcattctga
gaatagtgtatgcggcgaccgagttgctcttgcccggcgtcaatacgggataataccgcgccacatagca
gaactttaaaagtgctcatcattggaaaacgttcttcggggcgaaaactctcaaggatcttaccgctgtt
gagatccagttcgatgtaacccactcgtgcacccaactgatcttcagcatcttttactttcaccagcgtt
tctgggtgagcaaaaacaggaaggcaaaatgccgcaaaaaagggaataagggcgacacggaaatgttgaa
tactcatactcttcctttttcaatattattgaagcatttatcagggttattgtctcatgagcggatacat
atttgaatgtatttagaaaaataaacaaatagggggttccgcgcacatttccccgaaaagtgccacct

Figure 3.3: Annotated E391X pegRNA construct sequence that generated successfully mutated NEMO cell lines.

The pegRNA construct contains the following components: a U6 promoter site (uppercase and underlined), a spacer sequence (lowercase bold), a sgRNA scaffold (lowercase and underlined), a 3' extension containing the primer binding site (PBS) and reverse transcriptase (RT) template (uppercase bold), and the pU6-pegRNA-GG-acceptor backbone (lowercase).

U6-BsmBIcassette-Sp-sgRNA-QRSSPP-37:

gacgtcgctagctgtacaaaaaagcaggctttaaaggaaccaattcagtcgactggatccggtaccAAGG
TCGGGCAGGAAGAGGGCCTATTTCCCATGATTCCTTCATATTTGCATATACGATACAAGGCTGTTAGAGA
GATAATTAGAATTAATTTGACTGTAAACACAAAGATATTAGTACAAAATACGTGACGTAGAAAGTAATAA
TTTCTTGGGTAGTTTGCAGTTTTAAAATTATGTTTTAAAATGGACTATCATATGCTTACCGTAACTTGAA
AGTATTTCGATTTCTTGGCTTTATATATCTTGTGGAAAGGACGAAACACCG**AGCCTACCTCTCCTCTCCC**
CgttttagagctagaaatagcaagttaaaataaggctagtccgttatcaacTTGAAAAAGTGGCACCGAG
TCGgtgctttttttaagcttgggccgctcgaggtacctctctacatatgacatgtgagcaaaaggccagc
aaaaggcCAGGAACCGTAAAAAGGCcgcgttgctggcgttttccataggctccgccccccctgacgagca
tcacaaaaatcgacgctcaagtcagaggtggcgaaacccgacaggactataaagataccaggcgtttccc
cctggaagctccctcgtgcgctctcctgttccgaccctgccgcttaccggatacctgtccgcctttctcc
cttcgggaagcgtggcgctttctcatagctcacgctgtaggtatctcagttcggtgtaggtcgttcgctc
caagctgggctgtgtgcacgaaccccccgttcagcccgaccgctgcgccttatccggtaactatcgtctt
gagtccaacccggtaagacacgacttatcgccactggcagcagccactggtaacaggattagcagagcga
ggtatgtaggcggtgctacagagttcttgaagtggtggcctaactacggctacactagaagaacagtatt
tggtatctgcgctctgctgaagccagttaccttcggaaaaagagttggtagctcttgatccggcaaacaa
accaccgctggtagcggtggtttttttgtttgcaagcagcagattacgcgcagaaaaaaaggatctcaag
aagatcctttgatcttttctacggggtctgacgctcagtggaacgaaaactcacgttaagggattttggt
catgagattatcaaaaaggatcttcacctagatccttttaaattaaaaatgaagttttaaatcaatctaa
agtatatatgagtaaacttggtctgacagttaccaatgcttaatcagtgaggcacctatctcagcgatct
gtctatttcgttcatccatagttgcctgactccccgtcgtgtagataactacgatacgggagggcttacc
atctggccccagtgctgcaatgataccgcgagacccacgctcaccggctccagatttatcagcaataaac
cagccagccggaagggccgagcgcagaagtggtcctgcaactttatccgcctccatccagtctattaatt
gttgccgggaagctagagtaagtagttcgccagttaatagtttgcgcaacgttgttgccattgctacagg
catcgtggtgtcacgctcgtcgtttggtatggcttcattcagctccggttcccaacgatcaaggcgagtt
acatgatcccccatgttgtgcaaaaaagcggttagctccttcggtcctccgatcgttgtcagaagtaagt
tggccgcagtgttatcactcatggttatggcagcactgcataattctcttactgtcatgccatccgtaag
atgcttttctgtgactggtgagtactcaaccaagtcattctgagaatagtgtatgcggcgaccgagttgc
tcttgcccggcgtcaatacgggataataccgcgccacatagcagaactttaaaagtgctcatcattggaa
aacgttcttcggggcgaaaactctcaaggatcttaccgctgttgagatccagttcgatgtaacccactcg
tgcacccaactgatcttcagcatcttttactttcaccagcgtttctgggtgagcaaaaacaggaaggcaa
aatgccgcaaaaaagggaataagggcgacacggaaatgttgaatactcatactcttccttttcaatatt
attgaagcatttatcagggttattgtctcatgagcggatacatatttgaatgtatttagaaaaataaaca
aatagggttccgcgcacatttccccgaaaagtgccacct

Figure 3.4: Annotated 6G ngRNA plasmid sequences of successfully mutated NEMO cell lines.

The ngRNA construct contains the following components: a U6 promoter (uppercase and underlined), a nicking guide sequence (uppercase bold), and the BPK1520 (U6-BsmBI-cassette-Sp-sgRNA) backbone (black).

U6-BsmBIcassette-Sp-sgRNA-D311N-73:

gacgtcgctagctgtacaaaaaagcaggctttaaaggaaccaattcagtcgactggatccggtaccAAGG
TCGGGCAGGAAGAGGGCCTATTTCCCATGATTCCTTCATATTTGCATATACGATACAAGGCTGTTAGAGA
GATAATTAGAATTAATTTGACTGTAAACACAAAGATATTAGTACAAAATACGTGACGTAGAAAGTAATAA
TTTCTTGGGTAGTTTGCAGTTTTAAAATTATGTTTTAAAATGGACTATCATATGCTTACCGTAACTTGAA
AGTATTTCGATTTCTTGGCTTTATATATCTTGTGGAAAGGACGAAACACCG**CACCCACCAGGCACTGCGC**
CgttttagagctagaaatagcaagttaaaataaggctagtccgttatcaacTTGAAAAAGTGGCACCGAG
TCGgtgctttttttaagcttgggccgctcgaggtacctctctacatatgacatgtgagcaaaaggccagc
aaaaggcCAGGAACCGTAAAAAGGCcgcgttgctggcgtttttccataggctccgccccccctgacgagca
tcacaaaaatcgacgctcaagtcagaggtggcgaaacccgacaggactataaagataccaggcgtttccc
cctggaagctccctcgtgcgctctcctgttccgaccctgccgcttaccggatacctgtccgcctttctcc
cttcgggaagcgtggcgctttctcatagctcacgctgtaggtatctcagttcggtgtaggtcgttcgctc
caagctgggctgtgtgcacgaaccccccgttcagcccgaccgctgcgccttatccggtaactatcgtctt
gagtccaacccggtaagacacgacttatcgccactggcagcagccactggtaacaggattagcagagcga
ggtatgtaggcggtgctacagagttcttgaagtggtggcctaactacggctacactagaagaacagtatt
tggtatctgcgctctgctgaagccagttaccttcggaaaaagagttggtagctcttgatccggcaaacaa
accaccgctggtagcggtggtttttttgtttgcaagcagcagattacgcgcagaaaaaaaggatctcaag
aagatcctttgatcttttctacggggtctgacgctcagtggaacgaaaactcacgttaagggattttggt
catgagattatcaaaaaggatcttcacctagatccttttaaattaaaaatgaagttttaaatcaatctaa
agtatatatgagtaaacttggtctgacagttaccaatgcttaatcagtgaggcacctatctcagcgatct
gtctatttcgttcatccatagttgcctgactccccgtcgtgtagataactacgatacgggagggcttacc
atctggccccagtgctgcaatgataccgcgagacccacgctcaccggctccagatttatcagcaataaac
cagccagccggaagggccgagcgcagaagtggtcctgcaactttatccgcctccatccagtctattaatt
gttgccgggaagctagagtaagtagttcgccagttaatagtttgcgcaacgttgttgccattgctacagg
catcgtggtgtcacgctcgtcgtttggtatggcttcattcagctccggttcccaacgatcaaggcgagtt
acatgatcccccatgttgtgcaaaaaagcggttagctccttcggtcctccgatcgttgtcagaagtaagt
tggccgcagtgttatcactcatggttatggcagcactgcataattctcttactgtcatgccatccgtaag
atgcttttctgtgactggtgagtactcaaccaagtcattctgagaatagtgtatgcggcgaccgagttgc
tcttgcccggcgtcaatacgggataataccgcgccacatagcagaactttaaaagtgctcatcattggaa
aacgttcttcggggcgaaaactctcaaggatcttaccgctgttgagatccagttcgatgtaacccactcg
tgcacccaactgatcttcagcatcttttactttcaccagcgtttctgggtgagcaaaaacaggaaggcaa
aatgccgcaaaaaagggaataagggcgacacggaaatgttgaatactcatactcttccttttcaatatt
attgaagcatttatcagggttattgtctcatgagcggatacatatttgaatgtatttagaaaaataaaca
aatagggttccgcgcacatttccccgaaaagtgccacct

Figure 3.5: Annotated D311N ngRNA plasmid sequences of successfully mutated NEMO cell lines.

The ngRNA construct contains the following components: a U6 promoter (uppercase and underlined), a nicking guide sequence (uppercase bold), and the BPK1520 (U6-BsmBI-cassette-Sp-sgRNA) backbone (black).

U6-BsmBIcassette-Sp-sgRNA-E391X-133:

gacgtcgctagctgtacaaaaaagcaggctttaaaggaaccaattcagtcgactggatccggtaccAAGG
TCGGGCAGGAAGAGGGCCTATTTCCCATGATTCCTTCATATTTGCATATACGATACAAGGCTGTTAGAGA
GATAATTAGAATTAATTTGACTGTAAACACAAAGATATTAGTACAAAATACGTGACGTAGAAAGTAATAA
TTTCTTGGGTAGTTTGCAGTTTTAAAATTATGTTTTAAAATGGACTATCATATGCTTACCGTAACTTGAA
AGTATTTCGATTTCTTGGCTTTATATATCTTGTGGAAAGGACGAAACACCG**CATGAGTGGCCTGTGAGAC**
CgttttagagctagaaatagcaagttaaaataaggctagtccgttatcaacTTGAAAAAGTGGCACCGAG
TCGgtgctttttttaagcttgggccgctcgaggtacctctctacatatgacatgtgagcaaaaggccagc
aaaaggcCAGGAACCGTAAAAAGGCcgcgttgctggcgtttttccataggctccgccccccctgacgagca
tcacaaaaatcgacgctcaagtcagaggtggcgaaacccgacaggactataaagataccaggcgtttccc
cctggaagctccctcgtgcgctctcctgttccgaccctgccgcttaccggatacctgtccgcctttctcc
cttcgggaagcgtggcgctttctcatagctcacgctgtaggtatctcagttcggtgtaggtcgttcgctc
caagctgggctgtgtgcacgaaccccccgttcagcccgaccgctgcgccttatccggtaactatcgtctt
gagtccaacccggtaagacacgacttatcgccactggcagcagccactggtaacaggattagcagagcga
ggtatgtaggcggtgctacagagttcttgaagtggtggcctaactacggctacactagaagaacagtatt
tggtatctgcgctctgctgaagccagttaccttcggaaaaagagttggtagctcttgatccggcaaacaa
accaccgctggtagcggtggtttttttgtttgcaagcagcagattacgcgcagaaaaaaaggatctcaag
aagatcctttgatcttttctacggggtctgacgctcagtggaacgaaaactcacgttaagggattttggt
catgagattatcaaaaaggatcttcacctagatccttttaaattaaaaatgaagttttaaatcaatctaa
agtatatatgagtaaacttggtctgacagttaccaatgcttaatcagtgaggcacctatctcagcgatct
gtctatttcgttcatccatagttgcctgactccccgtcgtgtagataactacgatacgggagggcttacc
atctggccccagtgctgcaatgataccgcgagacccacgctcaccggctccagatttatcagcaataaac
cagccagccggaagggccgagcgcagaagtggtcctgcaactttatccgcctccatccagtctattaatt
gttgccgggaagctagagtaagtagttcgccagttaatagtttgcgcaacgttgttgccattgctacagg
catcgtggtgtcacgctcgtcgtttggtatggcttcattcagctccggttcccaacgatcaaggcgagtt
acatgatcccccatgttgtgcaaaaaagcggttagctccttcggtcctccgatcgttgtcagaagtaagt
tggccgcagtgttatcactcatggttatggcagcactgcataattctcttactgtcatgccatccgtaag
atgcttttctgtgactggtgagtactcaaccaagtcattctgagaatagtgtatgcggcgaccgagttgc
tcttgcccggcgtcaatacgggataataccgcgccacatagcagaactttaaaagtgctcatcattggaa
aacgttcttcggggcgaaaactctcaaggatcttaccgctgttgagatccagttcgatgtaacccactcg
tgcacccaactgatcttcagcatcttttactttcaccagcgtttctgggtgagcaaaaacaggaaggcaa
aatgccgcaaaaaagggaataagggcgacacggaaatgttgaatactcatactcttccttttcaatatt
attgaagcatttatcagggttattgtctcatgagcggatacatatttgaatgtatttagaaaaataaaca
aatagggttccgcgcacatttccccgaaaagtgccacct

Figure 3.6: Annotated E391X ngRNA plasmid sequences of successfully mutated NEMO cell lines.

The ngRNA construct contains the following components: a U6 promoter (uppercase and underlined), a nicking guide sequence (uppercase bold), and the BPK1520 (U6-BsmBI-cassette-Sp-sgRNA) backbone (black).

3.2 Transfection of prime editing plasmids into HEK293T cells

To visually confirm successful transfection, confocal images of GFP-expressing HEK293T cells were acquired on the ImageXpress® Pico Automated Cell Imaging System (Molecular Devices) using transmitted light and fluorescein isothiocyanate (FITC) optics (Figure 3.7). Transmitted light imaging revealed a dense field of cells, while the FITC channel identified individual cells expressing GFP, confirming successful uptake of the CRISPR plasmid. The merged image of both channels demonstrated that GFP-positive transfected cells represented a minority population surrounded by a majority of non-transfected cells, which shows low efficiency in transfection.

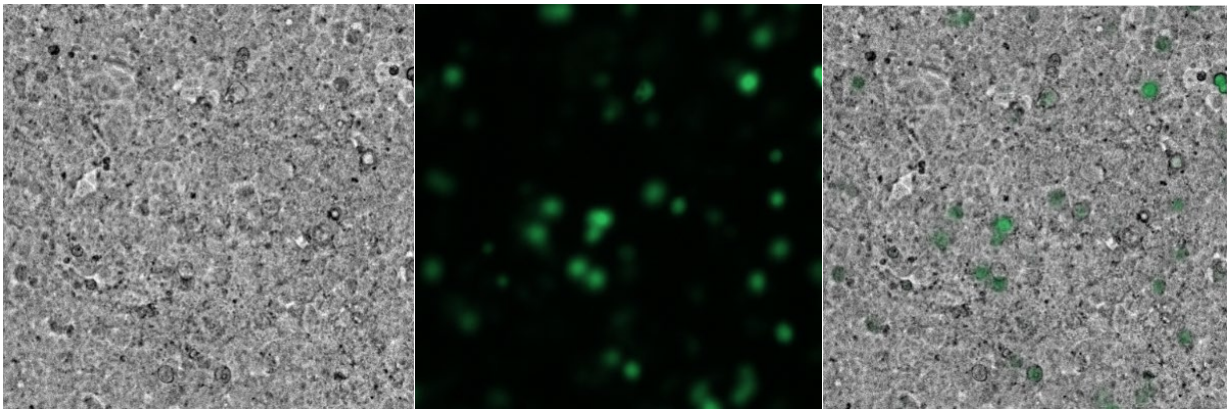

Figure 3.7: Confocal images of transfected HEK293T cells taken at 10X magnification.

From left to right: transmitted light image showing a dense field of cells, FITC channel image showing GFP fluorescence in individual transfected cells, and the merged image of both channels. The merged image demonstrates that GFP-positive transfected cells represent a minority population surrounded by non-transfected cells.

3.3 Fluorescence Activated Cell Sorting (FACS)

Flow cytometry was used to identify and sort single-cell particles based on GFP fluorescence intensity. Parental HEK293T cells served as the negative control, setting the baseline for GFP signal. Transfected HEK293T cells for 6G, D311N, and E391X NEMO mutations displayed an increase in GFP fluorescence compared to the parental control, confirming successful uptake and expression of the GFP co-expressing CRISPR-Cas9 plasmid prior to single-cell sorting (Figure 3.8). The cells in the GFP gate were sorted into 1 cell per well in a 96-well plate and the surviving cells were subjected to Sanger sequencing.

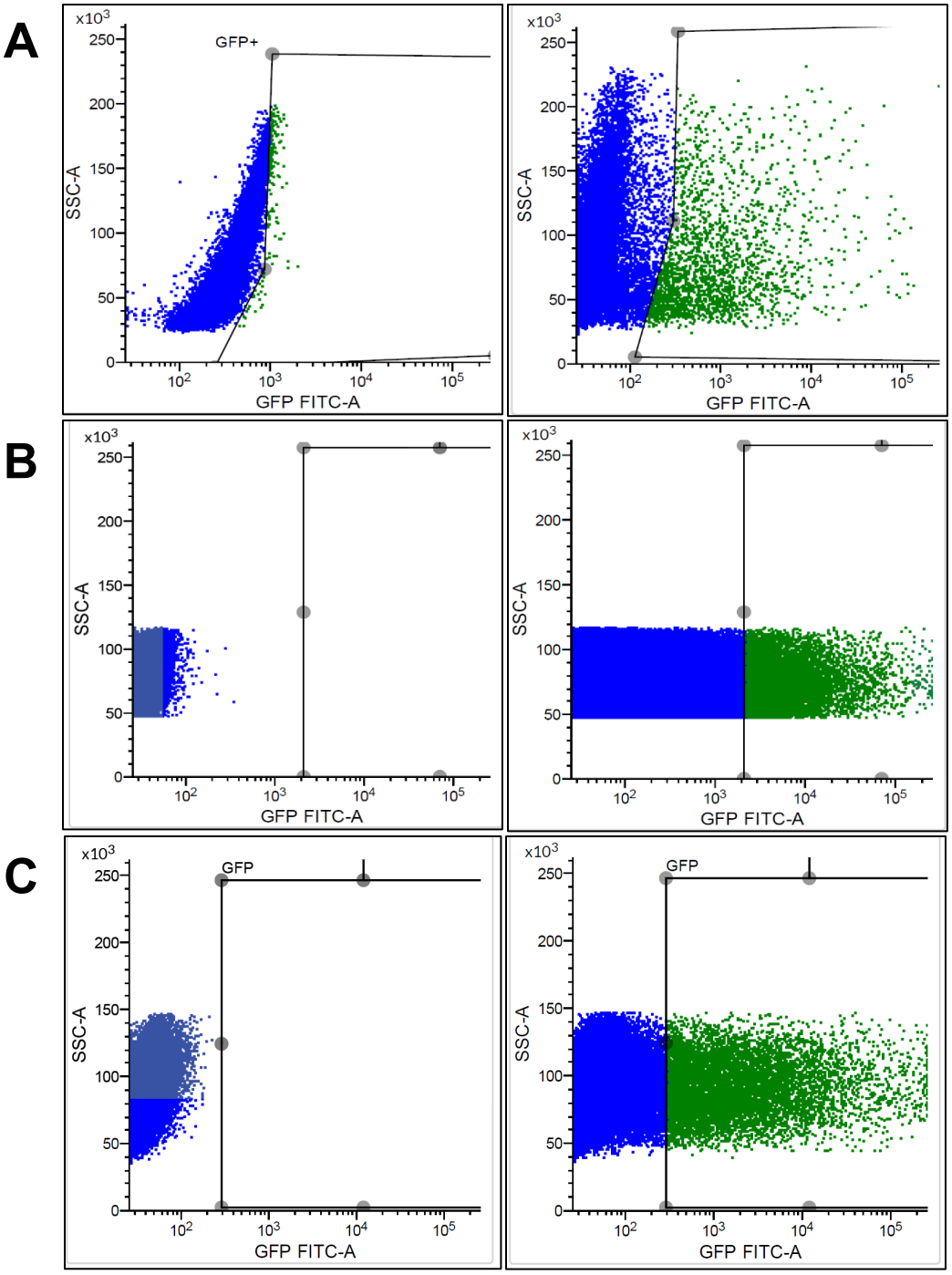

Figure 3.8: Flow cytometry dot plots of single-cell sorting for parental and NEMO mutant HEK293T cell lines.

Wild-type parental and CRISPR plasmid-transfected HEK293T cells were sorted by GFP fluorescence intensity via flow cytometry into 96-well plates. For each mutant, two dot plots are shown: the left plot displays the wild-type parental HEK293T cells as the untransfected control and the right plot displays the GFP-positive population selected for single-cell sorting. GFP-positive cells from the 6G (A), D311N (B), and E391X (C) mutant transfections were individually gated and sorted into 96-well plates for single-cell clonal expansion.

3.4 IKBKG mutation region PCR amplification agarose gel

Following single-cell sorting, the exon region harboring each respective mutation was amplified by PCR for subsequent Sanger sequencing verification. For all NEMO mutant cell lines with the exception of the NEMO knockout, primers targeting the exon 8–10 region of IKBKG were used to amplify the respective mutation sites, generating a PCR product of 2,100 bp. For the NEMO knockout cell line, which harbors a mutation in exon 1, primers targeting the promoter region were used for PCR amplification, generating a product of 680 bp. PCR products were resolved on a 1% agarose gel alongside a no-template control. Both primer sets produced clear amplification bands at the expected sizes with no evidence of off-target amplification or primer dimers in the no-template control, confirming the specificity of the PCR amplification.

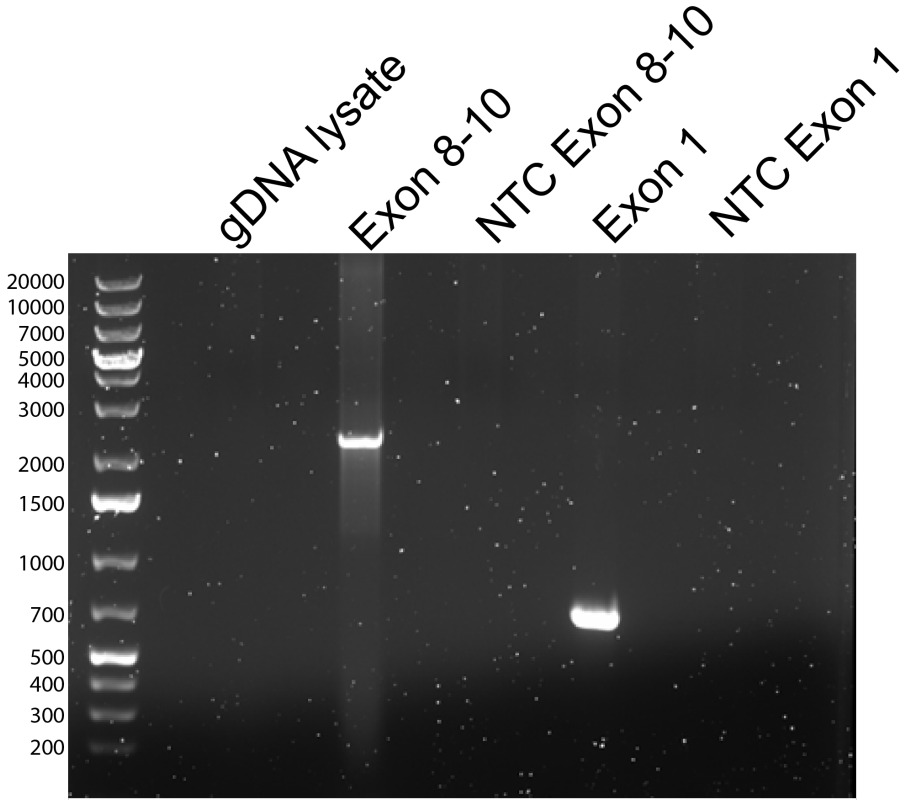

Figure 3.9: Agarose gel of amplified exon 8 – 10 and promoter 1.

Amplified DNAs were loaded onto a 1% agarose gel and ran alongside 1kb plus gene ruler (ThermoFisher). From left to right the lanes show genomic DNA lysate, amplified exon 8-10 region, no template control exon 8-10, amplified exon 1 region, and no template control exon 1 region.

3.5 Sequences of mutated NEMO HEK293T cell lines

Amplified PCR fragments were gel extracted and combined with the respective exon 8, exon 10, or exon 1 forward primers before submission for Sanger sequencing to confirm successful incorporation of each mutation. Sanger sequencing of chromosome X regions 154,564,343–154,564,379 bp and 154,563,560–154,563,596 bp confirmed homozygous introduction of the 6G secondary binding site mutation and the D311N linear polyubiquitin binding mutation, respectively.

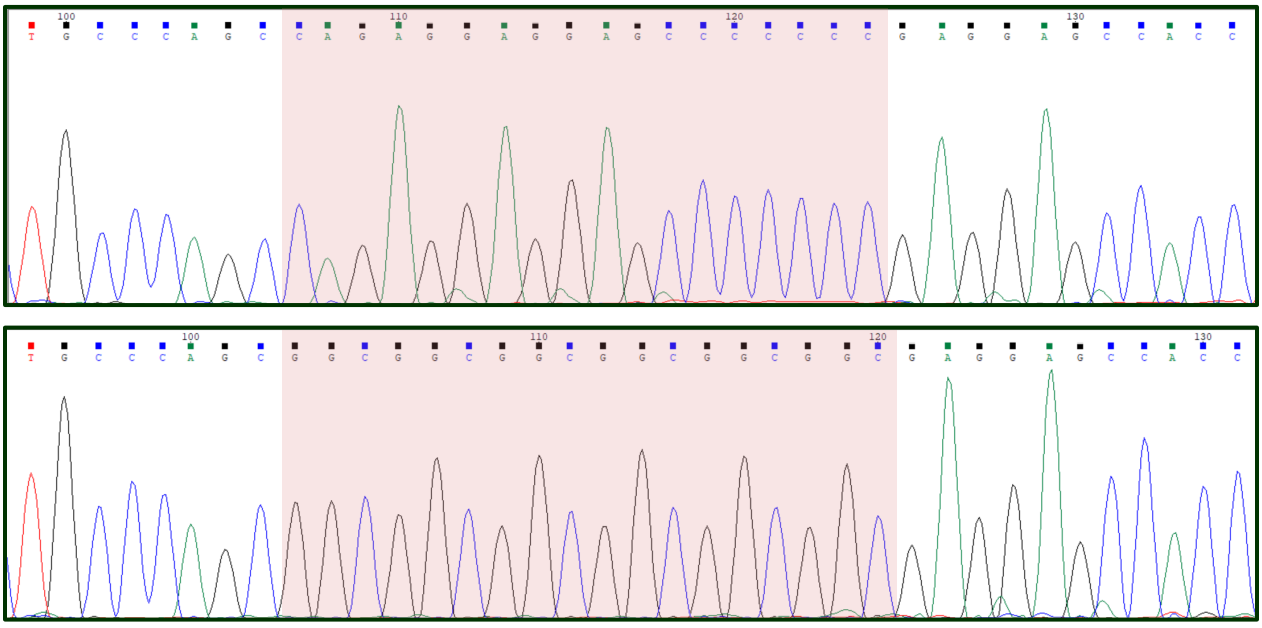

Figure 3.10: DNA chromatograms of wild-type and 6G NEMO sequences in the IKBKG exon 10 region.

Top chromatogram shows wild-type HEK293T sequence of IKBKG exon 10. Bottom corresponding chromatogram shows 6G mutant sequence of IKBKG exon 10, confirming the successful substitution of amino acid positions 384–389 to glycine.

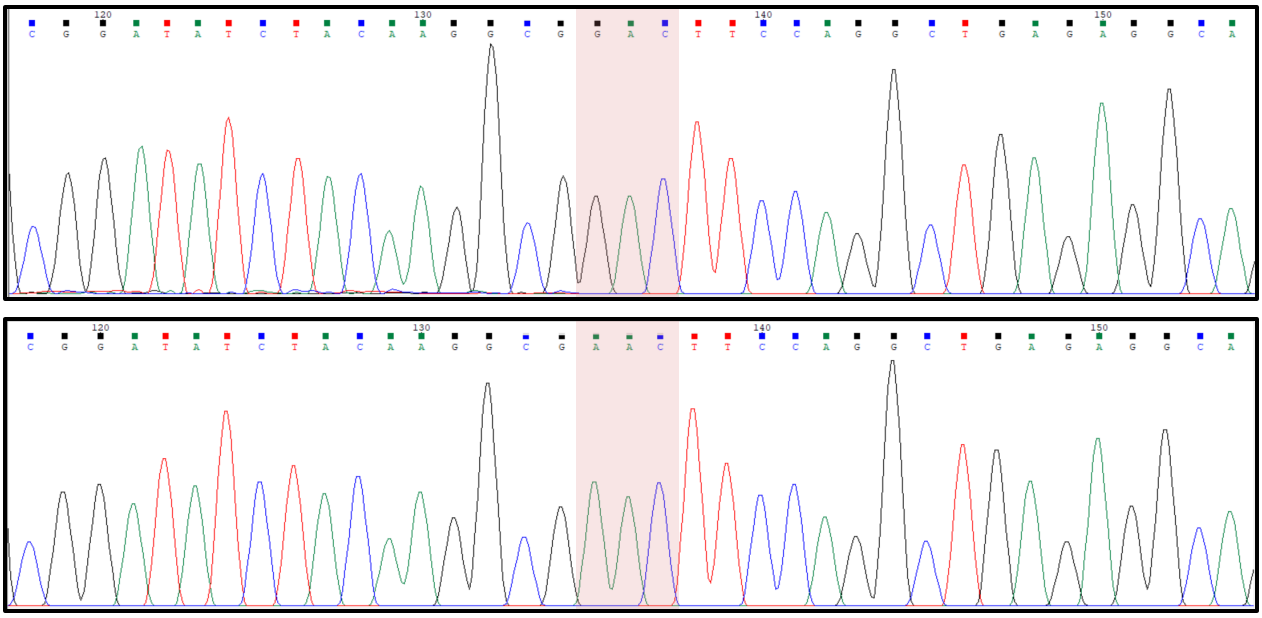

Figure 3.11: DNA chromatograms of wild-type and D311N NEMO sequences in the IKBKG exon 8 region.

The top chromatogram shows the wild-type HEK293T sequence of IKBKG exon 8, and the bottom chromatogram shows the corresponding D311N mutant sequence, confirming the successful introduction of the GAC→AAC substitution at codon 311.

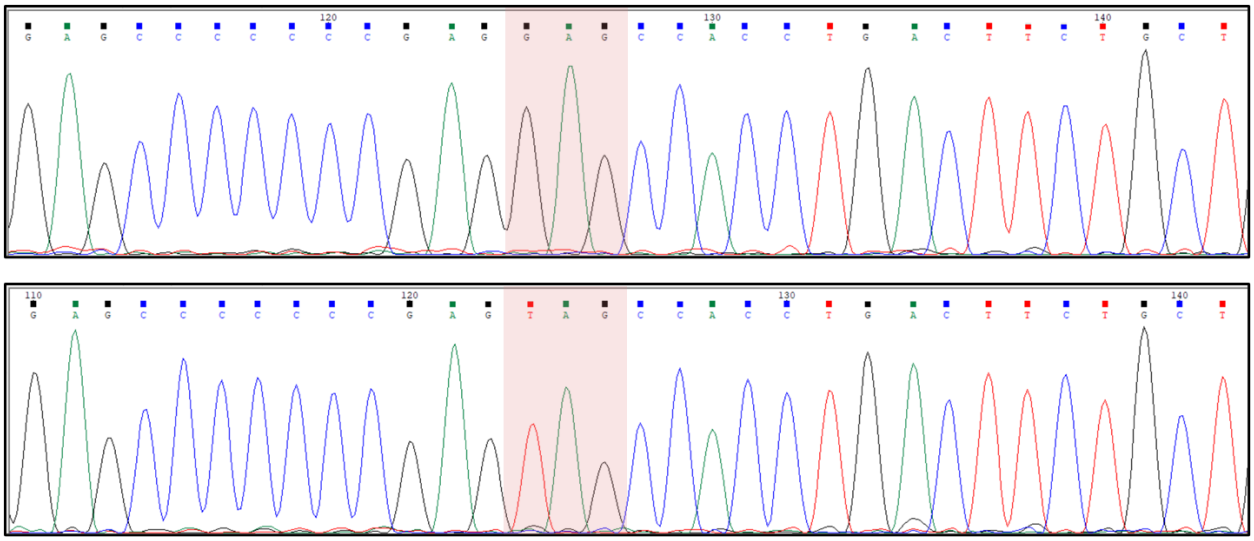

Figure 3.12: DNA chromatograms of wild-type and E391X NEMO sequences in the IKBKG exon 10 region.

The top chromatogram shows the wild-type HEK293T sequence of IKBKG exon 10, and the bottom chromatogram shows the corresponding E391X mutant sequence, confirming the successful introduction of the GAG→TAG substitution at codon 391.

3.6 Verifying NF-κB activation of TNF-α induced mutant NEMO HEK293T cell lines

Wild type, AbCam NEMO knockout, 6G, and D311N NEMO HEK293T cell lines were stimulated with 10 ng/mL TNF-α and harvested at 0, 10, and 30 minutes post-stimulation for cytoplasmic and nuclear fractionation. The E391X mutant cell line was not included in this analysis as it could not be recovered during cell line generation. Lamin A/C and β-actin were used as endogenous nuclear and cytoplasmic markers, respectively, to confirm successful fractionation. All the proteins were probed simultaneously with each protein of interest antibodies and imaged together. In wild-type cells, the bands for nuclear fraction of NF-κB p65 increased over time indicated by the increase size of the band as well as intensity. This canonical activation was accompanied by IκBα degradation in the cytoplasmic fraction, shown by the decrease of size and intensity over time. The combination of the NF-κB band increasing over time and IκBα band decreasing over time shows an intact canonical pathway.

The AbCam NEMO knockout cell line displayed a similar pattern of NF-κB nuclear accumulation and IκBα degradation but with lighter bands compared to wild type. This indicates that the NF-κB activation was not impaired in this "KO" cell line and NEMO may still present. The 6G NEMO mutant also exhibited NF-κB nuclear accumulation and IκBα degradation. However, nuclear translocation appeared delayed due to the bands appearing lighter and less intense compared to wild type, suggesting that disruption of the secondary IKK2 binding site partially impairs but does not abolish NF-κB activation. In contrast, the D311N NEMO mutant showed no detectable accumulation of NF-κB p65 in the nuclear fraction over time and no IκBα degradation, indicating that disruption of the linear polyubiquitin binding site abolished canonical NF-κB activation in response to TNF-α.

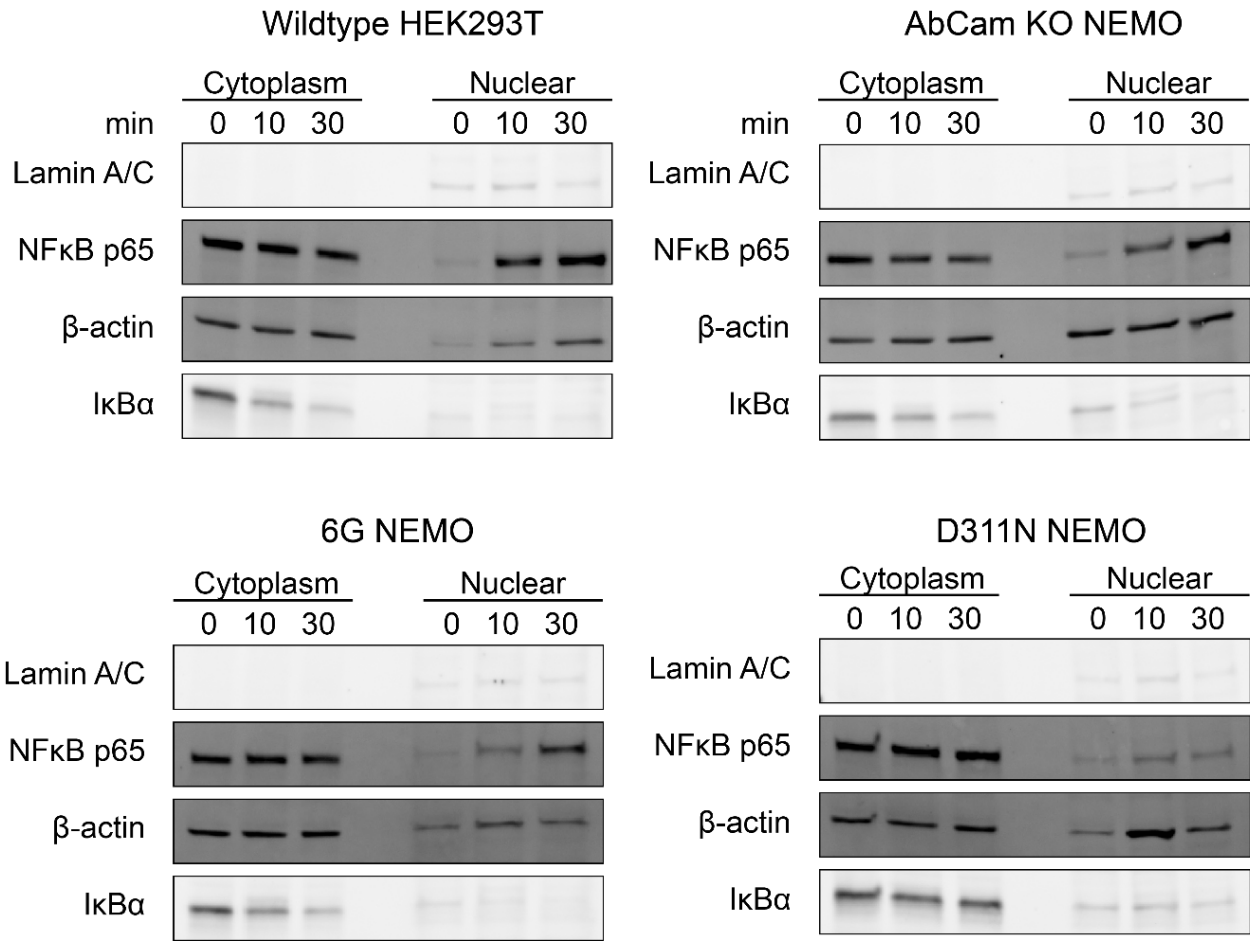

Figure 3.13: TNF-α induced NF-κB activation pathway of NEMO mutant HEK293T cells.

Wild-type HEK293T, AbCam NEMO knockout HEK293T, 6G NEMO, and D311N NEMO cells were treated with 10 ng/mL TNF-α and harvested at 0, 10, and 30 minutes post-stimulation. Cells were fractionated into cytoplasmic and nuclear fractions, normalized for protein concentration, and resolved by SDS-PAGE before transfer onto nitrocellulose membrane. Membranes were probed with antibodies against NF-κB p65, IκBα, Lamin A/C, and β-actin.

Discussion

Four NEMO mutant cell lines were attempted using CRISPR-Cas9 prime editing, targeting distinct binding mechanisms involved in canonical NF-κB activation. Of the four intended constructs, three mutations were successfully confirmed by Sanger sequencing. However, only two mutant cell lines, 6G and D311N, were ultimately recovered for downstream analysis. The third sequencing-confirmed mutant cell line (E391X) was lost during expansion, and time constraints prevented further recovery attempts. Chromatogram analysis of the 6G, D311N, and E391X cell lines confirmed the presence of the intended mutations with no evidence of insertions or deletions (indels) within the sequenced regions, indicating that prime editing introduced the desired substitutions with high fidelity.

The 6G and D311N NEMO mutant cell lines were further validated by stimulation with TNF-α to assess their effect on canonical NF-κB activation. The complete disruption of NF-κB activation observed in the D311N mutant is consistent with previous studies demonstrating the critical role of linear polyubiquitin binding in NEMO-mediated IKK complex activation. In contrast, the delayed but not abolished NF-κB nuclear translocation observed in the 6G mutant provides new insight into the role of the secondary IKK2 binding site, suggesting that this interaction contributes to but is not strictly required for NF-κB activation. This finding challenges the previously held assumption that disruption of the secondary IKK2 binding site would be equally detrimental to NF-κB activation as disruption of the linear polyubiquitin binding site and instead points to a modulatory rather than essential role for this interaction in the canonical TNF-α signaling pathway.

Collectively, the findings presented in this chapter establish the successful generation and functional validation of two NEMO mutant cell lines, 6G and D311N, providing a robust cellular platform for dissecting the distinct contributions of NEMO's secondary IKK2 binding site and linear polyubiquitin binding site to canonical NF-κB activation in subsequent chapters.

Appendix

3A.1 List of all pegRNA and ngRNA oligos used for respective NEMO mutations

Table 3A.1: Oligonucleotide sequences for constructing KO NEMO pegRNA plasmids.

Constructs of 8 bp deletion KO NEMO	Sequence (5' – 3')
pegRNA spacer top	caccGAGCCGGAAGCGTGGTAGGGAgtttt
pegRNA spacer bottom	ctctaaaacTCCCTACCACGCTTCCGGCTC
pegRNA extension top (17-10-25)	gtgcGTCCCAGTTTCGCGGTCGCCCTTCCCTACCACGCT
pegRNA extension bottom (17-10-25)	aaaaAGCGTGGTAGGGAAGGGCGACCGCGAAACTGGGAC
pegRNA extension top (17-13-25)	gtgcGTCCCAGTTTCGCGGTCGCCCTTCCCTACCACGCTTCC
pegRNA extension bottom (17-13-25)	aaaaGGAAGCGTGGTAGGGAAGGGCGACCGCGAAACTGGGAC
pegRNA extension top (17-16-25)	gtgcGTCCCAGTTTCGCGGTCGCCCTTCCCTACCACGCTTCCGGC
pegRNA extension bottom (17-16-25)	aaaaGCCGGAAGCGTGGTAGGGAAGGGCGACCGCGAAACTGGGAC
ngRNA top (-37)	caccGGTGTCATAGCTGTGGGATC
ngRNA bottom (-37)	aaacGATCCCACAGCTATGACACC

Table 3A.2: Oligonucleotide sequences for constructing QRRSPP mutant pegRNA plasmids.

Constructs of QRRSPP Mutation	Sequence (5' – 3')
pegRNA spacer top (20)	caccGAGAAGTCAGGTGGCTCCTCGgtttt
pegRNA spacer bottom (20)	ctctaaaacCGAGGAGCCACCTGACTTCTC
pegRNA extension top (20-39-10)	gtgcTCCCCTGGCCCTGCCCAGCggcggcggcggcggcggcGAGGAGCCACCT
pegRNA extension bottom (20-39-10)	aaaaAGGTGGCTCCTCgccgccgccgccgccgccGCTGGGCAGGGCCAGGGGA
pegRNA extension top (20-39-13)	gtgcTCCCCTGGCCCTGCCCAGCggcggcggcggcggcggcGAGGAGCCACCTGAC
pegRNA extension bottom (20-39-13)	aaaaGTCAGGTGGCTCCTCgccgccgccgccgccgccGCTGGGCAGGGCCAGGGGA
pegRNA extension top (20-39-16)	gtgcTCCCCTGGCCCTGCCCAGCggcggcggcggcggcggcGAGGAGCCACCTGACTTC
pegRNA extension bottom (20-39-16)	aaaaGAAGTCAGGTGGCTCCTCgccgccgccgccgccgccGCTGGGCAGGGCCAGGGGA
ngRNA top (-37)	caccGAGCCTACCTCTCCTCTCCCC
ngRNA bottom (-37)	aaacGGGGAGAGGAGAGGTAGGCTC

Table 3A.3: Oligonucleotide sequences for constructing D311N mutant pegRNA plasmids.

Constructs of D311N Linear Ubiquitin Mutation	Sequence (5' – 3')
pegRNA spacer top (6)	caccGCCAGGCGGATATCTACAAGGgtttt
pegRNA spacer bottom (6)	ctctaaaacCCTTGTAGATATCCGCCTGGC
pegRNA extension top (6-16-14)	gtgcGCCTGGAAGTtCGCCTTGTAGATATCCGCC
pegRNA extension bottom (6-16-14)	aaaaGGCGGATATCTACAAGGCGaACTTCCAGGC
pegRNA extension top (6-21-16)	gtgcTCTCAGCCTGGAAGTtCGCCTTGTAGATATCCGCCTG
pegRNA extension bottom (6-21-16)	aaaaCAGGCGGATATCTACAAGGCGaACTTCCAGGCTGAGA
pegRNA extension top (6-28-16)	gtgcGCCTGCCTCTCAGCCTGGAAGTtCGCCTTGTAGATATCCGCCTG
pegRNA extension bottom (6-28-16)	aaaaCAGGCGGATATCTACAAGGCGaACTTCCAGGCTGAGAGGCAGGC
ngRNA top (-70)	caccGCACCCACCAGGCACTGCGCC
ngRNA bottom (-70)	aaacGGCGCAGTGCCTGGTGGGTGC

Table 3A.4: Oligonucleotide sequences for constructing E391X mutant pegRNA plasmids

Constructs of E391X Zinc Finger Mutation	Sequence (5' – 3')
pegRNA spacer top	caccGCAGAAGTCAGGTGGCTCCTgtttt
pegRNA spacer bottom	ctctaaaacAGGAGCCACCTGACTTCTGC
pegRNA extension top (11)	gtgcCCCCCCCGAGtAGCCACCTGACTTCT
pegRNA extension bottom (11)	aaaaAGAAGTCAGGTGGcTACTCGGGGGGG
pegRNA extension top (13)	gtgcAGCCCCCCCGAGtAGCCACCTGACTTCT
pegRNA extension bottom (13)	aaaaAGAAGTCAGGTGGcTACTCGGGGGGGCT
pegRNA extension top (15)	gtgcGGAGCCCCCCCGAGtAGCCACCTGACTTCT
pegRNA extension bottom (15)	aaaaAGAAGTCAGGTGGcTACTCGGGGGGGCTCC
ngRNA top	caccGCATGAGTGGCCTGTGAGACC
ngRNA bottom	aaacGGTCTCACAGGCCACTCATGC

3A.2 FACS sort and gating of 8-bp KO NEMO

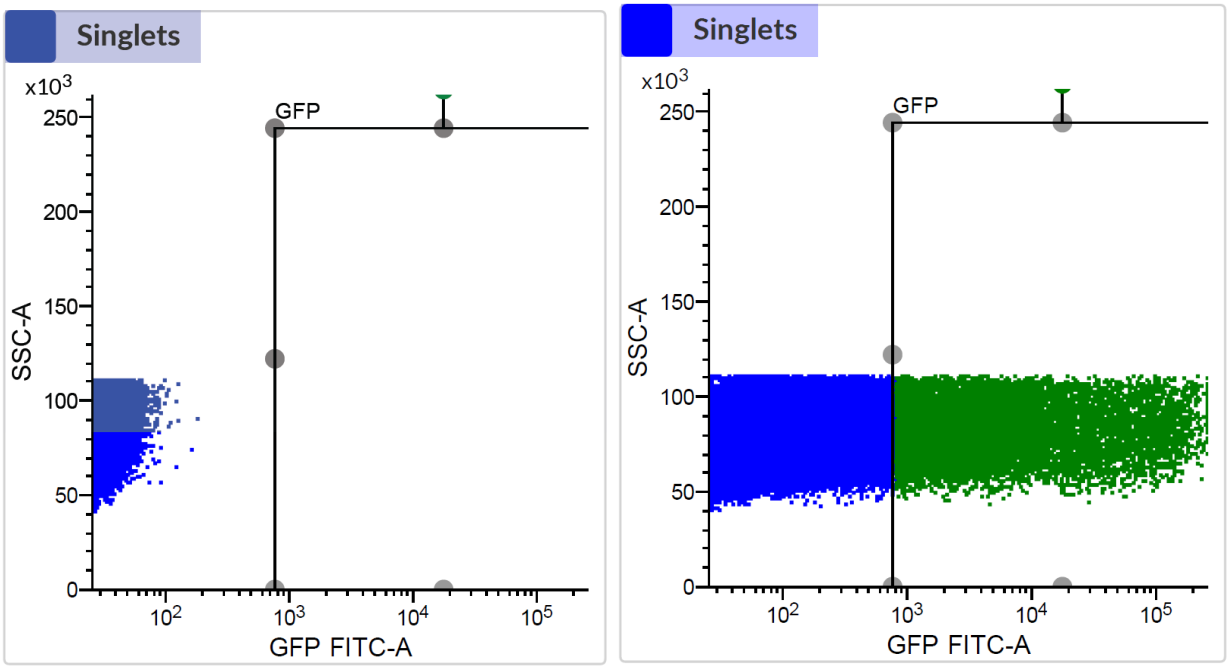

Figure 3A.1: 8-bp KO NEMO transfected HEK293T cells were sorted by GFP fluorescence intensity via FACS into 96-well plates.

Left plot displays the wild-type parental HEK293T cells as the untransfected control and the right plot displays the GFP-positive population selected for single-cell sorting. GFP-positive cells KO NEMO transfection was gated and sorted into 96-well plates for single-cell clonal expansion.

Acknowledgements

Chapter 3, in part is currently being prepared for submission for publication of the material. Luong, Sally; Huxford, Tom. The dissertation author was the primary researcher and author of this material.

Chapter 4 Utilization of mutant NEMO HEK293T cell lines

Introduction

Having established and validated the 6G and D311N NEMO mutant HEK293T cell lines, these cells were utilized alongside wild-type HEK293T cells to dissect the contributions of distinct NEMO binding interactions to canonical TNF-α induced NF-κB activation. The 6G mutation disrupts the secondary IKK2 binding site of NEMO, while the D311N mutation disrupts the linear polyubiquitin binding site, together providing two mechanistically distinct points of intervention within the NF-κB signaling pathway.

Prior to pathway analysis, the responsiveness of HEK293T cells to a panel of canonical and potentially canonical NF-κB inducers was assessed, including TNF-α, LPS, IL-1β, flagellin, and S1P. Of these, only TNF-α was found to activate NF-κB in HEK293T cells, establishing it as the sole inducer used for all subsequent experiments. This finding is consistent with the known limited receptor repertoire of HEK293T cells and confirms that any observed NF-κB activation in this study is attributable specifically to TNF-α mediated canonical signaling[99].

To comprehensively characterize the effect of each NEMO mutation on NF-κB pathway activation, three complementary approaches were used. Western blotting was used to monitor the abundance and phosphorylation status of key proteins involved in NF-κB activation, including IKK1/2, IκBα, and NF-κB p65. NF-κB transcriptional activity was quantified using a luciferase reporter assay, providing a functional readout of pathway activation across multiple time points and conditions. Finally, RT-qPCR was used to measure the expression of NF-κB target genes, capturing the downstream transcriptional consequences of altered NEMO function. Together, these approaches provide a multi-level analysis of how disruption of specific NEMO binding interactions affects the initiation, magnitude, and duration of canonical NF-κB signaling.

The mechanistic contribution of the secondary IKK2 binding site was further investigated by using the 6G NEMO mutant cell line to probe NF-κB pathway activation in the presence of small molecule NF-κB inhibitors. While the genetic disruption of the secondary IKK2 binding site

in 6G NEMO demonstrated a partial reduction in NF-κB activation, the use of pharmacological inhibitors allowed for a more precise dissection of how this mutation affects the responsiveness of the IKK complex to upstream or downstream inhibition. Specifically, if the 6G NEMO mutant responds differently to IKK2 inhibitors compared to wild-type cells, it would suggest that the secondary binding site plays a role in mediating how NEMO interacts with and responds to IKK2 activity. Of particular interest is whether the 6G mutant displays reduced sensitivity to IKK2 inhibition relative to wild-type cells, which would indicate that the secondary IKK2 binding site normally contributes to the inhibitor's mechanism of action and by extension, that this interaction is a functionally relevant point of regulation within the canonical NF-κB signaling pathway. Together, the genetic and pharmacological approaches provide complementary lines of evidence for understanding the precise role of the secondary IKK2 binding site in NEMO-mediated NF-κB activation.

Results

4.1 Assessment of canonical NF-κB activation in HEK293T cells by multiple NF-κB inducers

Lipopolysaccharide (LPS), interleukin-1β (IL-1β), flagellin, sphingosine-1-phosphate (S1P), and phorbol myristate acetate (PMA) were screened as potential NF-κB inducers in wild-type HEK293T cells. Each stimulus was applied at their respective concentrations and at various time points, and cells were harvested for cytoplasmic and nuclear fractionation following the same protocol used for TNF-α stimulation.

LPS failed to activate NF-κB, consistent with the well-documented absence of Toll-like receptor 4 (TLR4) expression in HEK293T cells, which is required for LPS recognition and downstream signaling[99]. PMA, while capable of inducing NF-κB nuclear translocation, does not represent a canonical inducer as it bypasses IκBα degradation and activates NF-κB through a protein kinase C (PKC)-dependent mechanism[100,101]. For the remaining inducers, IL-1β, flagellin, and S1P, it remains unclear whether HEK293T cells express the correct receptors for their recognition. Although some evidence of NF-κB pathway activation was observed with these inducers, the absence of confirmed receptor expression in HEK293T cells means these results cannot be conclusively attributed to canonical NF-κB signaling[35,102,103]. Collectively, these findings highlight the limited receptor repertoire of HEK293T cells and establish TNF-α as the only validated canonical NF-κB inducer in this cell line for use in subsequent experiments.

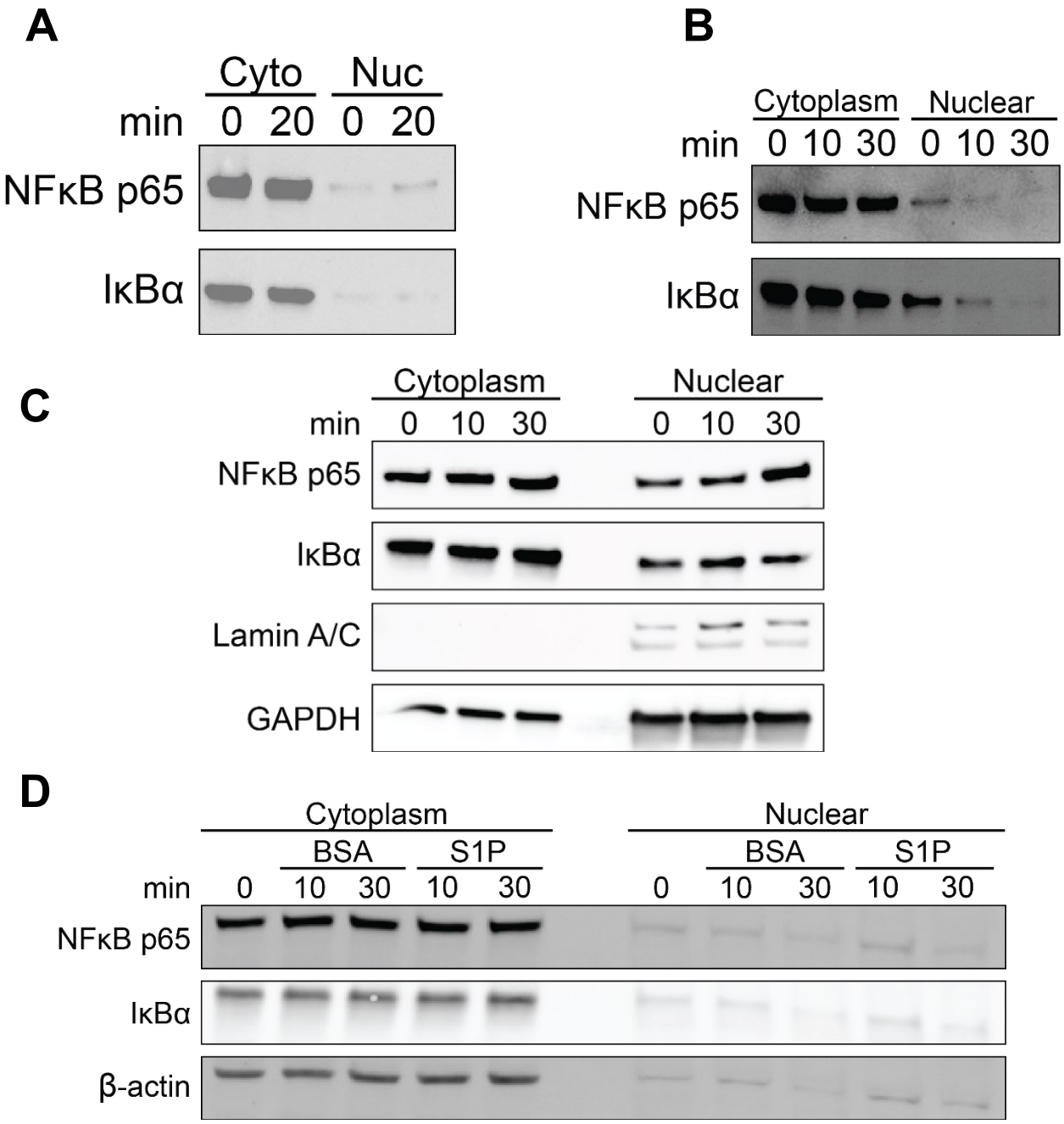

Figure 4.1: Activation of NF-κB over time by inducing wild-type HEK293T cell lines with various inducers.

Cells were treated with the inducer and nuclear extracted to separate cytoplasmic and nuclear fractions. The fractions were run on a gel, transferred onto nitrocellulose, and probed with NF-κB, IκBα, Lamin A/C, and β-actin antibodies. A) Cells were treated with 1 μg/mL LPS and harvested after 0 and 20 minutes. B) Cells were treated with 10 ng/mL IL-1β and harvested after 0, 10 and 30 minutes. C) Cells were treated with 1 μg/mL PMA and harvested after 0, 10 and 30 minutes. D) Cells were treated with 4 mg/mL BSA control and 1 μM S1P, respectively, and then harvested after 0, 10 and 30 minutes.

4.2 Probing the IKK2 activation and phosphorylation of TNF-α induced mutant NEMO HEK293T cell lines

Wild-type, AbCam NEMO knockout, 6G, and D311N NEMO mutant HEK293T cells were stimulated with 10 ng/mL TNF-α and harvested at 0, 10, and 30 minutes post-stimulation. Cytoplasmic fractions obtained from nuclear extraction were analyzed by western blot and probed for IKK2, phospho-IKK2, NEMO, and linear polyubiquitin, with either GAPDH or Ponceau S staining used as a loading control.

Anti-IKKγ/NEMO antibody was used to confirm the presence of NEMO within the cytoplasmic lysate of the cell lines (Figure 4.2). Wild-type cell line showed two bands in between the molecular weight marker of 50 kDa. The most common isotype form of NEMO is at 48 kDa, but there is also another form at 55kDa. The two bands we determine to be both isotypes. KO NEMO shows one band below the 50 kDa marker, which we could think would be the 48 kDa isotype but based on KO NEMO product description, it is a truncated version of NEMO. 6G NEMO cell line only shows one 55 kDa isoform instead of both isoforms and D311N NEMO have both, similar to wild-type. Anti-mouse IKKγ/NEMO antibody was used as a verifying antibody by accident however still showed cross-reactivity with human NEMO. It shows a band below 50 kDa marker for all cell lines, which could mean that the first NEMO antibody may require a confirmational change in the protein that is attributed by the secondary binding site. Overall, these mutant cell lines have NEMO intact and present.

Qualitatively, in wild-type cells, phosphorylated IKK2 levels increased over time following TNF-α stimulation, consistent with intact canonical NF-κB pathway activation (Figure 4.3). The AbCam NEMO knockout cell line similarly displayed an increase in phospho-IKK2, the presence of a truncated NEMO protein, suggesting that residual NEMO activity is sufficient to support IKK2 phosphorylation and NF-κB activation. This finding further supports the exclusion of the AbCam NEMO knockout from subsequent assays, as it does not represent a true loss-of-function model. The 6G NEMO mutant exhibited detectable but reduced levels of IKK2 phosphorylation

compared to wild-type, indicating partial impairment of IKK complex activation in response to TNF-α stimulation. Notably, the D311N NEMO mutant also exhibited detectable levels of phospho-IKK2, which appears inconsistent with the complete absence of NF-κB nuclear translocation and IκBα degradation observed in the fractionation western blot.

Quantitative analysis on the western blot was also performed using ImageJ. The intensity, shape and size of the bands were processed, analyzed and inputted in Excel. The phosphorylated IKK2 bands were divided by total amount of IKK2 and then normalized using the time point 0. For wild-type cells, 10 minute stimulation was 28X more phosphorylation than unstimulated. KO NEMO was 15X more phosphorylation, 6G NEMO had about 9X more phosphorylation, and D311N showed a little more than 2X more than unstimulated. Although the total IKK2 protein differed between cell lines, the quantitative analysis still showed that 6G NEMO still was able to display phosphorylation of IKK2.

For D311N NEMO, we could visually see phosphorylation bands on the western blot however when we analyzed the data using ImageJ and dividing the phosphorylated protein by total protein, the data shows that D311N only has residual phosphorylation that does not complete the NF-κB pathway, consistent with the previous western blot. To see if linear ubiquitin accumulated in activated cells, anti-linear ubiquitin was used to probe the cytosolic lysates of the cells.

Linear polyubiquitin bands on the western blot did not reveal consistent or interpretable differences across cell lines (Figure 4.3). Unexpectedly, D311N cells displayed larger linear polyubiquitin bands relative to wild type, which is inconsistent with the expectation that disruption of linear polyubiquitin binding in D311N would reduce detectable linear polyubiquitin association with NEMO. Similarly, 6G NEMO cells showed lower linear polyubiquitin levels relative to wild-type, which is also unexpected given that the 6G mutation does not disrupt linear polyubiquitin binding and would therefore be predicted to show comparable levels to wild-type. These contradictory observations suggest that western blotting is not an appropriate method for

assessing NEMO-linear polyubiquitin association, as it reflects the total abundance of linear polyubiquitin present in the cytoplasmic fraction rather than the specific interaction between linear polyubiquitin and NEMO.

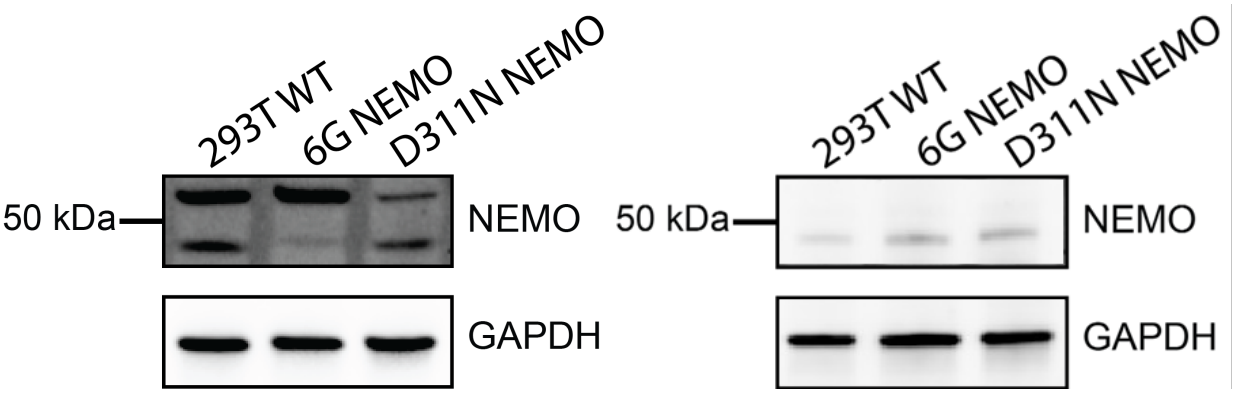

Figure 4.2: Protein expression of NEMO/IKKγ in cell lines.

Cell lysates were probed with either anti-human NEMO/IKKγ (left) or anti-mouse NEMO/IKKγ (right) and anti-human GAPDH for loading control.

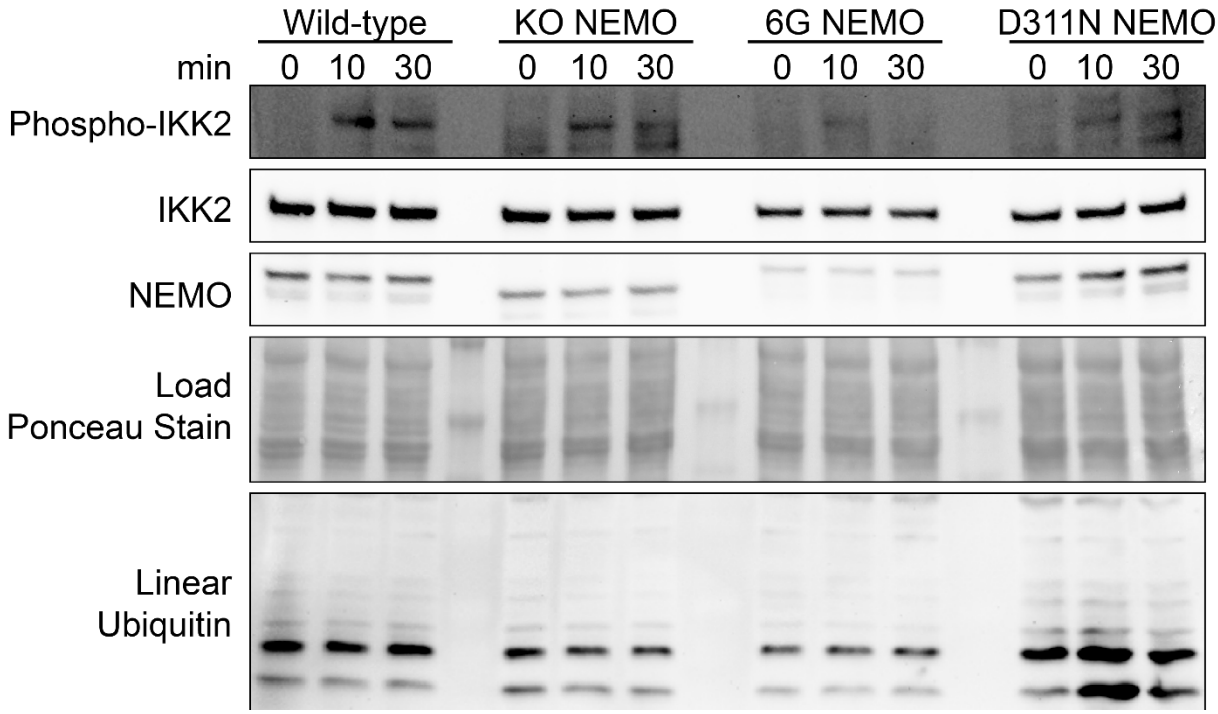

Figure 4.3: Monitoring activation of IKK2 over time through treatment of mutant HEK293T cell lines with TNF-α.

Cells were treated with 10 ng/mL TNF-α over 0, 10 and 30 minute time points. Cytoplasmic fractions were run on a gel, transferred to nitrocellulose membrane, and probed with phospho-IKK2, IKK2, NEMO, and linear ubiquitin antibodies. Ponceau stain was used to visualize loading.

4.3 Orthogonal validation of TNF-α induced NF-κB activation in NEMO mutant HEK293T cell lines

Stable NEMO mutant HEK293T cell lines containing the NF-κB luciferase reporter were stimulated with 20 ng/mL TNF-α and harvested at 10 minutes, 30 minutes, 1, 2, 3, 4, and 5 hours post-stimulation. Relative light units (RLU) were averaged across biological and technical triplicates at each time point and normalized to the lowest RLU time point (30 minutes) to calculate fold induction. Wild-type HEK293T cells exhibited the highest fold induction, with luciferase activity progressively increasing through 5 hours post-stimulation. The 6G NEMO mutant displayed fold induction values of at least half that of wild-type cells across all time points, while D311N NEMO exhibited approximately half the fold induction of the 6G mutant, indicating a stepwise reduction in NF-κB transcriptional activity corresponding to the degree of NEMO functional impairment seen in the western blot.

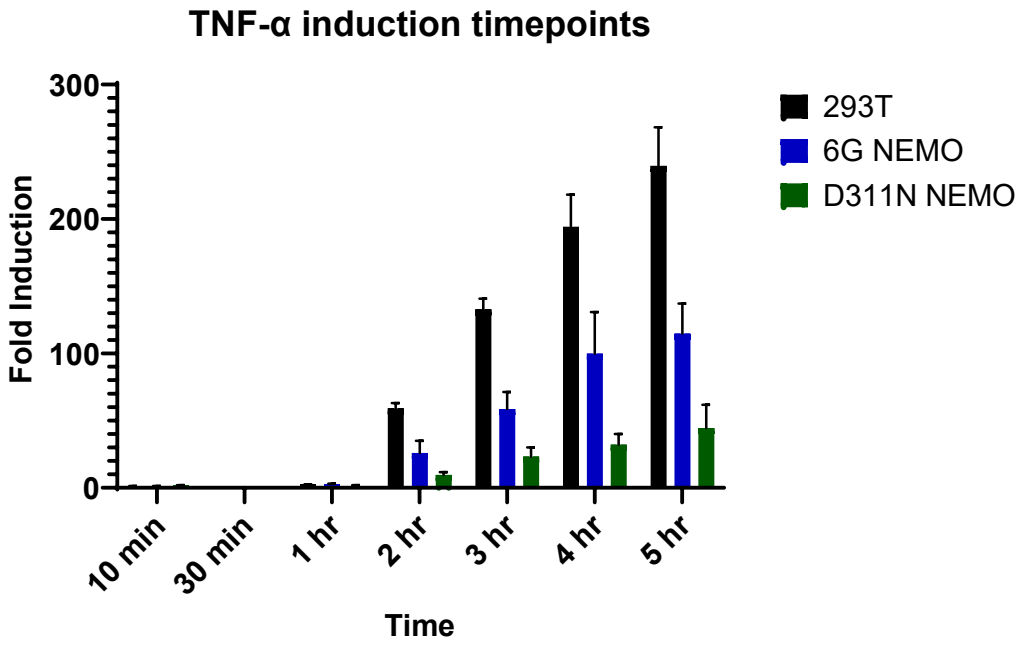

Figure 4.4: Nano-Glo luciferase assay NF-κB reporter of mutant NEMO cell lines against TNF-α.

10 minutes to 5 hours stimulation of TNF-α on HEK293T wild type, 6G NEMO 293T, and D311N NEMO 293T and fold induction was calculated on luminescence. 293T had the largest increase of fold induction followed by 6G NEMO and then D311N NEMO.

4.4 Differences in gene expression profile of TNF-α induced NF-κB activation between mutant cell lines

The relative gene expression of IκBα was measured in wild-type, 6G, and D311N NEMO HEK293T cells following TNF-α stimulation up to 120 minutes using the 2^−ΔΔCt method, normalized to the reference housekeeping gene and the 0-minute time point. IκBα expression peaked at 60 minutes post-stimulation across all cell lines before declining at 120 minutes, reflecting the well-characterized negative feedback loop in which NF-κB-driven IκBα resynthesis terminates NF-κB transcriptional activity (Figure 4.5). IκBα induction followed a stepwise pattern consistent with the luciferase assay results, with wild-type cells exhibiting the highest expression, 6G NEMO cells approximately half that of wild-type, and D311N cells approximately half that of 6G NEMO. These results support the well-established role of linear polyubiquitin binding to NEMO in canonical NF-κB activation, while the partial retention of activity in the 6G mutant suggests that the secondary IKK2 binding site contributes to but is not strictly required for IKK complex activation, as NEMO retains its ability to bind linear polyubiquitin in its absence.

Several additional NF-κB target genes were assessed at 60 minutes post-stimulation, corresponding to the peak of IκBα gene expression (Figure 4.6). IκBζ is a nuclear IκB protein that is primarily induced by LPS or IL-1 but can be upregulated at lower levels through TNF-α-mediated NF-κB activation[104–106]. Wild-type cells displayed a detectable increase in IκBζ gene expression. However, this was approximately 3-fold lower than the IκBα response, consistent with TNF-α being a weaker inducer of IκBζ relative to LPS or IL-1. Both 6G and D311N NEMO mutants showed a comparable reduction in IκBζ gene expression relative to wild-type, reflecting the impaired NF-κB transcriptional activity observed in these cell lines.

A20 is a negative regulator of NF-κB that promotes deubiquitination of RIPK1 and TRAF6 to attenuate NF-κB signaling[66,107,108]. Its gene expression followed the same trend as IκBα and IκBζ, with wild-type cells displaying the highest gene expression, followed by a stepwise reduction in 6G and then D311N NEMO mutants. c-FLIP, an anti-apoptotic gene induced by NF-κB, showed

no change in gene expression in wild-type cells following TNF-α stimulation, while both 6G and D311N NEMO mutants displayed a small but detectable decrease in c-FLIP expression[109]. Because there is an ambiguous upregulation in wild type cFLIP, increasing the timepoint at which RNA is harvested could show a more significant upregulation and a clearer difference between wild type and the mutants[110]. SOD1, a stress response gene reported to be induced by NF-κB, showed no significant change in gene expression across any of the cell lines. This is consistent with SOD1 upregulation being predominantly regulated through the PI3K/Akt signaling pathway rather than canonical NF-κB activation[111,112].

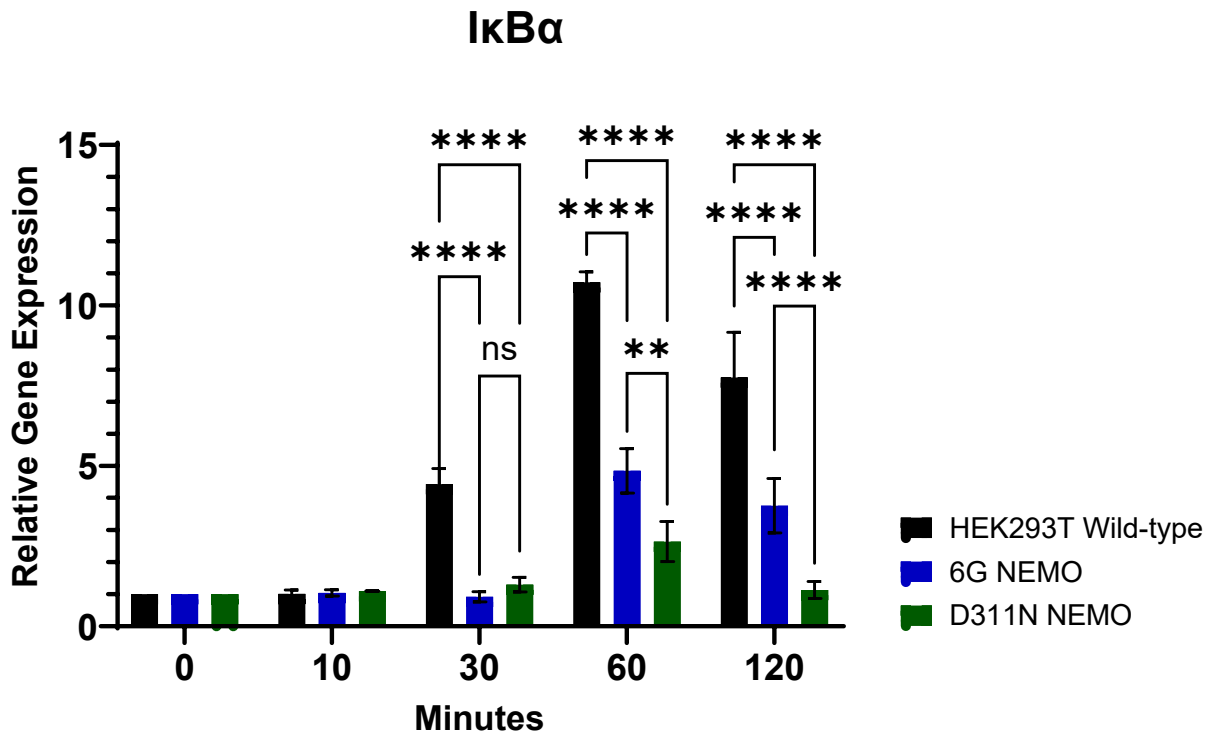

Figure 4.5: Relative gene expression of IκBα in TNF-α stimulated cells over 2 hours.
Wild-type, 6G NEMO and D311N NEMO were stimulated with 10 ng/mL TNF-α over 10, 30, 60 and 120 minutes. RNA was harvested from each timepoint and converted into cDNA. Relative gene expressions were quantified by RT-qPCR using SYBR Green. Data was normalized to its zero timepoint and significance was calculated through GraphPad Prism.

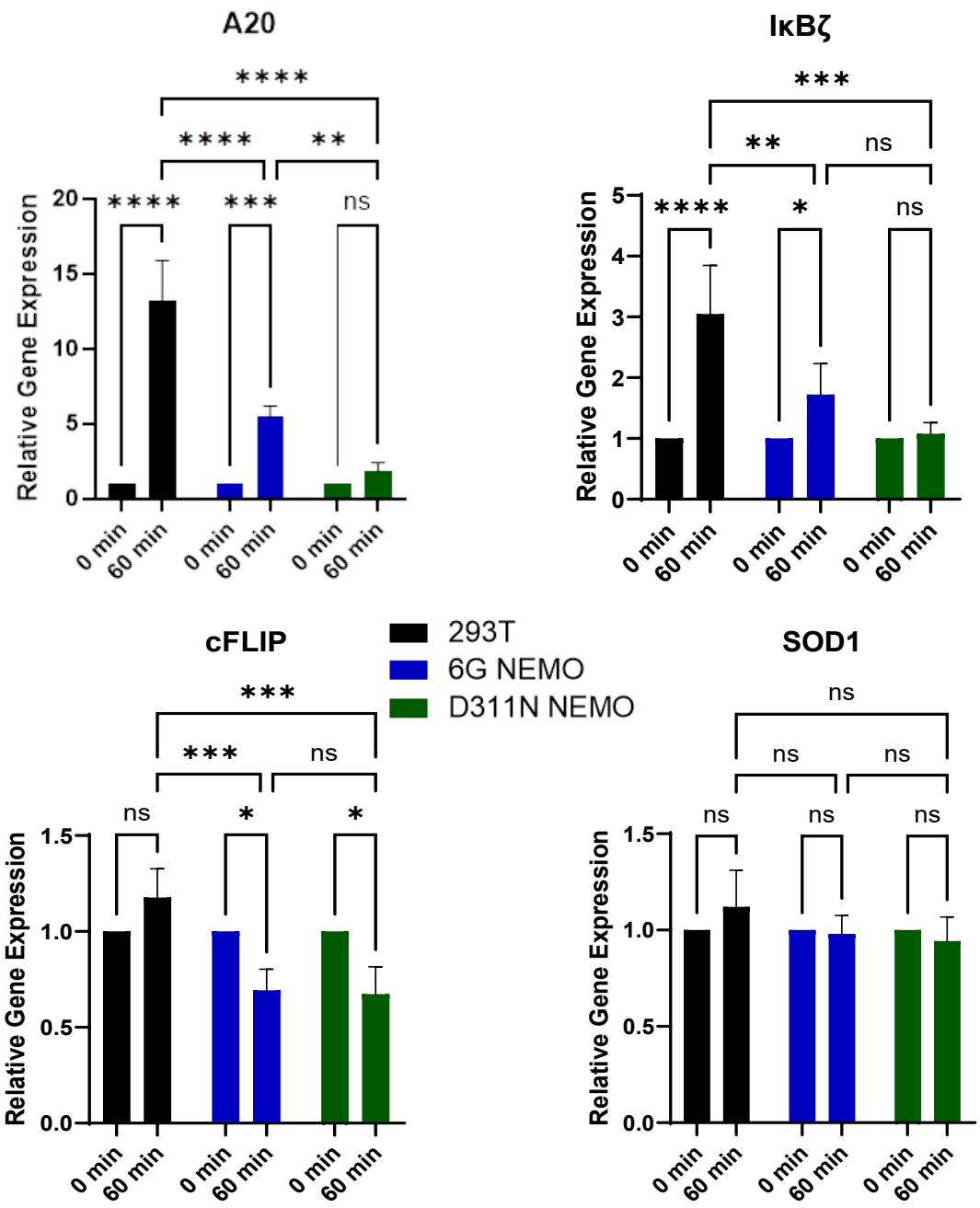

Figure 4.6: Relative gene expression of NF-κB target genes in TNF-α-stimulated NEMO mutant cell lines.

Wild-type, 6G, and D311N NEMO HEK293T cells were stimulated with 10 ng/mL TNF-α for 60 minutes and harvested for total RNA extraction. RNA was reverse transcribed into cDNA and relative gene expression of A20, IκBζ, c-FLIP, and SOD1 was quantified by RT-qPCR using SYBR Green. Expression values were normalized to the 0-minute time point and statistical significance was determined using GraphPad Prism.

4.5 Initial testing of NF-κB activation pathway inhibitors against mutant cell lines

Wild-type and 6G NEMO mutant HEK293T cells were treated with three small molecule NF-κB inhibitors: MLN120B, an IKK2 inhibitor; BMS-345541, an allosteric IKK1/IKK2 inhibitor; and Hoipin-8, a LUBAC inhibitor that blocks HOIL-1L, a component of the LUBAC complex responsible for attaching linear polyubiquitin chains to NEMO[113–115]. Wild-type cells served as the positive control and D311N NEMO was included as a negative control for the luciferase assay. The rationale for testing inhibitors on wild-type and 6G NEMO cells was to determine whether the secondary IKK2 binding site mutation affects the sensitivity of the pathway to upstream inhibition. If the inhibitors suppress NF-κB activation in wild-type cells but not in 6G NEMO, it suggests that 6G NEMO is insensitive to IKK2 inhibition, potentially due to altered IKK complex dynamics resulting from loss of the secondary binding site. Conversely, if both cell lines are inhibited to the same extent, it would indicate that 6G NEMO remains downstream of the inhibitor's target, as is expected for Hoipin-8, which acts upstream of NEMO at the level of LUBAC-mediated linear polyubiquitin chain generation.

Despite multiple attempts, MLN120B failed to reproducibly inhibit NF-κB activation, likely due to solubility issues under the experimental conditions that prevented the compound from remaining in solution. BMS-345541 and Hoipin-8 both demonstrated inhibitory effects on NF-κB activation in western blot assays, though the results were inconsistent across experiments. In an assay where inhibitors were pre-incubated for 24 hours, BMS-345541 showed modest inhibition as evidenced by reduced IκBα degradation and NF-κB nuclear translocation compared to the stimulated control, while Hoipin-8 showed less inhibition under the same conditions. In contrast, when the inhibitor pre-incubation was reduced to 1 hour, Hoipin-8 demonstrated greater inhibitory effects while BMS-345541 showed little inhibition. These inconsistencies suggest that the two inhibitors have different optimal incubation requirements. BMS-345541 may require prolonged incubation to achieve sufficient intracellular concentration to inhibit NF-κB

activation, while extended incubation may lead to degradation of Hoipin-8 and loss of its inhibitory activity over time.

To complement the western blot data, a luciferase reporter assay was performed as an orthogonal readout of NF-κB transcriptional activity. Fold induction was plotted by normalizing stimulated cells treated with or without inhibitors to unstimulated cells and analyzed by two-way ANOVA using GraphPad Prism. Statistical analysis revealed no significant difference between the inhibitor-treated groups and the untreated stimulated control, indicating that the experimental conditions require further optimization before definitive conclusions can be drawn regarding the effect of these inhibitors on NF-κB activation in the 6G NEMO mutant background. Future experiments should systematically optimize inhibitor concentration, pre-incubation time, and solvent conditions to establish reproducible inhibition before evaluating the differential sensitivity of wild-type and 6G NEMO cells to each inhibitor.

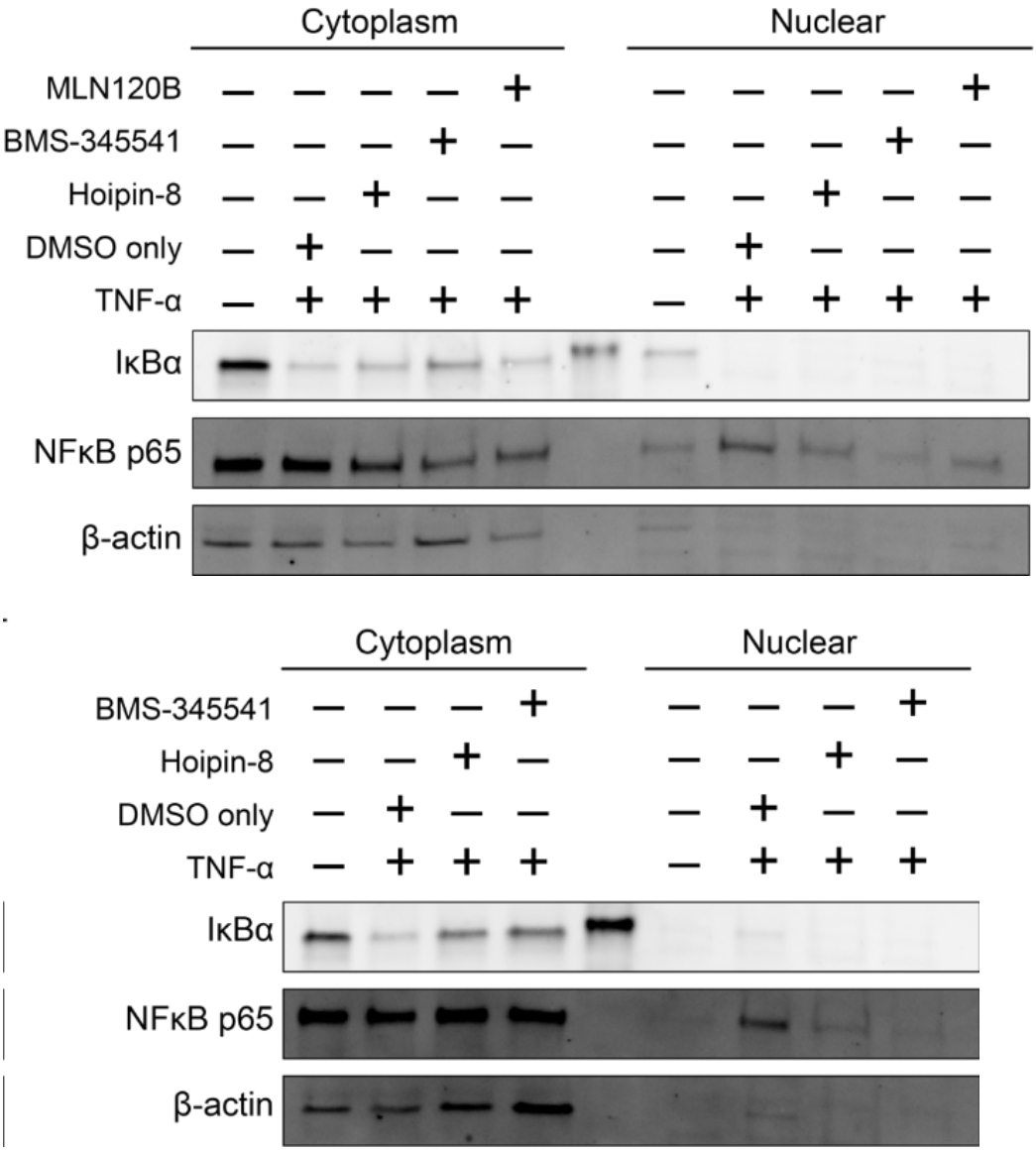

Figure 4.7: Effect of 24-hour inhibitor pre-incubation on TNF-α-induced NF-κB activation in wild-type and 6G NEMO HEK293T cells.

Wild-type and 6G NEMO HEK293T cells were pre-incubated for 24 hours with serum-free media alone, DMSO vehicle control, Hoipin-8, BMS-345541, or MLN120B prior to TNF-α stimulation for 30 minutes to induce NF-κB activation. Top blot shows wild-type HEK293T cells and bottom blot shows 6G NEMO mutant cells.

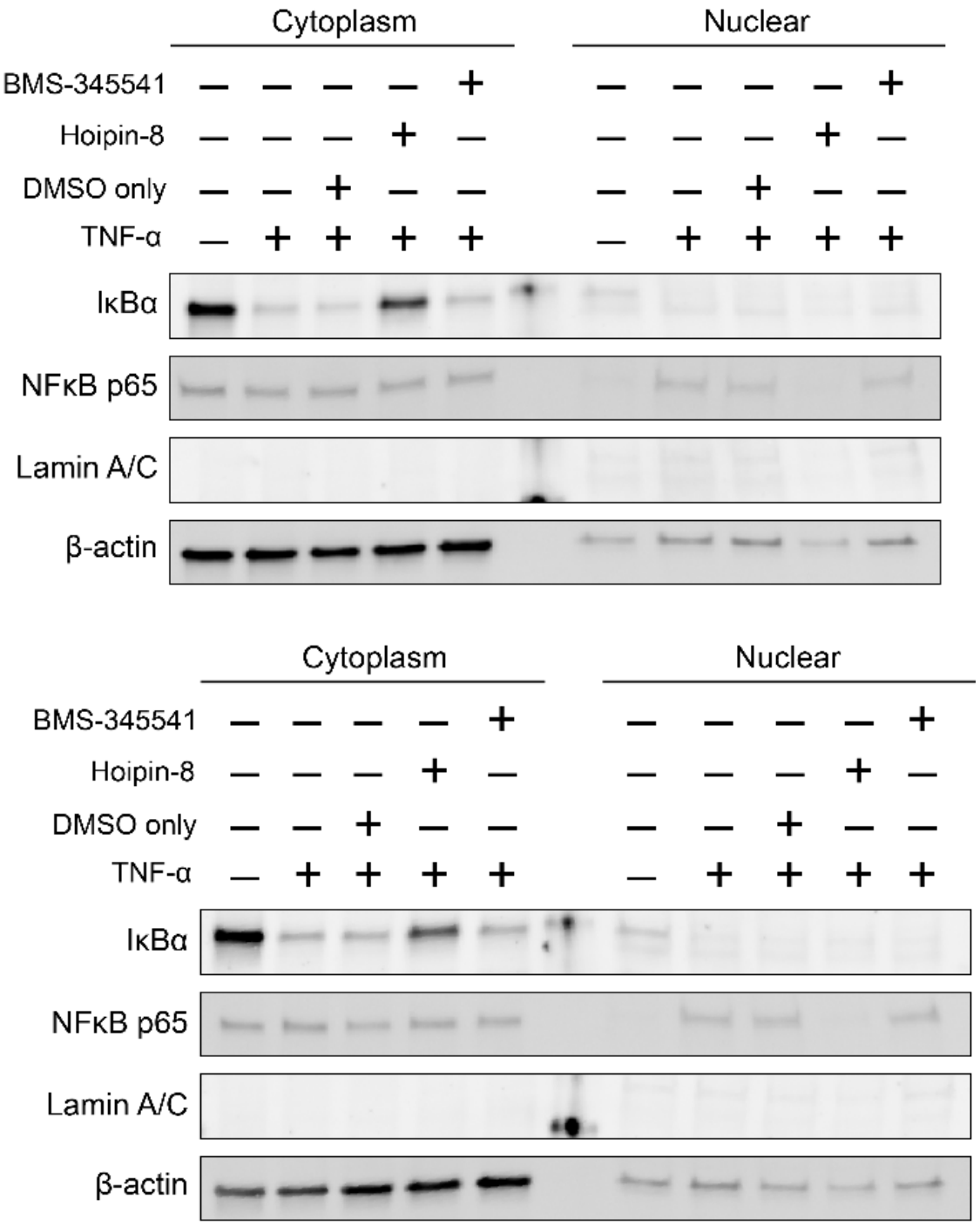

Figure 4.8: Effect of 1 hour inhibitor pre-incubation on TNF-α-induced NF-κB activation in wild-type and 6G NEMO HEK293T cells.

Wild-type and 6G NEMO HEK293T cells were pre-incubated for 1 hour with serum-free media alone, DMSO vehicle control, Hoipin-8 or BMS-345541 prior to TNF-α stimulation for 30 minutes to induce NF-κB activation. Top blot shows wild-type HEK293T cells and bottom blot shows 6G NEMO mutant cells.

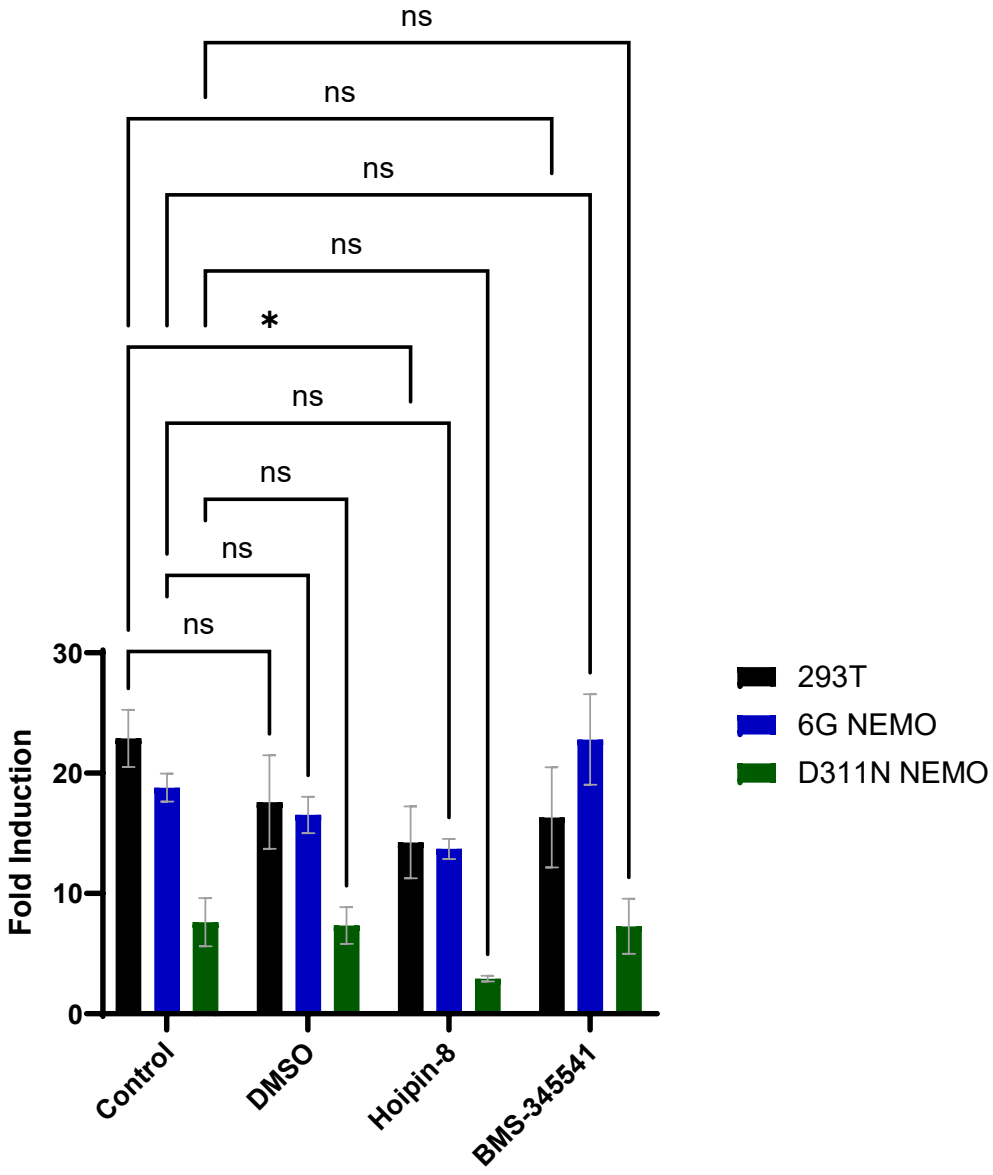

Figure 4.9: NF-κB luciferase reporter activity in inhibitor-treated NEMO mutant HEK293T cell lines.

Wild-type, 6G, and D311N NEMO HEK293T cells were pre-incubated with serum-free media alone, DMSO vehicle control, Hoipin-8, or BMS-345541 for 24 hours prior to TNF-α stimulation for 5 hours. Statistical significance between cell lines and inhibitor-treated groups was determined by two-way ANOVA using GraphPad Prism software, with no significant differences detected between the uninhibited positive control and inhibitor-treated conditions.

Discussion

NEMO is an essential regulatory subunit of the IKK complex, playing a central role in canonical NF-κB activation through multiple binding interactions, including linear polyubiquitin chain association and conformational changes that facilitate IKK complex assembly. Given the diversity of canonical NF-κB inducers and the convergence of their signaling on NEMO, we hypothesized that NEMO plays a role in differentiating the cellular response to distinct canonical inducers. To investigate this, two NEMO mutant HEK293T cell lines were generated by CRISPR-Cas9 prime editing: the 6G mutant, disrupting the secondary IKK2 binding site, and the D311N mutant, disrupting the linear polyubiquitin binding site. Before continuing to analysis pathway differences, HEK293T cells were screened against a panel of canonical NF-κB inducers, TNF-α, LPS, IL-1β, flagellin, and S1P, and found to be responsive only to TNF-α. As TNF-α was the only canonical inducer capable of activating NF-κB in HEK293T cells, subsequent analyses focused on characterizing the role of each NEMO mutation in TNF-α-induced canonical NF-κB activation.

Differences in NF-κB activation between the NEMO mutants and wild-type cells were assessed using three complementary approaches. Western blot analysis of cytoplasmic fractions probed for IKK2, phospho-IKK2, NEMO, and linear polyubiquitin. An AbCam NEMO knockout cell line was initially included as a control but was found to retain NF-κB activation due to the presence of a truncated NEMO protein and was therefore excluded from further analysis, leaving wild-type, 6G, and D311N NEMO as the three cell lines carried forward for all further experiments.

Among these cell lines, IKK2 phosphorylation increased over time in all cases following TNF-α stimulation, with wild-type cells displaying the highest levels. Notably, the detection of phospho-IKK2 in D311N cells, despite the complete absence of IκBα degradation and NF-κB nuclear translocation, was clear and present. However, analyzing the western blot and normalizing the ratio of phosphorylated IKK2 to total protein showed that there was minimal phosphorylation compared to wild-type, concluding that D311N shows insignificant phosphorylation that does not lead to clear activation of NF-κB signaling pathway. Linear

polyubiquitin band intensities were inconsistent across cell lines and did not follow the expected pattern of reduced linear polyubiquitin in the D311N mutant. This inconsistency is likely attributable to the nature of the western blot readout itself, which reflects the total abundance of linear polyubiquitin in the cytoplasmic fraction rather than the specific association of linear polyubiquitin with NEMO. As such, western blotting is not an appropriate method for assessing NEMO-linear polyubiquitin binding, and a more targeted approach such as co-immunoprecipitation would be required to specifically evaluate this interaction.

NF-κB transcriptional activity was quantified using a luciferase reporter assay in which wild-type, 6G, and D311N NEMO cell lines stably expressing the NF-κB luciferase reporter were stimulated with TNF-α for up to 5 hours. The 6G mutant exhibited approximately half the luciferase activity of wild-type cells, while D311N exhibited approximately half that of 6G, indicating a stepwise reduction in NF-κB transcriptional output consistent with the previous western blot results. This trend was further corroborated by RT-qPCR analysis of NF-κB target genes, including IκBα, IκBζ, and A20, all of which followed the same stepwise pattern across cell lines, confirming that the reduction in NF-κB activity in the NEMO mutants is reflected at the level of downstream gene expression. Overall, these three techniques showed the same results of 6G NEMO having the ability to activate NF-κB in a lower response compared to wild-type but higher than that of D311N. 6G NEMO results are not surprising because 6G NEMO has the ability to still binding to linear ubiquitin and thus IKK complex can still become activate with linear ubiquitin but without the secondary binding site.

To further probe the mechanism of the secondary IKK2 binding site, small molecule inhibitors targeting upstream and downstream components of the NF-κB pathway, Hoipin-8 and BMS-345541, were applied to wild-type and 6G NEMO cells. Western blot data from inhibitor-treated cells were inconsistent across experiments, and luciferase reporter assays revealed no statistically significant difference between inhibitor-treated and untreated conditions, indicating that the experimental conditions require further optimization before definitive conclusions can

be drawn. Nevertheless, these experiments establish a framework for using pharmacological inhibition to probe the functional consequences of the secondary IKK2 binding site mutation, and future studies with optimized inhibitor concentrations and incubation conditions may reveal differential sensitivity between wild-type and 6G NEMO cells. Collectively, the data presented in this chapter demonstrate that the 6G mutation produces a partial and modulatory impairment of canonical NF-κB activation, in contrast to the complete abolition observed in D311N, establishing that the secondary IKK2 binding site and the linear polyubiquitin binding site play distinct and non-redundant roles in NEMO-mediated NF-κB signaling.

Acknowledgements

Chapter 4, in part is currently being prepared for submission for publication of the material. Luong, Sally; Huxford, Tom. The dissertation author was the primary researcher and author of this material.

Chapter 5 Preparation of mutant NEMO U-2 OS cell lines using CRISPR-Cas9 prime editing

Introduction

Western blot analysis confirmed that HEK293T cells have a limited receptor repertoire, restricting canonical NF-κB activation to TNF-α stimulation alone. While this allowed for the characterization of differences in TNF-α induced NF-κB activation between the NEMO mutant cell lines, it did not address the broader question of how NEMO differentiates between distinct canonical NF-κB inducers. To investigate this, the same prime editing methodology used to generate the NEMO mutant HEK293T cell lines was applied to generate equivalent mutant cell lines in U-2 OS cells.

U-2 OS cells were selected as a complementary model system due to their responsiveness to a broader range of canonical NF-κB inducers, their established use in NF-κB signaling studies, and their responsiveness to transfection. Although U-2 OS cells are a hypertriploid female cell line, they have been successfully used in gene editing studies, confirming that genomic modification is achievable in this cell line, although with greater difficulty compared to HEK293T cells[116,80]. Prior to generating mutant cell lines, U-2 OS cells were stimulated with a panel of canonical NF-κB inducers to confirm pathway responsiveness. NF-κB activation was confirmed in response to both TNF-α and IL-1β, which signal through distinct upstream pathways providing two mechanistically distinct contexts in which to investigate the role of NEMO's binding interactions in canonical NF-κB signaling.

The validated 6G and D311N pegRNA and ngRNA constructs described in Chapter 3 were used to transfect U-2 OS cells, which were subsequently subjected to fluorescence-activated cell sorting and Sanger sequencing to assess the efficiency of prime editing in this cell line. However, U-2 OS cells presented unique challenges for gene editing that complicated the generation of stable mutant cell lines, as described in the results.

Results

5.1 Assessment of various NF-κB canonical inducers on U-2 OS cell line

U-2 OS cells were stimulated with a panel of canonical NF-κB inducers, TNF-α, IL-1β, LPS, flagellin, and PMA, for 10 and 30 minutes before harvesting for cytoplasmic and nuclear fractionation. Western blot analysis of both fractions probed for the hallmarks of canonical NF-κB activation: IκBα degradation in the cytoplasmic fraction and NF-κB p65 nuclear translocation. β-actin and Lamin A/C were used as cytoplasmic and nuclear loading controls, respectively.

TNF-α and IL-1β both robustly activated NF-κB, as evidenced by a marked reduction in cytoplasmic IκBα and a clear increase in nuclear NF-κB p65 at both time points. LPS and flagellin showed modest reductions in IκBα band intensity at 30 minutes compared to 10 minutes, suggesting partial or delayed NF-κB activation, though the response was considerably weaker than that observed with TNF-α and IL-1β. PMA, which canonically activates NF-κB through a protein kinase C-dependent mechanism that does not involve IκBα degradation, unexpectedly showed complete loss of the IκBα band at 30 minutes and a faint nuclear NF-κB p65 signal, suggesting that PMA may engage both IκBα-dependent and -independent NF-κB activation mechanisms in U-2 OS cells, though further investigation would be required to confirm this observation.

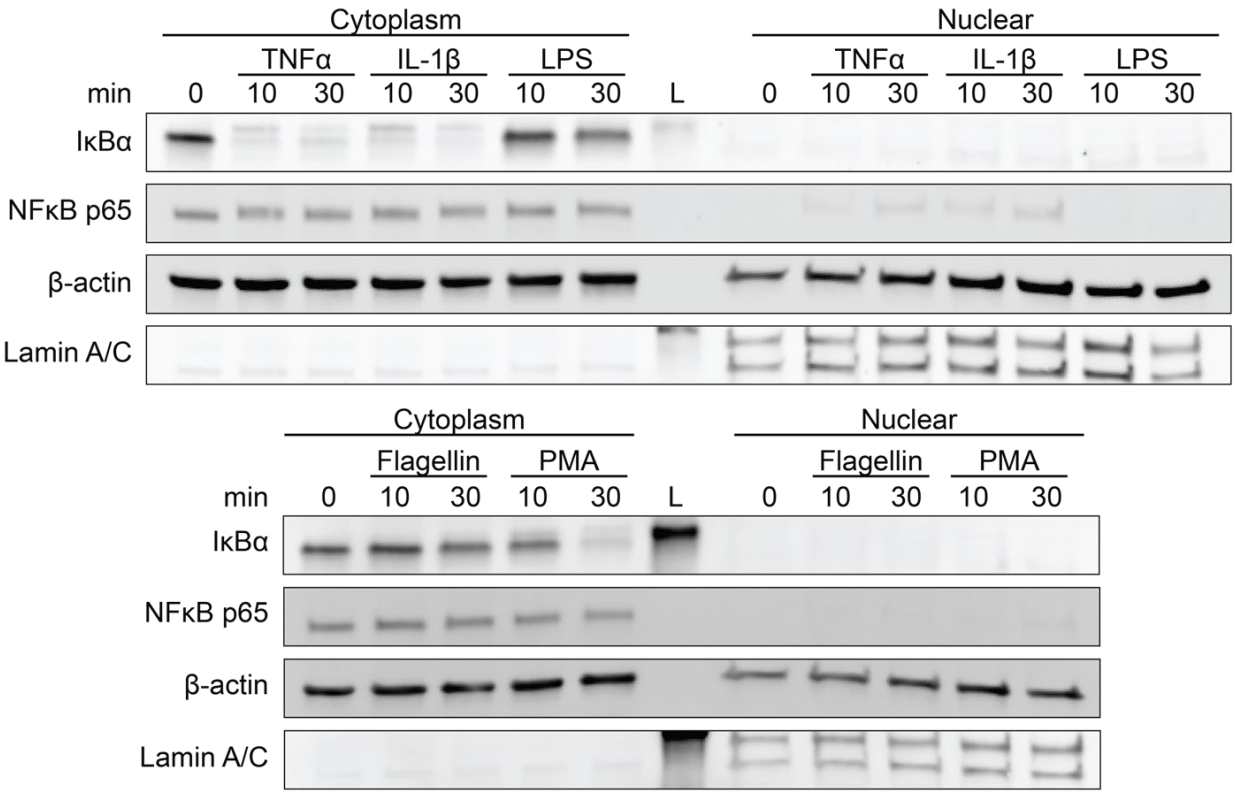

Figure 5.1: Western blot analysis of canonical NF-κB activation in U-2 OS cells stimulated with multiple NF-κB inducers.

Parental U-2 OS cells were stimulated with TNF-α (10 ng/mL), IL-1β (10 ng/mL), LPS (1 μg/mL), flagellin (10 ng/mL), or PMA (1 μg/mL) for 10 and 30 minutes before harvesting for cytoplasmic and nuclear fractionation. Membranes were probed with antibodies against IκBα, NF-κB p65, β-actin, and Lamin A/C.

5.2 Fluorescence Activated Cell Sorting (FACS)

Flow cytometry was used to identify and sort single-cell particles based on GFP fluorescence intensity. Parental U-2 OS cells served as the negative control, setting the baseline for GFP signal. Transfected U-2 OS cells for both the 6G and D311N mutations displayed an increase in GFP fluorescence compared to the parental control, confirming successful uptake and expression of the GFP co-expressing CRISPR-Cas9 plasmid prior to single-cell sorting. The cells in the GFP gate were sorted into 1 cell per well in a 96-well plate and the surviving cells were subjected to Sanger sequencing.

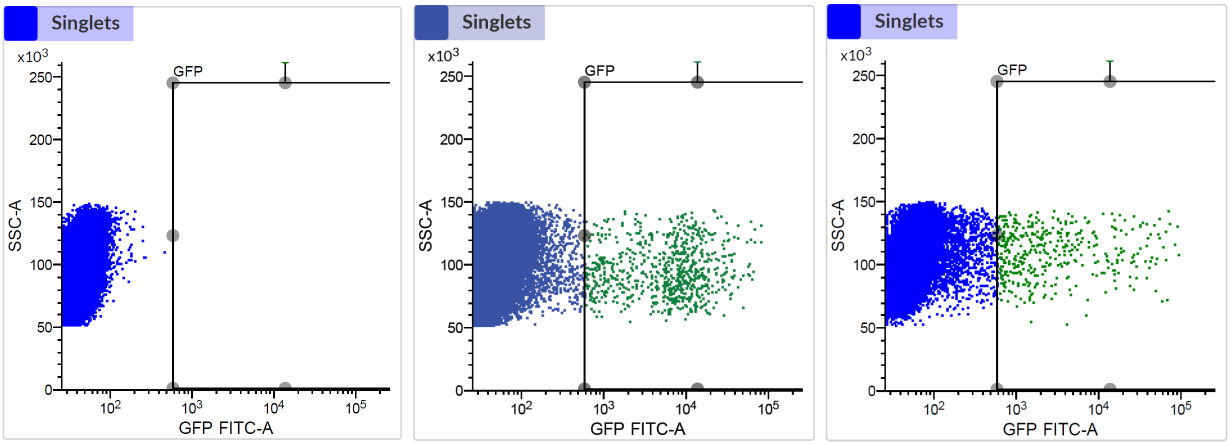

Figure 5.2: Flow cytometry dot plots of single-cell sorting for parental and NEMO mutant transfected U-2 OS cells.

Parental U-2 OS cells served as the untransfected control (left plot), 6G NEMO (middle plot) and D311N NEMO (right plot) transfected U-2 OS cells were gated on GFP fluorescence intensity to identify and sort GFP-positive single cells for clonal expansion.

5.3 Transfected U-2 OS chromatogram sequences

Following the same procedure used for HEK293T cell line generation, U-2 OS clones were expanded, harvested, and submitted for Sanger sequencing. Amplified PCR fragments were gel extracted and combined with the respective exon 8 and exon 10 forward primers before submission to confirm successful incorporation of each mutation. While 6G NEMO mutations were detected in several clonal lines, closer inspection of the chromatograms revealed evidence of insertions and deletions (indels) within the sequenced regions. One clonal line, indicated by a red arrow, harbored a 3 bp deletion on one X chromosome, resulting in a heterozygous indel evidenced by a smaller peak overlapping a larger peak in the chromatogram, indicative of a frameshift in one allele while the other retains the unedited sequence. A second 6G clonal line showed evidence of reversion to the wild-type sequence, marked by black and red asterisks indicating retention of the original cytosine and adenine base pairs, respectively, also present as a heterozygous pattern. Unfortunately, no D311N mutant sequences were identified among any of the clonal lines sequenced.

Although these results demonstrate that U-2 OS cells are susceptible to prime editing, the efficiency of editing is lower than that observed in HEK293T cells. This difference is likely attributable to the differential expression of mismatch repair (MMR) enzymes between the two cell lines. HEK293T cells lack specific MMR enzymes, which increases the probability of stable homozygous mutation incorporation following prime editing[117,118]. In contrast, U-2 OS cells possess a more intact MMR system, which increases the likelihood of indel formation and reversion of the edited sequence back to the wild-type, as prime editing products are known to be susceptible to MMR-mediated correction of the newly installed sequence[118]. The reversion to wild-type observed in the second 6G clonal line is consistent with this mechanism, highlighting MMR activity as a key barrier to efficient prime editing in U-2 OS cells.

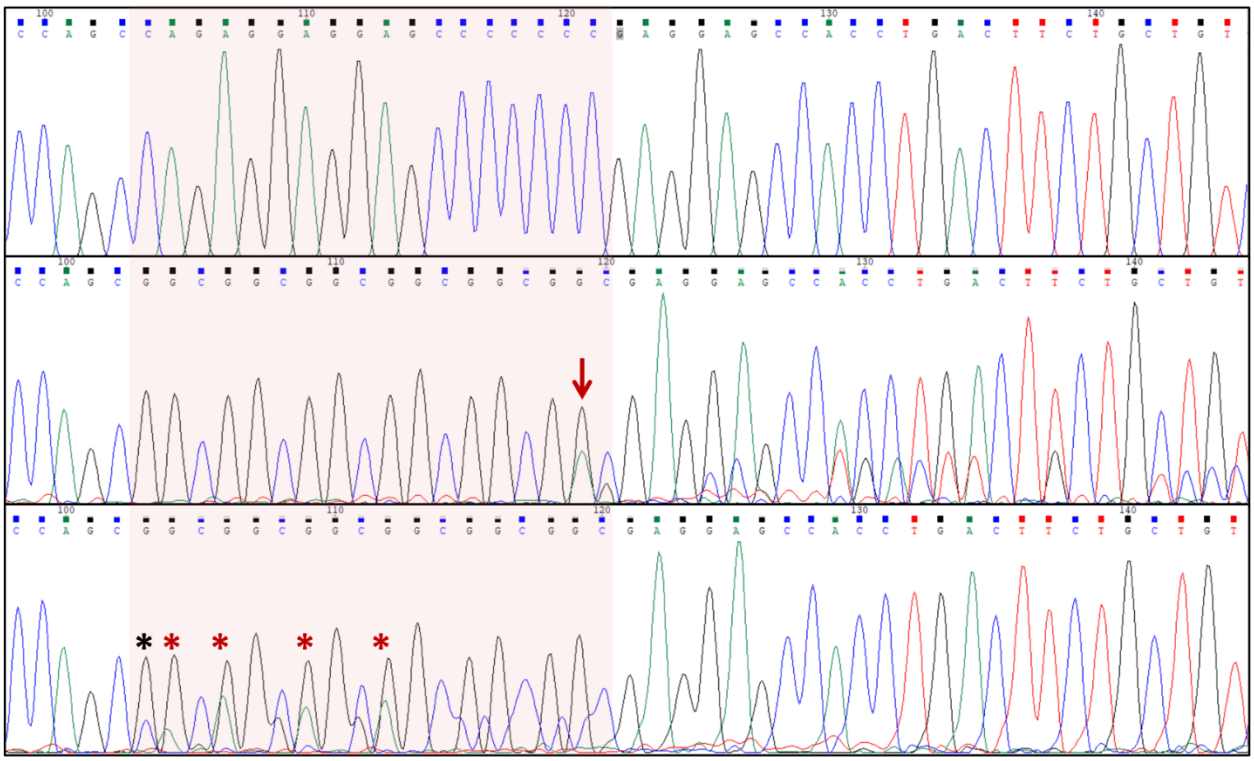

Figure 5.3: DNA chromatograms of wild-type and 6G NEMO sequences in the IKBKG exon 10 region of U-2 OS cells.

The top chromatogram shows the wild-type IKBKG exon 10 sequence, while the bottom two chromatograms show Sanger sequencing results from two independent 6G NEMO clonal cell lines. The red highlighted region spanning all three chromatograms denotes the location of the intended mutation site. The red arrow indicates the start of the indel within the mutant sequences, and black and red asterisks mark the positions retaining wild-type base identity.

Discussion

HEK293T cells provided the proof of concept for using CRISPR-Cas9 prime editing to introduce endogenous mutations into NEMO and demonstrated the feasibility of using these mutant cell lines to interrogate the NF-κB pathway. Building on this foundation, the same prime editing strategy was applied to U-2 OS cells, a well-established model system with a documented history of use in both NF-κB signaling and gene editing studies. U-2 OS cells were selected to address the broader question of how NEMO consolidates diverse canonical signals into distinct gene expression responses, as this cell line exhibits a broader responsiveness to canonical NF-κB inducers compared to HEK293T cells while remaining amenable to transfection and routine culture.

Initial NF-κB activation experiments in U-2 OS cells confirmed that both TNF-α and IL-1β activate the canonical NF-κB pathway, providing two mechanistically distinct inducers through which to investigate the role of NEMO's binding interactions. The same prime editing constructs and protocol used to generate the NEMO mutant HEK293T cell lines were applied to U-2 OS cells. However, Sanger sequencing of single-cell clones revealed that U-2 OS cells are considerably more susceptible to indel formation than HEK293T cells. Of the 6G NEMO clonal lines sequenced, two of which held evidence of the intended mutation but were accompanied by a 3 bp deletion in one clone and a heterozygous mutation pattern in another, indicating incomplete or imprecise editing. No D311N mutant sequences were identified in any clonal line. Collectively, these results demonstrate that while U-2 OS cells are amenable to prime editing, the use of an MMR-evasive prime editor variant should be considered to reduce indel frequency and improve the efficiency of mutation incorporation in future experiments.

Chapter 6 Conclusion

NEMO is an essential regulatory subunit of the IKK complex, required for canonical NF-κB activation through its ability to coordinate upstream signaling events with IKK complex assembly and activation. Linear polyubiquitin binding to NEMO has been shown to be a critical step in this process, facilitating IKK2 phosphorylation and subsequent IκBα phosphorylation and degradation to initiate NF-κB nuclear translocation. Despite its well-established functional importance, the structural characterization of NEMO remains incomplete, with only partial structural data available due to its intrinsically disordered nature. Given the central position of NEMO at the convergence of multiple canonical NF-κB signaling inputs and its multiple distinct binding interactions, we hypothesize that NEMO plays a role in decoding diverse upstream canonical stimuli and translating them into distinct downstream NF-κB-driven gene expression responses.

To address this hypothesis, several NEMO mutations were introduced to disrupt three key aspects of NEMO function: the secondary IKK2 binding site (6G), the linear polyubiquitin binding site (D311N), and the zinc finger domain. Of these, two mutant cell lines, 6G and D311N, were successfully generated and confirmed by Sanger sequencing. The presence of NEMO differed between wild-type and mutated cell lines, as it could mean that editing NEMO could affect the expression of NEMO.

As HEK293T cells lack the receptors necessary to respond to other canonical NF-κB inducers, TNF-α was the only inducer capable of activating the pathway and was used exclusively for all functional analyses. Functional validation confirmed that both mutations affected canonical NF-κB activation, though to markedly different degrees. Western blot, luciferase reporter assay, and RT-qPCR collectively demonstrated that 6G NEMO partially suppressed NF-κB activation, while D311N suppressed majority of the activation. Notably, the partial suppression observed in 6G NEMO contrasts with previous biochemical studies using recombinant IKK2 proteins, which showed no IKK2 phosphorylation upon disruption of the secondary binding site,

suggesting that the cellular context provides additional mechanisms that partially compensate for the loss of this interaction.

The stepwise reduction in NF-κB activity, with 6G NEMO exhibiting approximately half the activation of wild-type cells and D311N exhibiting approximately half that of 6G, was consistent across all three assays, reinforcing the reliability of this finding. The retention of partial NF-κB activation in 6G NEMO is consistent with the fact that this mutant retains the ability to bind linear polyubiquitin, which has been shown to be absolutely required for canonical NF-κB activation. Taken together, these findings indicate that the secondary IKK2 binding site plays a modulatory rather than essential role in canonical NF-κB activation, while linear polyubiquitin binding to NEMO is indispensable for pathway initiation.

To further probe the mechanism of the secondary IKK2 binding site, 6G NEMO cells were treated with a LUBAC inhibitor (Hoipin-8) and an allosteric IKK2 inhibitor (BMS-345541) to assess the sensitivity of the mutant to upstream and downstream pathway inhibition. While the data were inconclusive, the experiments demonstrated proof of concept that these inhibitors can suppress NF-κB activation in the mutated cell line, and further optimization of inhibitor concentrations and incubation conditions is required before definitive conclusions can be drawn regarding their effect on 6G NEMO.

The limited canonical inducer responsiveness of HEK293T cells, combined with the successful proof of concept of prime editing in this cell line, provided the rationale for extending the approach to U-2 OS cells. U-2 OS cells are more broadly responsive to canonical NF-κB inducers and have an established history of use in both NF-κB signaling and gene editing studies, making them a more suitable model for addressing the overarching hypothesis of how NEMO decodes diverse canonical stimuli. While evidence of 6G NEMO mutation was detected in U-2 OS clonal lines, the presence of indels rendered these cell lines unsuitable for downstream analysis. Co-expression of MMR-inhibiting proteins or the use of newer generation prime editor variants should be considered to improve editing fidelity in future attempts.

Collectively, the findings presented in this dissertation demonstrate that 6G NEMO exerts a modulatory effect on TNF-α induced canonical NF-κB activation, in contrast to the complete abolition observed in D311N, establishing that the secondary IKK2 binding site and the linear polyubiquitin binding site play distinct and non-redundant roles in NEMO-mediated NF-κB signaling. Furthermore, this work demonstrates that prime editing is a powerful tool for generating endogenous mutations in a biologically relevant cellular context to investigate the mechanistic properties of signaling proteins. However, careful consideration of cell line selection is critical, as the responsiveness of the chosen cell line to relevant signaling stimuli, its susceptibility to gene editing, and its ease of culture all significantly influence the quality and interpretability of the resulting data. With these considerations addressed, future studies utilizing U-2 OS or other more responsive cell lines will be well positioned to fully characterize the role of NEMO in decoding diverse canonical NF-κB signals.

Future directions

Given the limited responsiveness of HEK293T cells to canonical NF-κB inducers, transitioning to U-2 OS cells represents the most appropriate next step for investigating the role of NEMO in decoding diverse canonical signals. However, the initial attempts to recreate the 6G and D311N mutations in U-2 OS cells proved more challenging than anticipated, with indel formation presenting a significant barrier to generating clean homozygous mutant cell lines. To address this, the use of a newer generation prime editing system is recommended for future efforts.

Specifically, prime editing 7 (PE7), an optimized prime editing system that is human codon-optimized and incorporates mutations to improve Cas9 nickase activity, which offers several advantages over the PE3 system used in this study. PE7 also incorporates La, a small RNA-binding protein that acts as an exonuclease protection factor at the 3' end of pegRNAs, preventing exonuclease-mediated degradation and improving pegRNA stability and editing efficiency[119,120].

PE7 is available as a plasmid from Addgene and can be readily incorporated into the existing experimental workflow, though it does not co-express GFP as the current PE3 system does, which would require an alternative strategy for identifying successfully transfected cells.

To further streamline the screening process, the PE7 and pegRNA plasmids could be modified to incorporate antibiotic selection markers such as puromycin or blasticidin resistance, allowing for direct selection of transfected cells and reducing the time and resources required for mutation screening. The existing pegRNA oligonucleotides could be ligated into the modified plasmid backbone via Golden Gate assembly. The use of an ngRNA could also be omitted, as recent studies have demonstrated that it is not strictly required for PE7[119]. Following transfection, antibiotic selection over approximately two weeks would ensure for cells harboring both the PE7 and pegRNA constructs, after which FACS sorting into 96-well plates for single-cell clonal expansion could be performed. As antibiotic selection would guarantee for successful transfection of both plasmids into cells prior to sorting, the probability of identifying homozygous mutant clones would be substantially increased, reducing overall screening time and improving the efficiency of mutant cell line generation in U-2 OS cells.

APPENDIX

Miniprep protocol (Huxford Lab)

Solution I-
50 mM Glucose (made from filtered 1 M Glucose stock)
25 mM Tris-HCl (pH 8.0)
10 mM EDTA (pH 8.0)
Make 100 mL by adding 5 mL 1M Glucose, 2.5 mL 1 M Tris-HCl (pH 8.0) and 2 mL 0.5 M EDTA (pH 8.0) to 50 mL H_2O in 100 mL graduated cylinder. Fill to 100 mL mark with MilliQ water. Filter sterilize. Keep at 4°C. Check occasionally for bacterial growth. Good for more than 12 months at 4°C.

Solution II-
0.2 N NaOH
10% SDS
Make fresh each use. For 5 mL add 0.5 mL of 10 % SDS to 4 mL MilliQ H2O in a 15 mL Falcon tube. Add 0.2 mL of 5 M NaOH. Add MilliQ H_2O to the 5 mL mark. Note: do not use old 5 M NaOH stocks that have crusty deposits on the cap. 5 M NaOH should be kept air tight in a plastic bottle or Falcon tube. Keep at room temperature and throw away excess after use.

Solution III-
3 M Potassium Acetate
~2 M Acetic Acid
Make 100 mL by adding solid Potassium acetate to ~75 mL MilliQ H_2O in a 100 mL graduated cylinder. Add 11.5 mL of glacial acetic acid. Glacial acetic acid should be handled in the fume hood. Top with MilliQ H_2O to 100 mL mark. Filter sterilize and keep at 4°C. Good for more than 12 months at 4°C.

1) Sterilize platinum wire loop by immersing it in ethanol and flaming it. Working near an open flame, cool the wire by touching a clean spot on the agar plate. Drag loop over a well-isolated single bacterial colony. Touch the loop for a couple of seconds to 4.5 mL of LB broth with appropriate antibiotic in a 50 mL Falcon tube. Close tube and leave it for 12-18 hours shaking at approximately 250 rpm at 37° C.

2) Transfer 1.6 mL of overnight culture to eppie tube. Pellet cells at 13,200 rpm for 30 seconds. Draw off supernatant with a trapped vacuum. Note: If you need lots of plasmid for further cloning procedures, you may repeat this step two times in the same tube. Take care that you don't get the tubes mixed up. For sequencing or regular miniprep applications, 1.5 mL pellet is sufficient.

3) Pour 0.3 mL × (# of minipreps + 1) of solution I to a glass fraction tube so that the original bottle remains sterile. Add RNAse A to the fraction tube at a concentration of 100 μg/mL, mix it, label it, and leave it on ice.

4) Add 0.3 mL of solution I (+RNAse A) to each of the cell pellets. Bring them into solution by vortexing two tubes at a time. Make certain that the bacterial cell pellets are well homogenized before proceeding.

5) Gently add 0.3 mL of room temperature solution II to each of the tubes, four tubes at a time. Snap shut the tubes and mix by SLOWLY turning the tubes upside down and back up about ten times. Make sure that the entire inner surface of the eppie tube makes contact with the solution.

The mixture should be pale yellow and quite viscous. Leave at room temperature for no longer than five minutes.

6) Pour an appropriate amount [0.3 mL × (# of minipreps + 1)] of solution III into a glass fraction tube. Label it and leave it on ice. Gently add 0.3 mL of solution III to each of the tubes four at a time. Close and invert the tubes ten times, or until the solution has stopped changing to a thick white precipitate. Place tubes on ice for no longer than 10 minutes.

7) Pellet by centrifugation at 13,200 × g for 10 minutes (at 4°C, if possible).

8) While the tubes are spinning, prepare and label a new set of tubes. Add 0.8 mL isopropyl alcohol to each tube.

9) Carefully pipet 0.9 mL supernatant into the tubes containing isopropyl alcohol. Take care not to bring any white precipitate. This can be done by tipping the tube at about 45° and putting just the tip of the 1 mL pipet past the top of the solution. Draw up the supernatant slowly. Re-centrifuge if necessary.

10) Cap the tubes. Mix by vortexing. Leave on ice or in –20°C freezer for 10 minutes. Note: the tubes can be left overnight at this point without any problem.

11) Pellet DNA by centrifugation at 13,200 × g for 10 minutes at room temperature.

12) Remove supernatant with vacuum trap.

13) Add 0.5 mL 70% ethanol at room temperature. Invert the tube several times.

14) Pellet DNA by centrifugation at 13,200 × g for 5 minutes at room temperature.

15) Remove as much of the supernatant as possible with vacuum trap. Be careful not to suck up the DNA pellet. Leave tubes drying upside down on a paper towel for 5 minutes.

16) Resuspend DNA in 50 μL MilliQ H_2O (for sequencing) or in 150 μL TE (pH 8.0) buffer. Yield in 50 μL is approximately 250 ng/μL.

Golden gate assembly PCR cycle

Table A.1: pegRNA Golden Gate assembly PCR thermal cycling conditions

Step	**Cycles**	**Temperature**	**Time**
Incubation	30	16°C	5 minutes
		37°C	5 minutes
Inactivation	1	80°C	15 minutes
Hold	1	4°	Hold

REFERENCES

1. Singh, H., Sen, R., Baltimore, D. & Sharp, P. A. A nuclear factor that binds to a conserved sequence motif in transcriptional control elements of immunoglobulin genes. *Nature* **319**, 154–158 (1986).

2. Sen, R. & Baltimore, D. Inducibility of κ Immunoglobulin Enhancer-Binding Protein NFKB by a Posttranslational Mechanism. *Cell* **47**, 8 (1986).

3. Sen, R. & Baltimore, D. Multiple nuclear factors interact with the immunoglobulin enhancer sequences. *Cell* **46**, (1986).

4. Böhnlein, E., Lowenthal, J. W., Siekevitz, M., Ballard, D. W., Franza, B. R. & Greene, W. C. The same inducible nuclear proteins regulates mitogen activation of both the interleukin-2 receptor-alpha gene and type 1 HIV. *Cell* **53**, 827–836 (1988).

5. Baeuerle, A. Activation of DNA-Binding Activity in an Apparently Cytoplasmic Precursor of the NF-KB Transcription Factor. *Cell* (1988).

6. Lenardo, M. J. & Baltimore, D. NF-κB: A pleiotropic mediator of inducible and tissue-specific gene control. *Cell* **58**, 227–229 (1989).

7. Grilli, M. NF-κB and Rel: Participants in a Multiform Transcriptional Regulatory System. *International Review of Cytology* 62 (1993).

8. Ghosh, S., May, M. J. & Kopp, E. B. NF-κB AND REL PROTEINS: Evolutionarily Conserved Mediators of Immune Responses. *Annual Review of Immunology* **16**, 225–260 (1998).

9. Kopp, E. B. & Ghosh, S. NF-κB and Rel Proteins in Innate Immunity. in *Advances in Immunology* (ed. Dixon, F. J.) vol. 58 1–27 (Academic Press, 1995).

10. Blank, V., Kourilsky, P. & Israël, A. Cytoplasmic retention, DNA binding and processing of the NF-kappa B p50 precursor are controlled by a small region in its C-terminus. *The EMBO Journal* **10**, 4159–4167 (1991).

11. Ghosh, G., Wang, V. Y.-F., Huang, D.-B. & Fusco, A. NF-κB regulation: lessons from structures. *Immunological Reviews* **246**, 36–58 (2012).

12. Huxford, T. & Ghosh, G. A Structural Guide to Proteins of the NF-κB Signaling Module. *Cold Spring Harbor Perspectives in Biology* **1**, a000075–a000075 (2009).

13. Singh, V., Gupta, D. & Arora, R. NF-κB as a key player in regulation of cellular radiation responses and identification of radiation countermeasures. *Discoveries* **3**, e35 (2015).

14. Hinz, M., Arslan, S. Ç. & Scheidereit, C. It takes two to tango: IκBs, the multifunctional partners of NF-κB. *Immunological Reviews* **246**, 59–76 (2012).

15. Huxford, T., Hoffmann, A. & Ghosh, G. Understanding the Logic of IκB:NF-κB Regulation in Structural Terms. in *NF-kB in Health and Disease* (ed. Karin, M.) vol. 349 1–24 (Springer Berlin Heidelberg, Berlin, Heidelberg, 2010).

16. Schuster, M., Annemann, M., Plaza-Sirvent, C. & Schmitz, I. Atypical IκB proteins – nuclear modulators of NF-κB signaling. *Cell Commun Signal* **11**, 23 (2013).

17. Rice, N. R., MacKichan, M. L. & Israël, A. The precursor of NF-κB p50 has IκB-like functions. *Cell* **71**, 243–253 (1992).

18. Naumann, M., Nieters, A., Hatada, E. N. & Scheidereit, C. NF-kappa B precursor p100 inhibits nuclear translocation and DNA binding of NF-kappa B/rel-factors. *Oncogene* **8**, 2275–2281 (1993).

19. Whiteside, S. T. & Israel, A. IκB proteins: structure, function and regulation. *Seminars in Cancer Biology* **8**, 75 (1997).

20. Chen, Z. J., Parent, L. & Maniatis, T. Site-Specific Phosphorylation of IκBα by a Novel Ubiquitination-Dependent Protein Kinase Activity. *Cell* **84**, 10 (1996).

21. Chen, Z., Hagler, J., Palombella, V. J., Melandri, F., Scherer, D., Ballard, D. & Maniatis, T. Signal-induced site-specific phosphorylation targets I kappa B alpha to the ubiquitin-proteasome pathway. *Genes Dev.* **9**, 1586–1597 (1995).

22. Alkalay, I., Yaron, A., Hatzubai, A., Orian, A., Ciechanover, A. & Ben-Neriah, Y. Stimulation-dependent I kappa B alpha phosphorylation marks the NF-kappa B inhibitor for degradation via the ubiquitin-proteasome pathway. *Proceedings of the National Academy of Sciences* **92**, 10599–10603 (1995).

23. DiDonato, J. A., Hayakawa, M., Rothwarf, D. M., Zandi, E. & Karin, M. A cytokine-responsive IκB kinase that activates the transcription factor NF-κB. *Nature* **388**, (1997).

24. Mercurio, F., Zhu, H., Murray, B. W., Shevchenko, A., Bennett, B. L., Li, J. wu, Young, D. B., Barbosa, M., Mann, M., Manning, A. & Rao, A. IKK-1 and IKK-2: Cytokine-Activated IκB Kinases Essential for NF-κB Activation. *Science* **278**, 860–866 (1997).

25. Yamaoka, S., Courtois, G., Bessia, C., Whiteside, S. T., Weil, R., Agou, F., Kirk, H. E., Kay, R. J. & Israël, A. Complementation Cloning of NEMO, a Component of the IκB Kinase Complex Essential for NF-κB Activation. *Cell* **93**, 1231–1240 (1998).

26. Rothwarf, D. M., Zandi, E., Natoli, G. & Karin, M. IKK-γ is an essential regulatory subunit of the IκB kinase complex. *Nature* **395**, 297–300 (1998).

27. Israel, A. The IKK Complex, a Central Regulator of NF-κB Activation. *Cold Spring Harbor Perspectives in Biology* **2**, a000158–a000158 (2010).

28. Bagnéris, C., Ageichik, A. V., Cronin, N., Wallace, B., Collins, M., Boshoff, C., Waksman, G. & Barrett, T. Crystal Structure of a vFlip-IKKγ Complex: Insights into Viral Activation of the IKK Signalosome. *Molecular Cell* **30**, 620–631 (2008).

29. Rahighi, S., Ikeda, F., Kawasaki, M., Akutsu, M., Suzuki, N., Kato, R., Kensche, T., Uejima, T., Bloor, S., Komander, D., Randow, F., Wakatsuki, S. & Dikic, I. Specific Recognition of Linear Ubiquitin Chains by NEMO Is Important for NF-κB Activation. *Cell* **136**, 1098–1109 (2009).

30. Lo, Y.-C., Lin, S.-C., Rospigliosi, C. C., Conze, D. B., Wu, C.-J., Ashwell, J. D., Eliezer, D. & Wu, H. Structural Basis for Recognition of Diubiquitins by NEMO. *Molecular Cell* **33**, 602–615 (2009).

31. Tokunaga, F., Sakata, S., Saeki, Y., Satomi, Y., Kirisako, T., Kamei, K., Nakagawa, T., Kato, M., Murata, S., Yamaoka, S., Yamamoto, M., Akira, S., Takao, T., Tanaka, K. & Iwai, K. Involvement of linear polyubiquitylation of NEMO in NF-κB activation. *Nat Cell Biol* **11**, 123–132 (2009).

32. Ko, M. S., Cohen, S. N., Polley, S., Mahata, S. K., Biswas, T., Huxford, T. & Ghosh, G. Regulatory subunit NEMO promotes polyubiquitin-dependent induction of NF-κB through a targetable second interaction with upstream activator IKK2. *Journal of Biological Chemistry* **298**, 101864 (2022).

33. Karin, M. How NF-kB is activated: the role of the IkB kinase (IKK) complex. *Oncogene* 8 (1999).

34. Pahl, H. L. Activators and target genes of Rel/NF-kB transcription factors. *Oncogene* **18**, 6853–6866 (1999).

35. Karin, M. & Ben-Neriah, Y. Phosphorylation Meets Ubiquitination: The Control of NF-κB Activity. *Annu. Rev. Immunol.* **18**, 621–663 (2000).

36. Shih, V. F.-S., Tsui, R., Caldwell, A. & Hoffmann, A. A single NFκB system for both canonical and non-canonical signaling. *Cell Res* **21**, 86–102 (2011).

37. Sun, S.-C. The non-canonical NF-κB pathway in immunity and inflammation. *Nat Rev Immunol* **17**, 545–558 (2017).

38. Scherer, D. C., Brockman, J. A., Chen, Z., Maniatis, T. & Ballard, D. W. Signal-induced degradation of I kappa B alpha requires site-specific ubiquitination. *Proceedings of the National Academy of Sciences* **92**, 11259–11263 (1995).

39. Kanarek, N., London, N., Schueler-Furman, O. & Ben-Neriah, Y. Ubiquitination and Degradation of the Inhibitors of NF-κB. *Cold Spring Harb Perspect Biol* **2**, a000166 (2010).

40. Catici, D. A. M., Horne, J. E., Cooper, G. E. & Pudney, C. R. Polyubiquitin Drives the Molecular Interactions of the NF-κB Essential Modulator (NEMO) by Allosteric Regulation. *Journal of Biological Chemistry* **290**, 14130–14139 (2015).

41. Deng, L., Wang, C., Spencer, E., Yang, L., Braun, A., You, J., Slaughter, C., Pickart, C. & Chen, Z. J. Activation of the IκB Kinase Complex by TRAF6 Requires a Dimeric Ubiquitin-Conjugating Enzyme Complex and a Unique Polyubiquitin Chain. *Cell* **103**, 351–361 (2000).

42. Ea, C.-K., Deng, L., Xia, Z.-P., Pineda, G. & Chen, Z. J. Activation of IKK by TNFα Requires Site-Specific Ubiquitination of RIP1 and Polyubiquitin Binding by NEMO. *Molecular Cell* **22**, 245–257 (2006).

43. Wu, C.-J., Conze, D. B., Li, T., Srinivasula, S. M. & Ashwell, J. D. Sensing of Lys 63-linked polyubiquitination by NEMO is a key event in NF-κB activation. *Nat Cell Biol* **8**, 398–406 (2006).

44. Kensche, T., Tokunaga, F., Ikeda, F., Goto, E., Iwai, K. & Dikic, I. Analysis of Nuclear Factor-κB (NF-κB) Essential Modulator (NEMO) Binding to Linear and Lysine-linked Ubiquitin Chains and Its Role in the Activation of NF-κB. *Journal of Biological Chemistry* **287**, 23626–23634 (2012).

45. Hauenstein, A. V., Xu, G., Kabaleeswaran, V. & Wu, H. Evidence for M1-Linked Polyubiquitin-Mediated Conformational Change in NEMO. *Journal of Molecular Biology* **429**, 3793–3800 (2017).

46. Shaffer, R., DeMaria, A. M., Kagermazova, L., Liu, Y., Babaei, M., Caban-Penix, S., Cervantes, A., Jehle, S., Makowski, L., Gilmore, T. D., Whitty, A. & Allen, K. N. A Central Region of NF-κB Essential Modulator Is Required for IKKβ-Induced Conformational Change and for Signal Propagation. *Biochemistry* **58**, 2906–2920 (2019).

47. Shishodia, S. & Aggarwal, B. B. Nuclear Factor-κB Activation Mediates Cellular Transformation, Proliferation, Invasion Angiogenesis and Metastasis of Cancer. in *Molecular Targeting and Signal Transduction* (ed. Kumar, R.) vol. 119 139–173 (Kluwer Academic Publishers, Boston, 2004).

48. Yu, H., Lin, L., Zhang, Z., Zhang, H. & Hu, H. Targeting NF-κB pathway for the therapy of diseases: mechanism and clinical study. *Sig Transduct Target Ther* **5**, 209 (2020).

49. Liu, T., Zhang, L., Joo, D. & Sun, S.-C. NF-κB signaling in inflammation. *Sig Transduct Target Ther* **2**, 17023 (2017).

50. Tak, P. P. & Firestein, G. S. NF-κB: a key role in inflammatory diseases. *J. Clin. Invest.* **107**, 7–11 (2001).

51. McInnes, I. B. The Pathogenesis of Rheumatoid Arthritis. *The new england journal of medicine* (2011).

52. Han, Z., Boyle, D. L., Manning, A. M. & Firestein, G. S. AP-1 and NF-kB Regulation in Rheumatoid Arthritis and Murine Collagen-Induced Arthritis. *Autoimmunity* **28**, 197–208 (1998).

53. Schreiber, S., Nikolaus, S. & Hampe, J. Activation of nuclear factor kappa B in inflammatory bowel disease. *Gut* **42**, 477–484 (1998).

54. Karin, M., Cao, Y., Greten, F. R. & Li, Z.-W. NF-κB in cancer: from innocent bystander to major culprit. *Nat Rev Cancer* **2**, 301–310 (2002).

55. Taniguchi, K. & Karin, M. NF-κB, inflammation, immunity and cancer: coming of age. *Nat Rev Immunol* **18**, 309–324 (2018).

56. Hanahan, D. & Weinberg, R. A. The Hallmarks of Cancer. *Cell* **100**, 57–70 (2000).

57. Huang, C.-Y., Fong, Y.-C., Lee, C.-Y., Chen, M.-Y., Tsai, H.-C., Hsu, H.-C. & Tang, C.-H. CCL5 increases lung cancer migration via PI3K, Akt and NF-κB pathways. *Biochemical Pharmacology* **77**, 794–803 (2009).

58. Vinod Prabhu, V., Elangovan, P., Niranjali Devaraj, S. & Sakthivel, K. M. Targeting NF-κB mediated cell signaling pathway and inflammatory mediators by 1,2-diazole in A549 cells in vitro. *Biotechnol Rep (Amst)* **29**, e00594 (2021).

59. Chen, W. NF-kappaB in lung cancer, a carcinogenesis mediator and a prevention and therapy target. *Front Biosci* **16**, 1172 (2011).

60. Chu, C.-Y., Cha, S.-T., Lin, W.-C., Lu, P.-H., Tan, C.-T., Chang, C.-C., Lin, B.-R., Jee, S.-H. & Kuo, M.-L. Stromal cell-derived factor-1α (SDF-1α/CXCL12)-enhanced angiogenesis of human basal cell carcinoma cells involves ERK1/2–NF-κB/interleukin-6 pathway. *Carcinogenesis* **30**, 205–213 (2009).

61. How, K. N., Leong, H. J. Y., Pramono, Z. A. D., Leong, K. F., Lai, Z. W. & Yap, W. H. Uncovering incontinentia pigmenti: From DNA sequence to pathophysiology. *Front. Pediatr.* **10**, (2022).

62. Smahi, A., Courtois, G., Vabres, P., Yamaoka, S., Heuertz, S., Munnich, A., Israël, A., Heiss, N. S., Klauck, S. M., Kioschis, P., Wiemann, S., Poustka, A., Esposito, T., Bardaro, T., Gianfrancesco, F., Ciccodicola, A., D'Urso, M., Woffendin, H., Jakins, T., Donnai, D., Stewart, H., Kenwrick, S. J., Aradhya, S., Yamagata, T., Levy, M., Lewis, R. A., Nelson, D. L., & The International Incontinentia Pigmenti (IP) Consortium. Genomic rearrangement in NEMO impairs NF-κB activation and is a cause of incontinentia pigmenti. *Nature* **405**, 466–472 (2000).

63. Rudolph, D., Yeh, W.-C., Wakeham, A., Rudolph, B., Nallainathan, D., Potter, J., Elia, A. J. & Mak, T. W. Severe liver degeneration and lack of NF-κB activation in NEMO/IKKγ-deficient mice. *Genes Dev.* **14**, 854–862 (2000).

64. Fusco, F., Bardaro, T., Fimiani, G., Mercadante, V., Miano, M. G., Falco, G., Israël, A., Courtois, G., D'Urso, M. & Ursini, M. V. Molecular analysis of the genetic defect in a large cohort of IP patients and identification of novel NEMO mutations interfering with NF-κB activation. *Hum Mol Genet* **13**, 1763–1773 (2004).

65. Döffinger, R., Smahi, A., Bessia, C., Geissmann, F., Feinberg, J., Durandy, A., Bodemer, C., Kenwrick, S., Dupuis-Girod, S., Blanche, S., Wood, P., Rabia, S. H., Headon, D. J., Overbeek, P. A., Le Deist, F., Holland, S. M., Belani, K., Kumararatne, D. S., Fischer, A., Shapiro, R., Conley, M. E., Reimund, E., Kalhoff, H., Abinun, M., Munnich, A., Israël, A., Courtois, G. & Casanova, J.-L. X-linked anhidrotic ectodermal dysplasia with immunodeficiency is caused by impaired NF-κB signaling. *Nat Genet* **27**, 277–285 (2001).

66. Zilberman-Rudenko, J., Shawver, L. M., Wessel, A. W., Luo, Y., Pelletier, M., Tsai, W. L., Lee, Y., Vonortas, S., Cheng, L., Ashwell, J. D., Orange, J. S., Siegel, R. M. & Hanson, E. P. Recruitment of A20 by the C-terminal domain of NEMO suppresses NF-κB activation and autoinflammatory disease. *Proc. Natl. Acad. Sci. U.S.A.* **113**, 1612–1617 (2016).

67. Maubach, G., Schmädicke, A.-C. & Naumann, M. NEMO Links Nuclear Factor-κB to Human Diseases. *Trends in Molecular Medicine* **23**, 1138–1155 (2017).

68. Monreal, A. W., Ferguson, B. M., Headon, D. J., Street, S. L., Overbeek, P. A. & Zonana, J. Mutations in the human homologue of mouse dl cause autosomal recessive and dominant hypohidrotic ectodermal dysplasia. *Nat Genet* **22**, 366–369 (1999).

69. Kere, J., Srivastava, A. K., Montonen, O., Zonana, J., Thomas, N., Ferguson, B., Munoz, F., Morgan, D., Clarke, A., Baybayan, P., Chen, E. Y., Ezer, S., Saarialho-Kere, U., De La Chapelle, A. & Schlessinger, D. X–linked anhidrotic (hypohidrotic) ectodermal dysplasia is caused by mutation in a novel transmembrane protein. *Nat Genet* **13**, 409–416 (1996).

70. Vinolo, E., Sebban, H., Chaffotte, A., Israël, A., Courtois, G., Véron, M. & Agou, F. A Point Mutation in NEMO Associated with Anhidrotic Ectodermal Dysplasia with Immunodeficiency Pathology Results in Destabilization of the Oligomer and Reduces Lipopolysaccharide- and Tumor Necrosis Factor-mediated NF-κB Activation. *Journal of Biological Chemistry* **281**, 6334–6348 (2006).

71. Luedde, T., Beraza, N., Kotsikoris, V., van Loo, G., Nenci, A., De Vos, R., Roskams, T., Trautwein, C. & Pasparakis, M. Deletion of NEMO/IKKγ in Liver Parenchymal Cells Causes Steatohepatitis and Hepatocellular Carcinoma. *Cancer Cell* **11**, 119–132 (2007).

72. Koerner, L., Schmiel, M., Yang, T.-P., Peifer, M., Buettner, R. & Pasparakis, M. NEMO- and RelA-dependent NF-κB signaling promotes small cell lung cancer. *Cell Death Differ* **30**, 938–951 (2023).

73. Tsesmelis, M., Büttner, U. F. G., Gerstenlauer, M., Manfras, U., Tsesmelis, K., Du, Z., Sperb, N., Weissinger, S. E., Möller, P., Barth, T. F. E., Maier, H. J., Chan, L. K. & Wirth, T. NEMO/NF-κB signaling functions as a double-edged sword in PanIN formation versus progression to pancreatic cancer. *Molecular Cancer* **23**, 103 (2024).

74. Khalil, A. M. The genome editing revolution: review. *Journal of Genetic Engineering and Biotechnology* **18**, 68 (2020).

75. Jiang, F. & Doudna, J. A. CRISPR–Cas9 Structures and Mechanisms. *Annu. Rev. Biophys.* **46**, 505–529 (2017).

76. Makarova, K. S., Wolf, Y. I., Alkhnbashi, O. S., Costa, F., Shah, S. A., Saunders, S. J., Barrangou, R., Brouns, S. J. J., Charpentier, E., Haft, D. H., Horvath, P., Moineau, S., Mojica, F. J. M., Terns, R. M., Terns, M. P., White, M. F., Yakunin, A. F., Garrett, R. A., van der Oost, J., Backofen, R. & Koonin, E. V. An updated evolutionary classification of CRISPR–Cas systems. *Nat Rev Microbiol* **13**, 722–736 (2015).

77. Xu, Y. & Li, Z. CRISPR-Cas systems: Overview, innovations and applications in human disease research and gene therapy. *Comput Struct Biotechnol J* **18**, 2401–2415 (2020).

78. Jinek, M., Chylinski, K., Fonfara, I., Hauer, M., Doudna, J. A. & Charpentier, E. A Programmable Dual-RNA–Guided DNA Endonuclease in Adaptive Bacterial Immunity. *Science* **337**, 816–821 (2012).

79. Pacesa, M., Pelea, O. & Jinek, M. Past, present, and future of CRISPR genome editing technologies. *Cell* **187**, 1076–1100 (2024).

80. Anzalone, A. V., Randolph, P. B., Davis, J. R., Sousa, A. A., Koblan, L. W., Levy, J. M., Chen, P. J., Wilson, C., Newby, G. A., Raguram, A. & Liu, D. R. Search-and-replace genome editing without double-strand breaks or donor DNA. *Nature* **576**, 149–157 (2019).

81. Oost, J. van der & Patinios, C. The genome editing revolution. *Trends in Biotechnology* **41**, 396–409 (2023).

82. Doman, J. L., Sousa, A. A., Randolph, P. B., Chen, P. J. & Liu, D. R. Designing and executing prime editing experiments in mammalian cells. *Nat Protoc* **17**, 2431–2468 (2022).

83. Graham, F. L., Smiley, J., Russell, W. C. & Nairn, R. Characteristics of a Human Cell Line Transformed by DNA from Human Adenovirus Type 5. *Journal of General Virology* **36**, 59–72 (1977).

84. Louis, N., Evelegh, C. & Graham, F. L. Cloning and Sequencing of the Cellular–Viral Junctions from the Human Adenovirus Type 5 Transformed 293 Cell Line. *Virology* **233**, 423–429 (1997).

85. Stepanenko, A. A. & Dmitrenko, V. V. HEK293 in cell biology and cancer research: phenotype, karyotype, tumorigenicity, and stress-induced genome-phenotype evolution. *Gene* **569**, 182–190 (2015).

86. Lin, Y.-C., Boone, M., Meuris, L., Lemmens, I., Van Roy, N., Soete, A., Reumers, J., Moisse, M., Plaisance, S., Drmanac, R., Chen, J., Speleman, F., Lambrechts, D., Van de Peer, Y., Tavernier, J. & Callewaert, N. Genome dynamics of the human embryonic kidney 293 lineage in response to cell biology manipulations. *Nat Commun* **5**, 4767 (2014).

87. Rio, D. C., Clark, S. G. & Tjian, R. A Mammalian Host-Vector System That Regulates Expression and Amplification of Transfected Genes by Temperature Induction. *Science* **227**, 23–28 (1985).

88. Dubridge, R. B., Hsia, H. C., Leong, P.-M., Miller, J. H. & Calos, M. P. Analysis of Mutation in Human Cells by Using an Epstein-Barr Virus Shuttle System. *MOL. CELL. BIOL.* **7**, (1987).

89. Tan, E., Chin, C. S. H., Lim, Z. F. S. & Ng, S. K. HEK293 Cell Line as a Platform to Produce Recombinant Proteins and Viral Vectors. *Front. Bioeng. Biotechnol.* **9**, (2021).

90. Ponten, J. & Saksela, E. Two established in vitro cell lines from human mesenchymal tumours. *Intl Journal of Cancer* **2**, 434–447 (1967).

91. Bayani, J., Zielenska, M., Pandita, A., Al-Romaih, K., Karaskova, J., Harrison, K., Bridge, J. A., Sorensen, P., Thorner, P. & Squire, J. A. Spectral karyotyping identifies recurrent complex rearrangements of chromosomes 8, 17, and 20 in osteosarcomas. *Genes, Chromosomes and Cancer* **36**, 7–16 (2003).

92. Al-Romaih, K., Bayani, J., Vorobyova, J., Karaskova, J., Park, P. C., Zielenska, M. & Squire, J. A. Chromosomal instability in osteosarcoma and its association with centrosome abnormalities. *Cancer Genetics and Cytogenetics* **144**, 91–99 (2003).

93. Windheim, M., Stafford, M., Peggie, M. & Cohen, P. Interleukin-1 (IL-1) Induces the Lys63-Linked Polyubiquitination of IL-1 Receptor-Associated Kinase 1 To Facilitate NEMO Binding and the Activation of IκBα Kinase. *Molecular and Cellular Biology* **28**, 1783–1791 (2008).

94. Chow, R. D., Chen, J. S., Shen, J. & Chen, S. A web tool for the design of prime-editing guide RNAs. *Nat Biomed Eng* **5**, 190–194 (2021).

95. Hsu, J. Y., Anzalone, A. V., Grünewald, J., Lam, K. C., Shen, M. W., Liu, D. R., Joung, J. K. & Pinello, L. PrimeDesign software for rapid and simplified design of prime editing guide RNAs. *bioRxiv* 2020.05.04.077750 (2020) doi:10.1101/2020.05.04.077750.

96. Kleinstiver, B. P., Prew, M. S., Tsai, S. Q., Topkar, V. V., Nguyen, N. T., Zheng, Z., Gonzales, A. P. W., Li, Z., Peterson, R. T., Yeh, J.-R. J., Aryee, M. J. & Joung, J. K. Engineered CRISPR-Cas9 nucleases with altered PAM specificities. *Nature* **523**, 481–485 (2015).

97. Ko, M. S., Biswas, T., Mulero, M. C., Bobkov, A. A., Ghosh, G. & Huxford, T. Structurally plastic NEMO and oligomerization prone IKK2 subunits define the behavior of human IKK2:NEMO complexes in solution. *Biochimica et Biophysica Acta (BBA) - Proteins and Proteomics* **1868**, 140526 (2020).

98. Cordier, F. The Zinc Finger of NEMO Is a Functional Ubiquitin-binding Domain. *Journal of Biological Chemistry* **284**, (2009).

99. Medvedev, A. E. & Vogel, S. N. Overexpression of CD14, TLR4, and MD-2 in HEK 293T cells does not prevent induction of in vitro endotoxin tolerance. *Journal of Endotoxin Research* **9**, 60–64 (2003).

100. Krappmann, D., Patke, A., Heissmeyer, V. & Scheidereit, C. B-Cell Receptor- and Phorbol Ester-Induced NF-κB and c-Jun N-Terminal Kinase Activation in B Cells Requires Novel Protein Kinase C's. *Molecular and Cellular Biology* **21**, 6640–6650 (2001).

101. Holden, N. S., Squires, P. E., Kaur, M., Bland, R., Jones, C. E. & Newton, R. Phorbol ester-stimulated NF-κB-dependent transcription: Roles for isoforms of novel protein kinase C. *Cellular Signalling* **20**, 1338–1348 (2008).

102. Gewirtz, A. T., Navas, T. A., Lyons, S., Godowski, P. J. & Madara, J. L. Cutting Edge: Bacterial Flagellin Activates Basolaterally Expressed TLR5 to Induce Epithelial Proinflammatory Gene Expression. *The Journal of Immunology* **167**, 1882–1885 (2001).

103. Siehler, S., Wang, Y., Fan, X., Windh, R. T. & Manning, D. R. Sphingosine 1-Phosphate Activates Nuclear Factor-κB through Edg Receptors. *Journal of Biological Chemistry* **276**, 48733–48739 (2001).

104. Müller, A., Hennig, A., Lorscheid, S., Grondona, P., Schulze-Osthoff, K., Hailfinger, S. & Kramer, D. IκBζ is a key transcriptional regulator of IL-36–driven psoriasis-related gene expression in keratinocytes. *Proc. Natl. Acad. Sci. U.S.A.* **115**, 10088–10093 (2018).

105. IκBζ is a key driver in the development of psoriasis | PNAS. https://www.pnas.org/doi/10.1073/pnas.1509971112?url_ver=Z39.88-2003&rfr_id=ori%3Arid%3Acrossref.org&rfr_dat=cr_pub++0pubmed.

106. Daly, A. E., Yeh, G., Soltero, S. & Smale, S. T. *Selective Regulation of a Defined Subset of Inflammatory and Immunoregulatory Genes by an NF-κB P50-IκBζ Pathway*. http://biorxiv.org/lookup/doi/10.1101/2024.01.23.576959 (2024) doi:10.1101/2024.01.23.576959.

107. Priem, D., van Loo, G. & Bertrand, M. J. M. A20 and Cell Death-driven Inflammation. *Trends in Immunology* **41**, 421–435 (2020).

108. Martens, A. & Loo, G. van. A20 at the Crossroads of Cell Death, Inflammation, and Autoimmunity. *Cold Spring Harb Perspect Biol* **12**, a036418 (2020).

109. Micheau, O., Lens, S., Gaide, O., Alevizopoulos, K. & Tschopp, J. NF-κB Signals Induce the Expression of c-FLIP. *Molecular and Cellular Biology* **21**, 5299–5305 (2001).

110. Zhang, R., Xue, T., Shao, A., Lang, Y., Qin, C., Zhao, M., Kuang, Y., Yu, Z., Geng, Y., Zhao, C. & Tang, J. Bclaf1 regulates c-FLIP expression and protects cells from TNF-induced apoptosis and tissue injury. *EMBO Rep* **23**, EMBR202152702 (2021).

111. Rojo, A. I., Salinas, M., Martín, D., Perona, R. & Cuadrado, A. Regulation of Cu/Zn-Superoxide Dismutase Expression via the Phosphatidylinositol 3 Kinase/Akt Pathway and Nuclear Factor-κB. *J. Neurosci.* **24**, 7324–7334 (2004).

112. Dresselhaus, E. C. & Meffert, M. K. Cellular Specificity of NF-κB Function in the Nervous System. *Front. Immunol.* **10**, 1043 (2019).

113. Hideshima, T., Neri, P., Tassone, P., Yasui, H., Ishitsuka, K., Raje, N., Chauhan, D., Podar, K., Mitsiades, C., Dang, L., Munshi, N., Richardson, P., Schenkein, D. & Anderson, K. C. MLN120B, a Novel IκB Kinase β Inhibitor, Blocks Multiple Myeloma Cell Growth *In vitro* and *In vivo*. *Clinical Cancer Research* **12**, 5887–5894 (2006).

114. Burke, J. R., Pattoli, M. A., Gregor, K. R., Brassil, P. J., MacMaster, J. F., McIntyre, K. W., Yang, X., Iotzova, V. S., Clarke, W., Strnad, J., Qiu, Y. & Zusi, F. C. BMS-345541 Is a Highly Selective Inhibitor of IκB Kinase That Binds at an Allosteric Site of the Enzyme and Blocks NF-κB-dependent Transcription in Mice *. *Journal of Biological Chemistry* **278**, 1450–1456 (2003).

115. Katsuya, K., Oikawa, D., Iio, K., Obika, S., Hori, Y., Urashima, T., Ayukawa, K. & Tokunaga, F. Small-molecule inhibitors of linear ubiquitin chain assembly complex (LUBAC), HOIPINs, suppress NF-κB signaling. *Biochemical and Biophysical Research Communications* **509**, 700–706 (2019).

116. Niforou, K. N., Anagnostopoulos, A. K., Vougas, K., Kittas, C., Gorgoulis, V. G. & Tsangaris, G. T. The Proteome Profile of the Human Osteosarcoma U2OS Cell Line. *CANCER GENOMICS* (2008).

117. Trojan, J., Zeuzem, S., Randolph, A., Hemmerle, C., Brieger, A., Raedle, J., Plotz, G., Jiricny, J. & Marra, G. Functional analysis of *hMLH1* variants and HNPCC-related mutations using a human expression system. *Gastroenterology* **122**, 211–219 (2002).

118. Chen, P. J., Hussmann, J. A., Yan, J., Knipping, F., Ravisankar, P., Chen, P.-F., Chen, C., Nelson, J. W., Newby, G. A., Sahin, M., Osborn, M. J., Weissman, J. S., Adamson, B. & Liu, D. R. Enhanced prime editing systems by manipulating cellular determinants of editing outcomes. *Cell* **184**, 5635-5652.e29 (2021).

119. Yan, J., Oyler-Castrillo, P., Ravisankar, P., Ward, C. C., Levesque, S., Jing, Y., Simpson, D., Zhao, A., Li, H., Yan, W., Goudy, L., Schmidt, R., Solley, S. C., Gilbert, L. A., Chan, M. M., Bauer, D. E., Marson, A., Parsons, L. R. & Adamson, B. Improving prime editing with an endogenous small RNA-binding protein. *Nature* **628**, 639–647 (2024).

120. Yu, J., Park, J.-C., Uhm, H., Kim, Y.-W., Im, H. W. & Bae, S. Evolution of Prime Editing: Enhancing Efficiency and Expanding Capacity. *Advanced Science* **13**, e21015 (2026).